University College of Southeast Norway
Faculty of Technology, Natural Sciences
and Maritime Sciences

Doctoral dissertation no. 31
2017

Ole Kristian Sommersel

Hydrogen Leaks in Partially Confined Spaces - Dispersion and Explosions

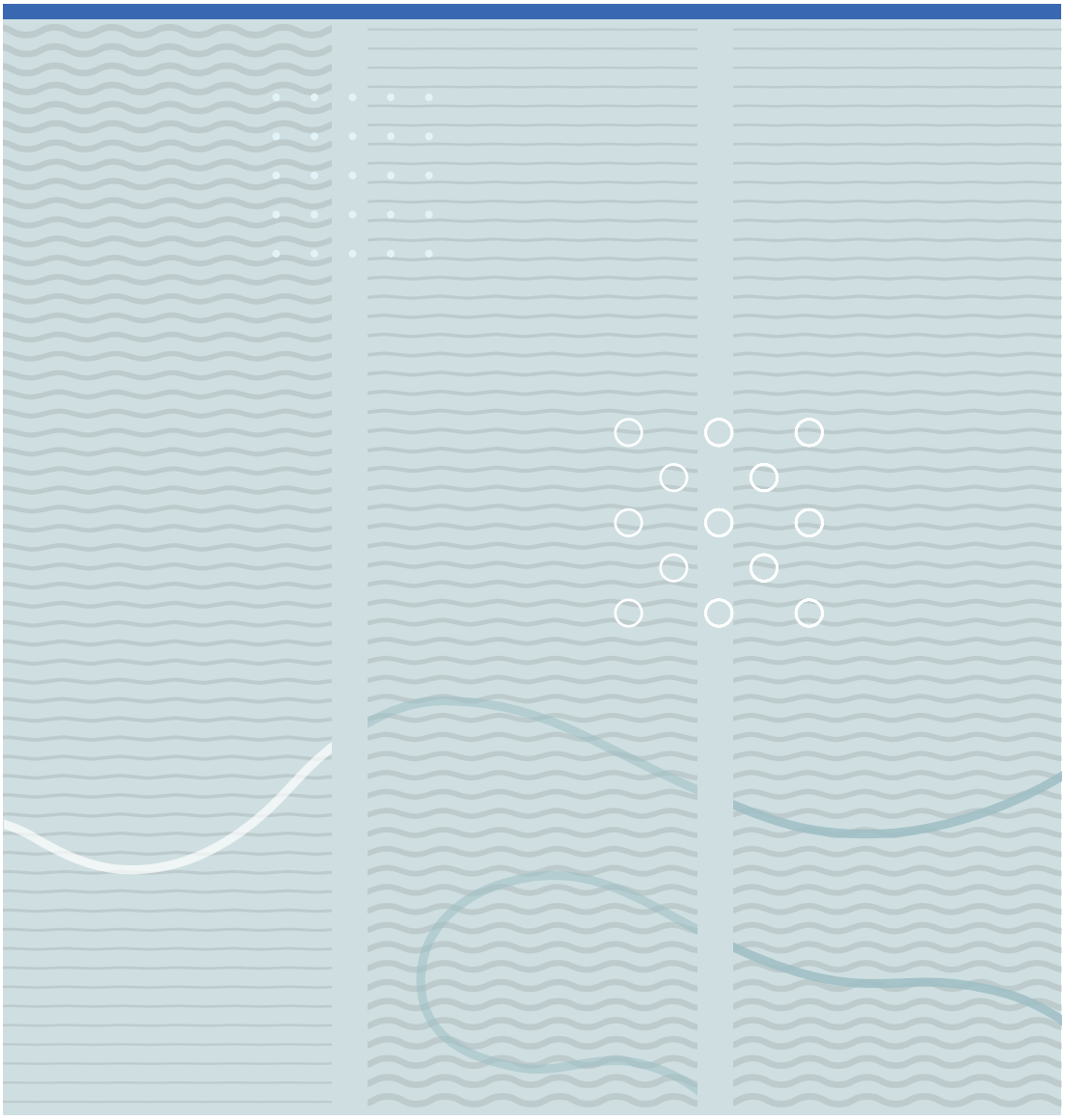

HSN

Ole Kristian Sommersel

Hydrogen Leaks in Partially Confined Spaces - Dispersion and Explosions

A PhD dissertation in
Process, Energy and Automation Engineering

Faculty of Technology, Natural Sciences and Maritime Sciences
University College of Southeast Norway
Kongsberg, 2017
Doctoral dissertations at the University College of Southeast Norway no. 31

ISSN: 2464-2770 (print)
ISSN: 2464-2483 (electronic)
ISBN: 978-82-7206-453-1 (print)
ISBN: 978-82-7206-454-8 (electronic)

Print: **University College of Southeast Norway**

Acknowledgements

This work has been carried out at Telemark University College (HiT) and University College of Southeast Norway (HSN), Faculty of Technology, Natural Sciences and Maritime Sciences.

The financial support from the Norwegian Research Council Programs, Strategiske Høgskoleprosjekter and RENERGI is gratefully acknowledged. This work has been a part of the International Energy Agency (IEA) Hydrogen Implement Agreement (HIA) task 19 (Hydrogen safety).

I especially thank my supervisor Professor Dag Bjerketvedt for the excellent, motivating and persevering guidance during my work on this PhD.

I would also like to thank Svein O. Christensen, Ottar Krest, Talleiv Skredtveit, Øyvind Johansen, Finn A. Haugen, Eivind Fjelddalen and Torstein Fanneløp for help with the experimental work.

Big thanks go to my fellow students and friends Knut Vågsæther, Andre Vagner Gaathaug, Joachim Lundberg, Vegeir Knudsen, Robin Lal Shresta, Kjetil Svendsen and Kanchan Rai. I would also like to thank Trygve Skjold for constructive feedback.

Special thanks go to my family; especially my wife Ellen, thank you for all the help, love and understanding. And of course, my sons Even, Gustav and Aksel.

Porsgrunn, October 2017

Ole Kristian Sommersel

Abstract

In Porsgrunn, Norway, there was an explosion in an ammonia plant in July 1985. The accident was caused by a hydrogen leak inside a factory building, called N1. The result was a severe hydrogen-air explosion and jet fire, which led to massive material damages and two fatalities. The 100 meter long building where the explosion occurred was completely destructed.

The basis for this thesis is the accident in the N1 ammonia plant hydrogen, where one of the main goals was to re-investigate the chain of events. The N1 factory building has been the model for both small-scale and field-scale experimental campaigns. The objective of the thesis is to get a better understanding of the dispersion of hydrogen and inhomogeneous hydrogen explosions in long buildings, channels and tunnels.

A laboratory scale experimental rig was built for studying dispersion and ignition of hydrogen gas clouds in an open channel. The rig was designed to study the gas cloud frontal velocity and the generated overpressure in the combustion of the hydrogen released. The experimental campaign was studied numerically, by use of the commercial CFD code FLACS.

A field-scale experimental rig was set up in Raufoss to study dispersion and ignition of inhomogeneous hydrogen gas clouds at a larger scale. The experimental campaign was designed to study the effects on generated explosion overpressures by varying mass flow rate, jet direction, time of ignition and level of obstructions. Subsequently, the experiments were studied numerically in FLACS.

Finally, FLACS was used to re-investigate the N1 accident through five different inhomogeneous hydrogen gas cloud scenarios. The scenarios were varied with respect to basic geometry and jet direction.

List of papers

Journal papers:

Application of background oriented schlieren for quantitative measurements of shock waves from explosions

Sommersel, O.K., Bjerketvedt, D. Christensen, S.O., Krest, O. and Vaagsaether, K. (2008) Shock Waves, vol 18, Issue 4, pp 291-297

Experiments with release and ignition of hydrogen gas in a 3 m long channel

Sommersel, O.K., Bjerketvedt, D., Vaagsaether, K., Fannelop, T.K. (2009) International Journal of Hydrogen Energy, vol 34, Issue 14, pp. 5869-5874

Hydrogen Explosions in 20' ISO container

Sommersel, O.K., Vaagsaether, K., Bjerketvedt, D. (2017) International Journal of Hydrogen Energy, vol 42, Issue 11, (2017) pp. 7740-7748

Conference proceedings:

Experiments with flame propagation in inhomogeneous hydrogen-air clouds in a small vessel

Sommersel, O.K, Shresta, R.L and Bjerketvedt, D. (2005) Proceedings of the 20th International Colloquium on the Dynamics of Explosion and Reactive Systems (ICDERS). Poster presentation

Application of background oriented schlieren (BOS) for quantitative measurements of shock waves from explosions

Sommersel, O.K., Bjerketvedt, D. Christensen, S.O., Krest, O. and Vaagsaether, K. (2007) Proceedings of the 24th International Colloquium on the Dynamics of Explosion and Reactive Systems (ICDERS). Oral presentation

Experiments with release and ignition of hydrogen gas in a 3m long channel

Sommersel, O.K., Bjerketvedt, D., Vaagsaether, K., Fannelop, T.K. (2007) 2nd International Conference on Hydrogen Safety (ICHS). Oral presentation by Bjerketvedt

Numerical simulations of a large hydrogen release in a process plant

Sommersel, O.K., Bjerketvedt, D. (2009) 3rd International Conference on Hydrogen Safety (ICHS). Poster presentation

Hydrogen Explosions in 20' ISO container

Sommersel, O.K., Vaagsaether, K., Bjerketvedt, D. (2015) 6th International Conference on Hydrogen Safety (ICHS). Oral presentation by Vaagsaether

Abbreviations

CFD	Computational Fluid Dynamics
DDT	Deflagration to Detonation Transition
FLACS	Flame Acceleration Simulator
fps	Frames per second
HySafe	The International Association for Hydrogen Safety (earlier EC funded Network of Excellence)
ICHS	International Conference on Hydrogen Safety
ICDERS	International colloquium on Dynamics of Explosions and Reactive Systems
ISHPMIE	International Symposium on Hazards, Prevention and Mitigation of Industrial Explosions
N1	Ammonia Plant 1, Norsk Hydro, Porsgrunn, Norway
NDEA	The Norwegian Defence Estates Agency
IEA	International Energy Agency
HIA	Hydrogen Implement Agreement

List of symbols

Latin symbols:

Symbol	Description	Unit
Fr	Froude number	[-]

g	acceleration of gravity	[m/s^2]
h	height of cloud	[m]
h_H	the height of a 100 % hydrogen layer in channel	[m]
L	length from end of channel to ignition point	[m]
Q	volume flow rate	[m^3/s]
u	velocity	[m/s]
u_F	frontal velocity	[m/s]
w	channel width	[m]
H	channel height	[m]

Greek symbols:

Symbol	Description	Unit
ρ_0	density of air	[kg/m³]
ρ_{H2}	density of hydrogen	[kg/m³]
$\Delta\tau$	time of ignition	[s]
Φ	dimensionless height, Φ=h/H	[-]

Table of contents

1 Introduction

1.1 Background

1.1.1 Hydrogen as an energy carrier

Large quantities of hydrogen are produced in the industry today (e.g. in the production of ammonia and in refineries), but hydrogen is not normally used for non-industrial energy purposes.

Four of the main advantages of the use of hydrogen as an energy carrier are energy reliability, local environment, global CO_2-emissions and industry development. As early as in 2004, the EC network of excellence for Hydrogen Safety (HySafe) was established in the sixth framework program of the European Commission (Hysafe 2004). Today, HySafe is an International Association for Hydrogen Safety, with a vision that hydrogen will be introduced as a safe and sustainable energy carrier. Partners in HySafe have in the last decade made progress in the research on several topics involved in safe commercial use of hydrogen, as the introduction of hydrogen as an energy carrier for the general public will make great demands on all aspects of safety. To ensure safe operation, a range of challenges must be accounted for; hydrogen has an ease of leaking, low ignition energy, wide range of combustible fuel-air mixtures, high buoyancy, and ability to embrittle metals.

The interest in hydrogen as an energy carrier has led to several studies of hydrogen safety issues, including studies on dispersions and explosions. The Sourcebook of hydrogen applications by Bain et al. (1998) states that 80% of industrial hydrogen leaks ignite, indicating the importance of preventing hydrogen leaks by means of fail-safe designs, control systems, personnel training and good knowledge of the process. It is well known that a hydrogen-air cloud can explode violently and thereby cause severe damage, Alcock et.al. (2001). The use of hydrogen in the transport sector raises

questions about the safety for hydrogen vehicles in buildings and road tunnels. The hazard is strongly linked to the dispersion of hydrogen inside partly confined spaces.

Large scale tests are expensive, in terms of costs, time and equipment. Computational Fluid Dynamics codes calculating dispersion and flame propagation are thus necessary tools for performing safety studies. Validation and benchmarking of these codes have been reported by Papanikolaou et al. (2010), Giannissi et al. (2015) and Middha and Hansen (2009), among others.

1.1.2 The N1 Ammonia plant accident

In Norway, there was an explosion in an ammonia plant in July 1985. The accident was caused by a hydrogen leak inside a factory building, called N1. The result was a severe hydrogen-air explosion and jet fire, which led to massive material damages and two fatalities. The 100 meter long building where the explosion occurred was completely destructed. A description of this accident was presented at the first International Conference on Hydrogen Safety (ICHS) conference in Pisa by Bjerketvedt and Mjaavatten (2005).

The investigation report from the N1 accident, written by Bjerketvedt and Mjaavatten (1986), did not include a detailed analysis of the dispersion of hydrogen inside the factory building (pump hall). The report contains basic estimates of the amount of flammable gas in a free jet, and a comparison of the dispersion phenomena to other explosion accidents. A series of numerical simulations of the explosion is included in the investigation report. These explosion simulations were performed with the commercial CFD tool FLACS, which was at the beginning of its development in 1985; the available numerical tools were limited. The simulations were performed with stoichiometric hydrogen gas clouds at different sizes. In the investigation report it is stated that even though FLACS then was a recognized code, the results had considerable uncertainties, due to a lack of experimental validation of hydrogen gas. The first commercial version of FLACS was released in 1986.

The N1 accident has been used as a specific background for the work performed in this thesis. Part of the objective of this work was to re-investigate the accident in the ammonia plant with a modern CFD tool.

1.1.3 FLACS

Throughout this thesis, the numerical simulations have been performed with FLACS. This CFD tool is now a well-known simulation tool for gas dispersion and gas explosions, developed by Gexcon (FLACS, 2016). The FLACS code has in the last decade been extensively validated for hydrogen dispersion and explosions. Gexcon, involved in the HySafe program, has published several papers on hydrogen dispersion and explosion both as benchmark exercises such as Venetsanos et al. (2009) and as independent work, among them Middha and Hansen (2009). The experimental campaign described in this thesis could further be used as validation of relevant CFD codes.

1.2 Aim of thesis

The basis for this thesis is the accident in the N1 ammonia plant hydrogen, where one of the main goals was to re-investigate the chain of events. The N1 factory building has been the model for both small-scale and field-scale experimental campaigns. The objective of the thesis is to get a better understanding of the dispersion of hydrogen and inhomogeneous hydrogen explosions in long buildings, channels and tunnels.

The work is structured as follows:

1. Laboratory scale; experiments in a 3 m long channel with small cross sectional area, and corresponding numerical simulations using the CFD code FLACS.
2. Field scale experiments of dispersion and ignition of hydrogen in a 6 m long container and numerical simulations of experiments in performed with FLACS.
3. Factory scale; numerical simulations of the N1 accident using the CFD code FLACS.

1.3 Thesis outline

This document consists of 7 chapters. The various chapters are further divided in sections. Literature studies are presented in the first part of the main chapters. Chapter 1 outlines the background and aim of this work. Chapter 2 addresses work performed in small scale in a 3 meter long channel; both experimentally and numerically. Chapter 3 gives a description of the experiments performed in field scale; dispersion and ignition of hydrogen in a standard shipping container. Shock wave investigations from these experiments are treated in Chapter 4, whereas the corresponding numerical simulations are presented in Chapter 5. Numerical simulations of the N1 ammonia plant accident are presented in Chapter 6. The conclusions with some recommendations for further work are presented in Chapter 7.

2 Small scale experiments and numerical simulations

2.1 Introduction

This chapter describes the work performed in laboratory scale. This include both laboratory experiments with hydrogen dispersions and explosions in a 3-meter-long channel, and numerical simulations of the same geometry. The objective was to study the dispersion mechanisms of inhomogeneous hydrogen gas clouds in a small-scale channel. The dimensions represent a small-scale version of the N1 ammonia plant factory building, and is the smallest scale investigated in this project.

The chapter is divided into 5 subsections. After a brief introduction in Chapter 2.1, the experimental equipment and data acquisition setup used in the experiments are explained in Chapter 2.2. In Chapter 2.3 the experimental results are presented and a Froude number expression is deduced to express the gas cloud dispersion. The experimental results are presented and discussed in Chapter 2.3. Numerical simulations are presented in Chapter 2.4, and finally the conclusions from the chapter are listed in Chapter 2.5.

2.2 Experiments, 3 m channel

A total of 5 test series were performed with flow rates of hydrogen from 1.8 dm^3/min to 75 dm^3/min (i.e. 3 to 112 mg/s). The propagation of the combustible hydrogen-air cloud in the channel was observed from high-speed video recordings. The hydrogen-air cloud in the channel behaves as a gravity current and the flow appears to be well described by Froude scaling with a length scale corresponding to the height of a layer of 100 % hydrogen. The Froude numbers observed in the experiments are in good agreement with the theory of “light-fluid intrusion” for gravity currents found in the literature. Numerical simulations with the FLACS code correlate well with the experimental results. The flame propagation indicated that approximately half the height of the channel was filled with combustible mixture. It is assumed that this Froude

scaling can be useful as a tool to analyse the consequences of hydrogen release in buildings, channels and tunnels.

2.2.1 Experimental setup

Figure 2.1 and Figure 2.2 show the experimental setup. It consisted of a horizontal square steel channel, 3 m long, 0.1 m wide and 0.1 m high. The top and bottom walls were made of painted steel, whereas the sidewalls were made of transparent polycarbonate. The channel was closed in one end and open to the atmosphere in the other end. The volume of the channel was 30.0 dm³.

Figure 2.1 Experimental setup of the 3 m long channel.

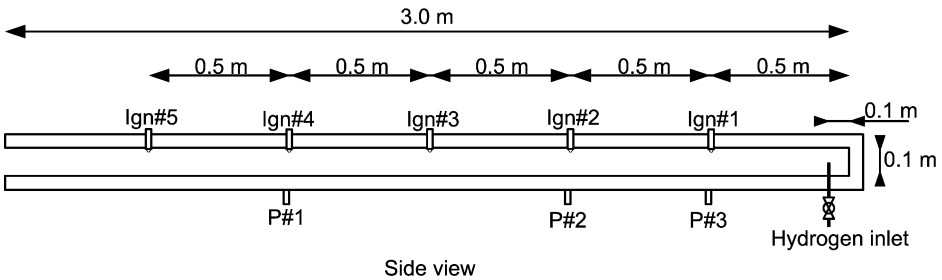

Figure 2.2 Schematic setup showing the ignition locations and hydrogen inlet.

2.2.2 Hydrogen gas supply

The hydrogen was supplied from a standard 200 barg gas cylinder. The hydrogen quality was 99.9 %. The volume flow, Q, was controlled by a F&P Purgemaster flow meter shown in Figure 2.3. The flow meter was calibrated prior to the experiments by a Ritter TG10-1.4571-PVC drum-type gas meter. By opening a fast acting Asco Joumatic pneumatic ball valve, the hydrogen gas was injected into the channel through a vertical 4 mm ID steel tube. The exit of the 4 mm tube was positioned 50 mm into the channel at the centreline and 0.1 m from the closed end. The release was directed vertically upwards and the flow velocities ranged from 2.4 m/s to 99.2 m/s.

Figure 2.3 F&P Purgemaster flow meter.

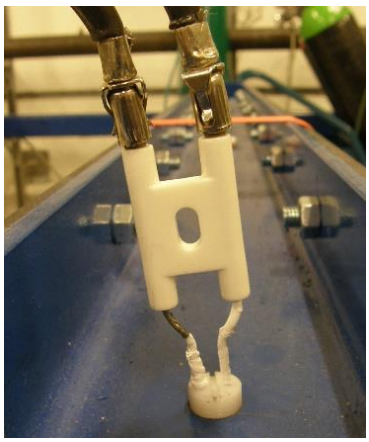

Figure 3.4 Electrode ignition source mounted on the top of the channel.

2.2.3 Ignition

The hydrogen-air mixture was ignited by a 5 kV spark between two electrodes mounted on the centreline of the channel, 5 mm from the upper wall. Figure 3.4 shows the spark electrodes seen from outside the channel. The current was supplied through a Siemens ZM 20/10 transformer. Figure 2.2 shows how the location of the ignition source was varied horizontally according to the 5 test series, 0.5 m, 1 m, 1,5 m, 2 m, and 2,5 m from

the closed end of the channel. The ignition source was switched on and off in a series of short pulses ten times per second.

2.2.4 Pressure recordings

Three Kistler 7001 pressure transducers measured the explosion pressures and the results were recorded digitally. The three pressure transducers were located 2 m, 1 m and 0.5 m from the closed end of the channel, as shown in Figure 2.2. They were flush mounted in the lower wall.

2.2.5 High-speed video

The experiments were recorded with a Photron Ultima APX-RS high-speed digital video camera equipped with a Nikkor 50 mm f/1.2 lens, shown in Figure 2.5. The monochrome camera can capture full 1024x1024 pixels resolution of up to 3000 frames per second, and with significantly higher frame rates at lower resolutions (max 250k fps). The camera has a 2 GB memory that can capture about 2000 images at full resolution. The Photron FASTCAM Viewer 2.4 software was used to control the camera.

During the experiments, the frame rate was typically 2000 fps, with a typical resolution of 1024x176 pixels. The videos were used to observe when the hydrogen release started, the time of ignition of the cloud and the following flame propagation. From observations on the videos, the opening of the pneumatic ball valve and the time of cloud ignition was determined.

Figure 2.5 Photron APX-RS high-speed camera.

2.3 Experimental results and discussion

2.3.1 Dispersion

The test conditions are shown in Table 2.1. Five test series with hydrogen flow rates ranging from 1.8 dm³/min to 75 dm³/min were carried out. For flow rates less than 1.8 dm³/min no ignition occurred.

Table 2.1. Experimental test conditions, with 5 different test series and corresponding hydrogen gas volume flows. The ignition positions in the channel was measured from the closed end wall.

Test series	1	2	3	4	5
Length, L [m]	0.5	1.0	1.5	2.0	2.5
Q_{min} [dm³/min]	1.8	2.7	4.6	10.3	17.5
Q_{max} [dm³/min]	75.0	75.0	75.0	75.0	75.0

2.3.2 Experimental flame propagation results

In this section a presentation of the results from the flame propagation in the channel is given. Figure 2.6 shows a typical development of the combustion process following the ignition of the cloud. In this particular experiment, the ignition source was located at L = 2.0 m from the end wall, with a flow rate Q = 17.5 dm^3/min. The time steps between each image are 30 milliseconds. Observations of the high-speed video show that the combustible gas filled approximately half of the height of the channel. For small flow rates, the high-speed videos show that the flame speeds were low and the combustion barely visible just below the upper wall. As the flame propagated towards the hydrogen inlet, the visible combustion occurred in the middle of the channel. This phenomenon is shown in Figure 2.6. For higher flow rates, the combustion was more turbulent, so the flames expanded over the full height of the channel. For the high flow rate experiments, it is possible that the flames were triple flames as discussed by Phillips (1965) and Chung (2007).

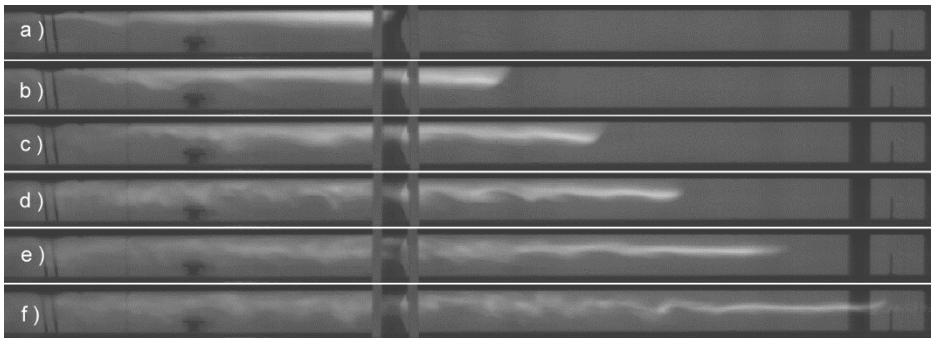

Figure 2.6 High-speed photos of the combustion of the hydrogen gas cloud at 30 ms time intervals. The ignition source is located at L=2.0 m and the flow rate is 17.5 dm³/min.

Explosion pressures were recorded in all the experiments. The maximum pressures versus the volume flow rate are shown in Figure 2.7. The explosion pressures in the experiments were less than 32 kPa, except for one experiment. In this test with Q = 75 dm³/min and L = 2.0, the transducer amplifiers were overloaded. Thus, maximum pressures were not recorded, but had at least 50 kPa and most likely less than 100 kPa (marked with an arrow in Figure 2.7).

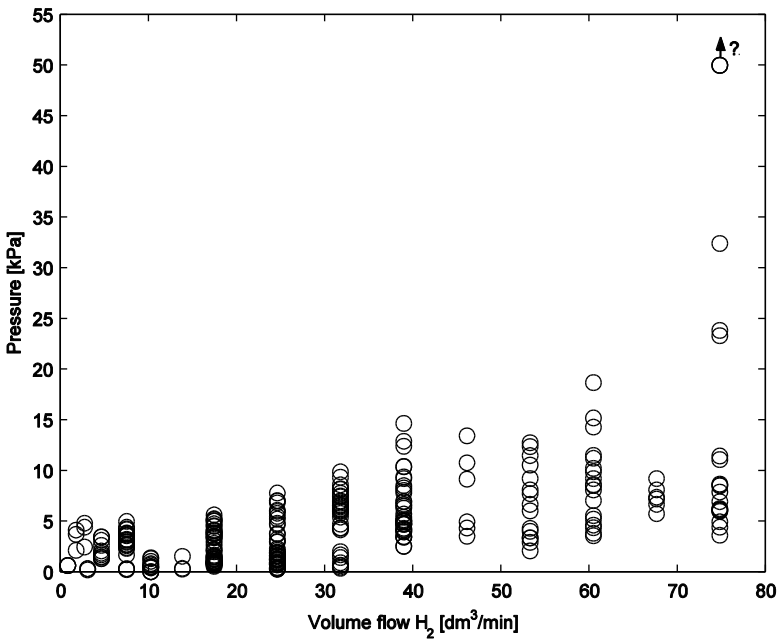

Figure 2.7 Maximum explosion pressures versus the volume flow rate Q, for the 5 test series.

2.3.3 Froude scaling

This chapter presents a set of equations developed to describe the propagation of the hydrogen gas cloud in the channel. The theory is related to fluid dynamics, where a gravity current is defined as a flow in a gravitational field driven by a density difference, Simpson (1997) and Fanneløp (1994). The frontal velocity of gravity currents can typically be expressed by the dimensionless Froude number. The Froude number is the ratio between momentum and gravity forces acting in a fluid flow. The Froude number is often defined as

$$\mathrm{Fr} = \frac{u_F}{(gh)^{\frac{1}{2}}} \qquad 3.1$$

where u is a velocity, g is the acceleration of gravity and h a length scale.

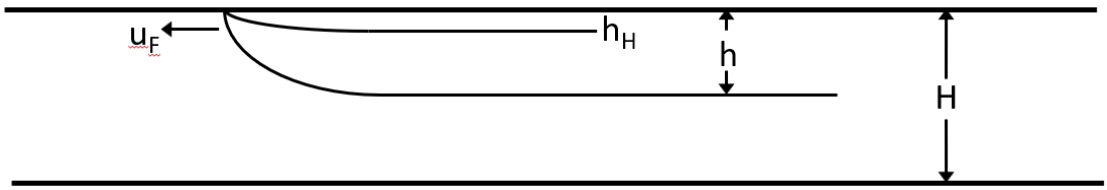

Figure 2.8 Sketch of channel with defined notation.

In this case the velocity is the frontal velocity of the hydrogen-air cloud, u_F. The flow rate of hydrogen gas into the channel, Q, can be related to the frontal velocity of the cloud by

$$Q = u_F h_H w \qquad 3.2$$

where h_H is the height of a 100 % hydrogen layer in the channel, shown in Figure 2.8. If h_H is selected as the characteristic length scale in defining the Froude number, then

$$Fr = \sqrt{\frac{u_F{}^3 w}{gQ}} \qquad 3.3$$

The average frontal velocity u_F can be expressed by L, the distance from the closed end of the channel to the ignition point and $\Delta\tau$, the time of ignition, i.e. time from the release started to the cloud is ignited.

$$u_F = \frac{L}{\Delta\tau} = \sqrt[3]{\frac{Fr^2 gQ}{w}} \qquad 3.4$$

This yields an expression for the Froude number;

$$Fr = \sqrt{\left(\frac{L}{\Delta\tau}\right)^3 w/gQ} \qquad 3.5$$

When the Froude number is known, the time of ignition can be estimated from

$$\Delta\tau = \sqrt[3]{\frac{wL^3}{Fr^2 gQ}} \qquad 3.6$$

Note that the expression in 3.1 is a variant of the dimensionless Richardson number (Ri) which expresses the ratio of the buoyancy term to the flow shear term. For a pure hydrogen layer with height h, the ratio $\frac{\Delta\rho}{\rho_0} \approx \frac{\rho_0 - \rho_{H_2}}{\rho_0} \approx 1$, leading to:

$$Ri^{-1} = \frac{\rho u^2}{\Delta\rho g h} = Fr^2 \qquad 3.7$$

The use of Froude scaling was presented by Sommersel et al. (2009) and was also presented by Rai et al. (2010) at the eight International Symposium on Hazards, Prevention and Mitigation of Industrial Explosions (ISHPMIE). Houf and Schefer (2008) report an experimental and numerical study on small-scale releases of hydrogen, where the buoyant and inertial forces are represented by Froude numbers.

Figure 2.9 and Figure 2.10 show the experimental results expressed in terms of Froude number, according to Eq. 3.5.

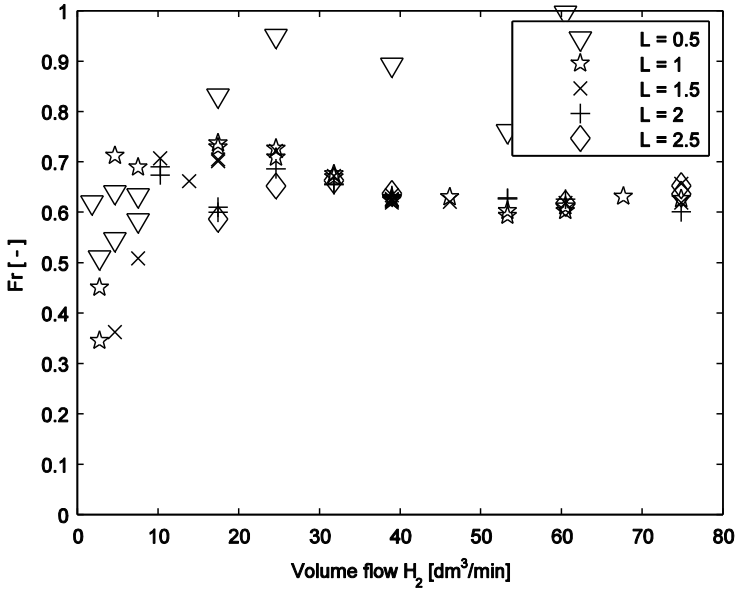

Figure 2.9 Froude numbers determined from hydrogen-air experiments.

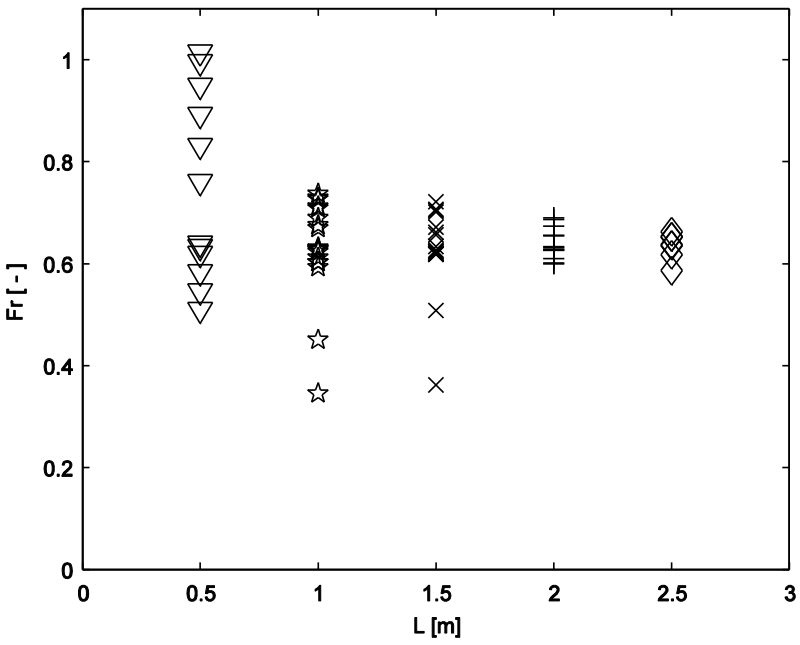

Figure 2.10 Experimentally obtained Froude number as function of distance between hydrogen discharge and ignition source.

For the higher flow rates, the Froude number approaches a constant value of about 0.65. Some scatter is present at the lower flow rates; this might be a result of error in the interpretation of time of ignition from the high-speed videos. At low flow rates, the initial flame was sometimes difficult to observe. Another factor that might influence the results is that the mixing caused by the low momentum jet cannot produce a well-mixed layer with a thickness of the upper half of the channel for low flow rates. Figure 2.9 and Figure 2.10 show that test series #1 has relatively large deviations from the Froude number found in the other series. In series #1 the distance between the hydrogen inlet and the ignition source is relatively short, and the deviation observed may be explained by the initial non-steady flow caused by the opening of the pneumatic ball valve.

The Froude numbers determined in the experiments are in accordance with the theory of "light-fluid intrusion" for gravity currents that can be found in the literature; Fanneløp (1994), Gröbelbauer et al. (1993) and Brooke (1968). Here, the model is extended for light-fluid intrusion given by Gröbelbauer et al. (1993) when the Froude number is based on the length scale $\mathrm{h_H}$.

$$\mathrm{Fr} = \frac{\mathrm{u_F}}{\sqrt{\mathrm{g h_H}}} = \frac{\mathrm{H}}{\mathrm{H} - \mathrm{h_H}} \sqrt{\frac{(\rho_0 - \rho_\mathrm{H})}{\rho_1} \left(\frac{(2-\Phi)(1-\Phi)}{(1+\Phi)} \right)} \qquad 3.8$$

In this expression, the dimensionless height $\Phi = {}^{\mathrm{h}}/_{\mathrm{H}}$ is an unknown. Observations from the flame propagation experiments, see Figure 2.6, show that the combustion products filled the upper half of the channel. This observation supports that the height $\Phi = 0.5$ is a reasonable assumption. Assuming that the height of the pure hydrogen layer $\mathrm{h_H} \ll \mathrm{H}$ then the Froude number Fr = 0.68 from Equation 3.8. When this Froude number is used in Equation 3.6 there is reasonable agreement with the experimental results, as shown in Figure 2.11. The solid lines are the calculated values for the time of ignition, Δτ. A change of 10 % in the value of h yields a Froude number interval between 0.63 and 0.74, when inserted into Equation 3.8.

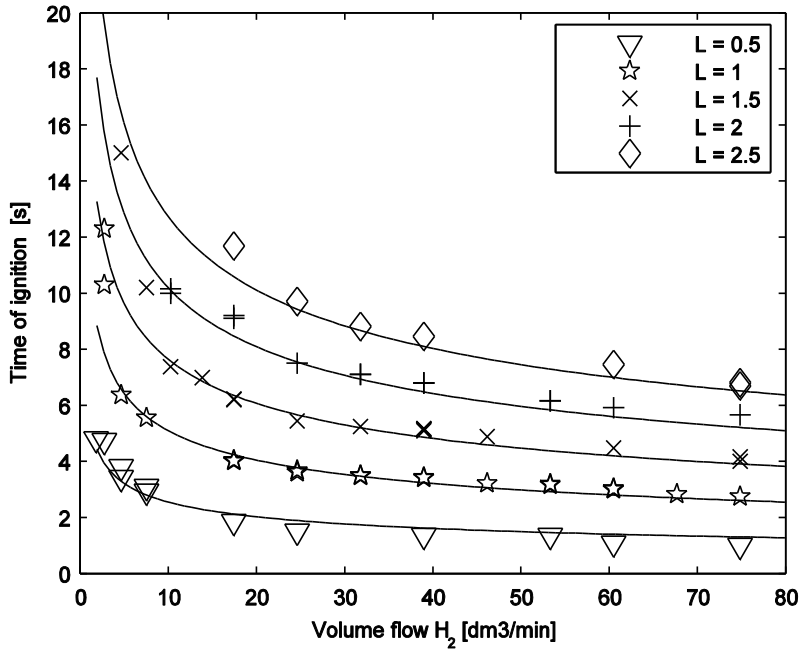

Figure 2.11 Time of ignition, Δτ, as function of volume flow rate, Q. The solid lines are calculated from Eq. 3.8, with Fr = 0.68

The change in h also result in Δτ = ±5.5%, obtained from Equation 3.6. The deviation from the experimental results becomes significant, and indicates that Φ≈0.5. It is likely that the expansion of the combustion products primarily will take place in the longitudinal direction, due to the open end of the channel and the relatively low flame speed (i.e. low Mach number).

It is interesting to note that when $^{h}/_{H}$ goes to zero, the Froude number becomes $Fr = 2 \cdot 0.68$. This indicates that the frontal velocity will likely be within a factor of about 2 and only dependent on Q, w, H and h. Factors influencing the height of the hydrogen-air cloud, h, needs to be studied in more detail. Dispersion experiments where a z-type Schlieren setup is applied on the 3 m long channel are presented in Chapter 2.3.5. The results show indications towards a degree of gas cloud filling, however, due to image quality the results were inconclusive. A more detailed analysis, where the dimensionless

height Φ was determined to ≈0.55 was presented in Rai et al. (2014). It should be noted that Φ is dependent of the test conditions, and different discharge conditions and other geometries will influence the value of Φ.

2.3.4 Hydrogen concentration

In assuming that $\Phi = {}^{h}/_{H} = 0.5$ and that Fr = 0.68, it is possible to estimate an average hydrogen concentration in the combustible cloud. Figure 2.12 shows this mole fraction for all the experiments.

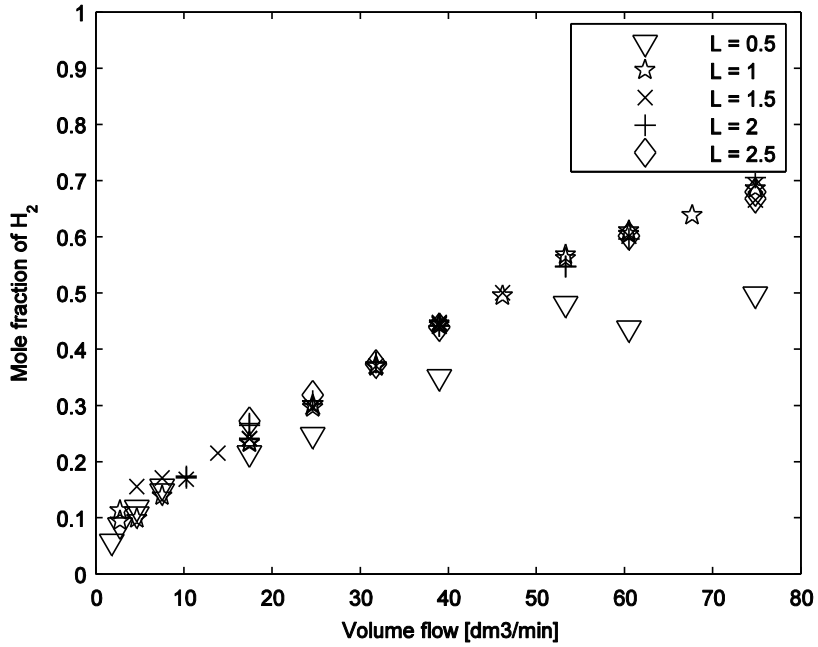

Figure 2.12 Average hydrogen concentration in the cloud, calculated with Φ = 0.5 and Fr = 0.68.

2.3.5 Schlieren visualization

A standard Z-type schlieren arrangement was used in an attempt to capture images of the development and dispersion of the hydrogen gas cloud in the channel. This method is widely used in flow visualization applications. Settles (2001) describes schlieren as gradient disturbances of inhomogeneous transparent media. They are relatively-small differences in refractive indexes, compared to the overall background. These differences are converted to shadows in a schlieren system. The customary schlieren setup employs

a bright light source, a knife edge and two concave mirrors that reflect the light through a subject gradient in a “Z” pattern, named the Z-type schlieren in Settles (2001). The schlieren images presented here were captured from a high-speed video recording of the light traveling through the 3 m long vessel.

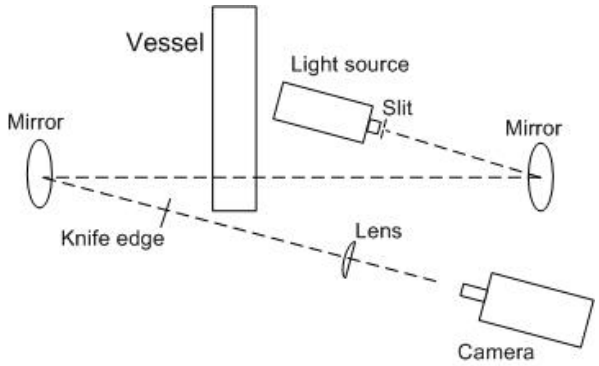

Figure 2.13 Z-type schlieren arrangement schematics (25° angles).

Figure 2.14 Palflash 501 light source used in the schlieren experiments.

The light source used in the experiments was a Palflash 501, shown in Figure 2.14, manufactured by Pulse Photonics ltd. The light was directed through a knife edge slit mounted on the light source and towards a 23.5 cm diameter spherical mirror with a 2.5 m focal length. The angle between the light source and the first mirror was 25°. The spherical mirror was then adjusted to direct the collimated light through the sides of the 3-meter-long vessel and towards the second spherical mirror, also with a 25° angle. The knife edge was positioned at the focal length of this second mirror, mounted on a slidebar together with a plano-convex lens. The films were captured on the APX-RS highspeed camera. The camera was used without a lens, and operated at frame speeds mainly in the range 250-500 fps, at typical resolutions of 1024x100 for capturing the full length of the channel.

Capturing good quality schlieren images of the development and dispersion of the hydrogen cloud was unsuccessful. The current setup was not able to capture the

gradient clearly between the hydrogen and air, probably due to insufficient lighting, and in some cases condensation of water vapor on the polycarbonate walls.

The high-speed videos show some gradients, especially close to the inlet. In the left-hand figure of Figure 2.16 the hydrogen discharge is barely visible. By studying the videos there are indications that the hydrogen gas cloud fills the upper half of the vessel, but producing high quality images of this phenomena was unsuccessful. Further work on experiments using schlieren photography was presented in Gaathaug et al. (2010), where angular schlieren was used to capture images of flame propagation in a similar channel.

Image processing of the schlieren based high-speed videos of the hydrogen dispersion have been tested out (a background subtraction method, further described in Chapter 4.2. Figure 2.15 shows an example of a treated image. The hydrogen inlet pipe is seen in the centre of the figure, and the white areas indicate that hydrogen is present. The hydrogen discharge, aimed vertically upwards, is seen as a wrinkled area in the centre of the image. A field of white is faintly visible centred along the horizontal axis, indicating a hydrogen gas cloud in the upper part of the channel.

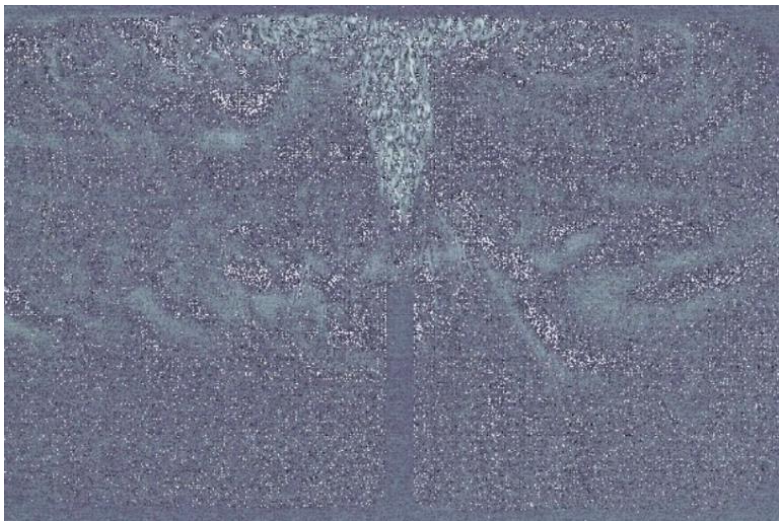

Figure 2.15 Image processed schlieren image of the hydrogen inlet in the channel. The white areas indicate that hydrogen is present. The image processing procedure is described in Chapter 4.

However, the combustion of the hydrogen gas cloud was clearly visible. Figure 2.16 shows a time series of dispersion and combustion of the hydrogen gas in the channel.

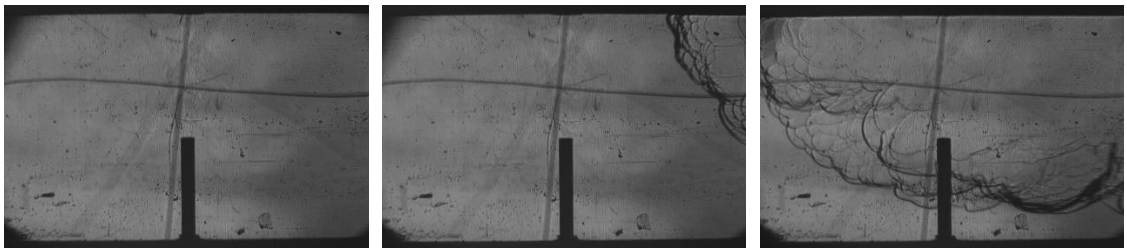

Figure 2.16 Images from schlieren test of dispersion and ignition of hydrogen in the 3 m long channel.

The schlieren visualization was intended to quantify the thickness of the hydrogen gas layer in the channel, in order to qualify the assumption $\Phi = 0.5$ used in the Froude number expression (Eq. 3.8). The results show indications towards a degree of gas cloud filling, however, due to image quality the results were inconclusive. Further work can be found in Rai et al. (2014).

2.4 Numerical simulations, 3 m channel

This section describes the numerical simulations performed on the small scale setup presented in chapter 2.2. The numerical setup and details are presented in chapter 2.4.1, and the results are presented in chapter 2.4.2.

2.4.1 Numerical setup

A series of numerical simulations have been performed with FLACS. This program is a commercial CFD simulation tool for gas dispersion and gas explosions. The modelling was performed with a total of 38200 control volumes. The 3D model grid consisted of grid cells of 50 mm. The grid was refined to 5 mm near the release point, and

smoothened up to 50 mm in the major part of the geometry. The jet was modelled with a 5 mm grid refinement with a smooth transition to 10 mm which was used in the rest of the channel. The grid was stretched in the longitudinal direction to 50 mm near the open end of the channel. The model was used to simulate hydrogen gas dispersions with 3 different mass flow rates, corresponding to 10 dm3/min, 30 dm3/min and 60 dm3/min respectively. The time of ignition criteria was the time when the hydrogen mole fraction reached 8 percent at the ignition location, i.e. the downward flammability limit of hydrogen.

2.4.2 Numerical results

Figure 2.17 shows an example of the numerical dispersion simulations. Here, the flow rate is 10 dm^3/min ($1.4 \cdot 10^{-5}$ kg/s $= 0.014$ g/s). The time series is presented with a 1 s interval, in a simulation where the nozzle was positioned 0.05 m above the channel floor (i.e. centred). The ignition source is located at 1.5 m, corresponding to test series 3, presented in Chapter 2.3.1.

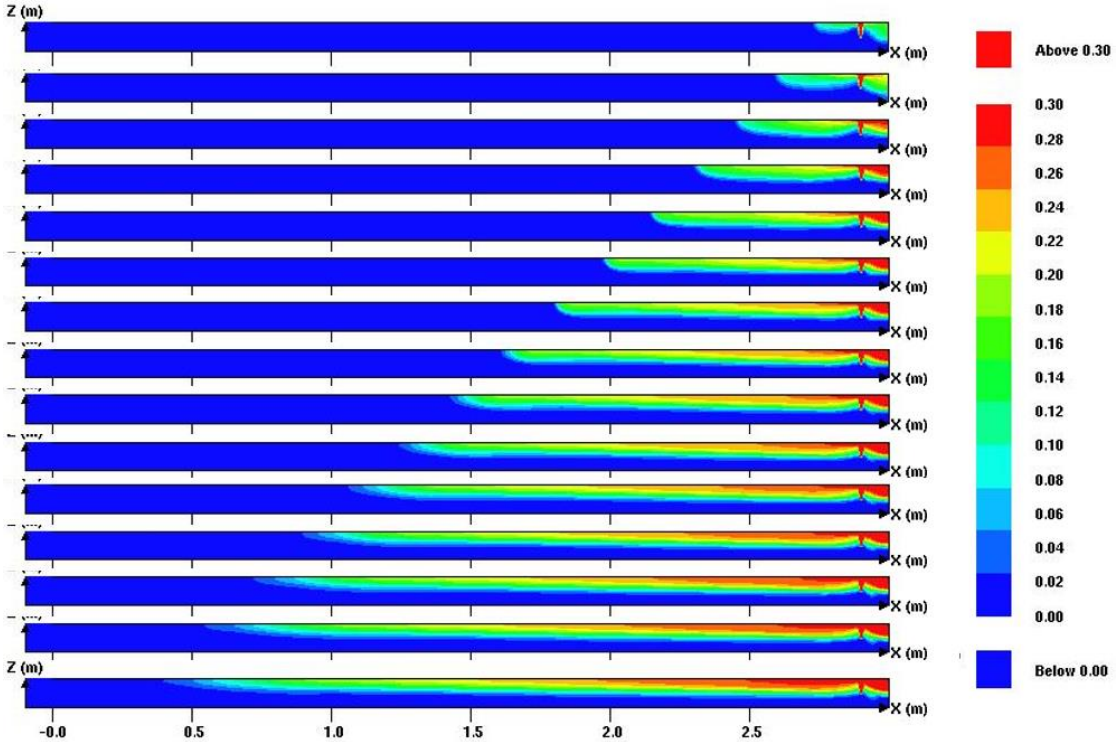

Figure 2.17 Time series of cut plane contour plots from numerical simulations in FLACS. The flow rate was 10 dm^3/min, with the nozzle positioned 0.05 m from the channel floor. Time step between images is 1 s. Blue colour corresponds to concentrations below LFL, whereas red colour corresponds to concentrations above stoichiometric.

Figure 2.18 compares the time of ignition from the FLACS simulations with the values from Equation 3.6, where Fr = 0.68. The FLACS dispersion simulations results correlate quite well with the experimental data. Sensitivity analyses with higher resolution in the FLACS simulations show similar results as with grid size 5 mm.

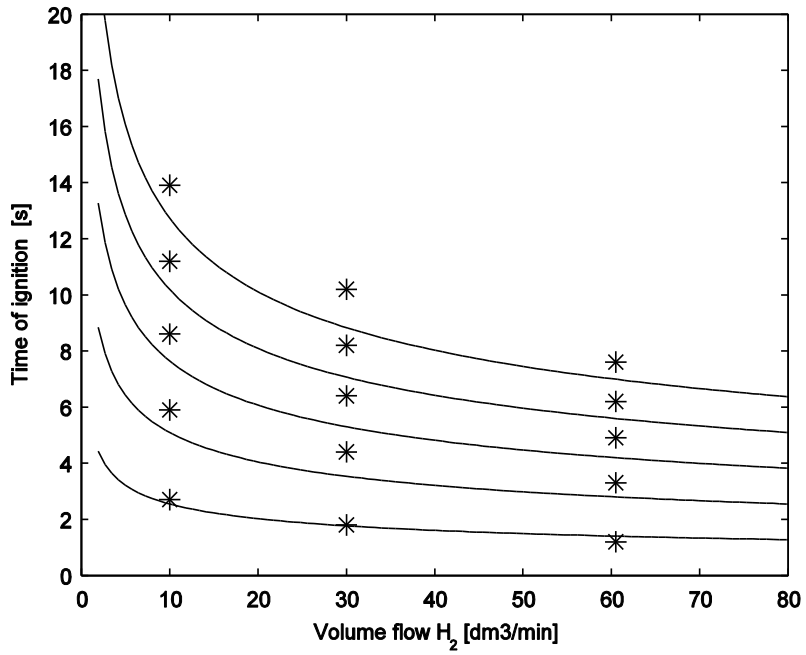

Figure 2.18 Comparison of numerical and theoretical results. The numerical calculations are performed in FLACS. The lines correspond to Equation 3.6, with Fr = 0.68.

2.5 Conclusions

A series of laboratory experiments with release of hydrogen gas inside a 3 m long horizontal channel with a cross section of 0.1 m by 0.1 m is reported in this chapter. The rig is considered to be a reasonable accurate small scale version of the N1 building, and therefore the experiments and simulations are considered to give small scale insight to the forming of gas clouds in such buildings. High-speed videos were used to observe when the hydrogen release started, the time of ignition of the cloud and the following flame propagation. Under the presented experimental conditions, the hydrogen-air cloud in the channel behaves as a gravity current.

The observed frontal velocity of the gas cloud, based on the time of arrival at the continuous ignition source, appear to be well described by Froude scaling with a length scale corresponding to the height of a layer of 100 % hydrogen in the channel. The Froude numbers observed in the experiments are in good agreement with the theory of light-fluid intrusion for gravity currents found in the literature.

The flame propagation in the channel was also observed on high-speed video. The flame propagation indicated that approximately half the height of the channel (i.e. $\Phi = 0.5$) was filled with combustible mixture, which supports the assumptions on which the Froude number is deduced. Numerical simulations with the FLACS code correlate well with the experimentally observed frontal velocities, and provides additional support in considering Froude scaling a useful tool to analyse the consequences of hydrogen release in buildings, channels and tunnels. Froude scaling will be used when N1 is reinvestigated in Chapter 6, both in evaluating the probable concentrations, and total release of hydrogen gas.

The maximum explosion pressures monitored was less than 32 kPa except for one test.

3 Experiments, ISO container

3.1 Introduction

This chapter presents setup and results from an experimental campaign with dispersion and explosion of hydrogen gas, performed in a 20 foot container. These experiments were field-scale, intended to represent the N1 ammonia plant factory building.

The purpose of the experiments was to study the dispersion and explosion mechanisms of inhomogeneous hydrogen gas clouds in a field-scale channel-like geometry. The main objectives were to obtain pressure- and high-speed data of the releases and explosions in the experiments.

The experiments were performed in June 2005 at the Norwegian Defence Estates Agency (NDEA) test facility at Raufoss in Norway, as part of an IEA-HIA task 19 project on hydrogen safety. The results from this work were presented at the International Conference on Hydrogen Safety (ICHS) in 2015, and have been published as an article in the Journal of Hydrogen Energy (Sommersel et al. 2017).

The test series consisted of calibration experiments with C-4 high explosives and 39 gas explosions experiments with inhomogeneous hydrogen air clouds in a standard ISO container. The results consisted of pressure records and high-speed videos. The first 37 experiments were performed with an empty container, and with both doors open. In experiments 38 and 39 the container was filled with obstacles, 2 and 8 ordinary euro pallets respectively. The explosion pressures from the experiments without obstacles were relatively low, in the range of 0.4 to 7 kPa. In the two experiments with obstacles the gas exploded more violently.

Initially the plan was to perform experiments with releasing the hydrogen both 1 m and 3 m from the closed end wall of the container. During the experimental campaign, it became clear that locating the nozzle closer to the container door opening (i.e. 3 m from closed end wall) led to an increased venting of the hydrogen into open air outside of the container, thus leading to lower explosion overpressures. The major part of the

experiments was therefore performed with the nozzle located close to the closed end wall of the container.

The experimental campaign was performed prior to the small scale experiments where the hydrogen gas cloud frontal velocity was expressed in terms of the Froude number as explained in Chapter 2.3.3.

3.2 Experimental setup

3.2.1 Module geometries

The hydrogen experiments were performed in a standard 20" ISO container, shown in Figure 3.1. The container had inner dimensions L = 6 m, W = 2.4 m and H = 2.4 m, and the steel walls and roof were corrugated. The doors shown on the container left hand side could be fully opened, whereas the end wall was solid (right side on Figure 3.1).

Figure 3.1 Image of the container used in the experiments.

The container was placed approximately 30 meters from a shooting range bunker, where the instruments and high-speed video cameras were set up. Figure 3.2 and Figure 3.3 show a schematic overview of the container with lengths and pressure monitor

placements. Two large web bands were used to tie the container to the ground. The gas filling system was placed behind the closed end wall.

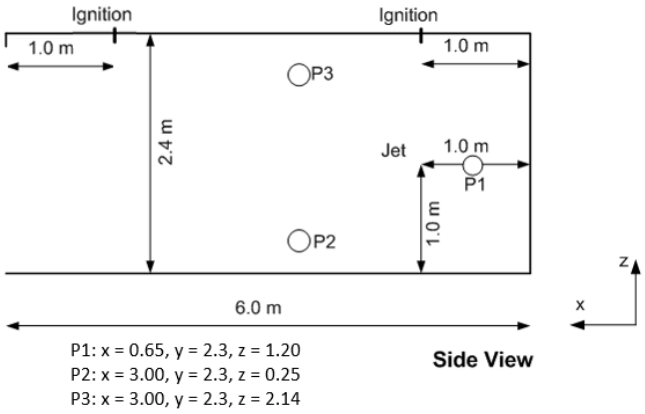

Figure 3.2 Side view of the container with measurements.

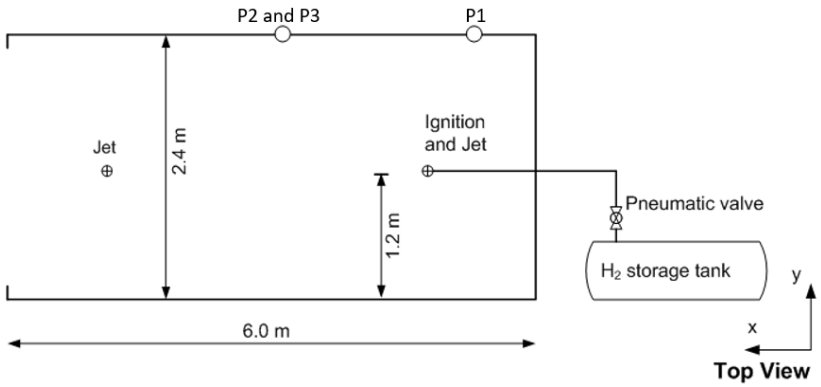

Figure 3.3 Top view of the container and filling system and measurements.

3.2.2 Fuel supply system

The fuel supply system consisted of a 0.3 m^3 storage tank and a steel tube connecting the tank and the container, shown in Figure 3.4. The tank was placed behind the closed end wall. A nozzle was mounted at the tube outlet, with nozzle diameters 5 and 9 mm, respectively. The nozzle was placed in two different locations, 1.0 m and 3.0 m from the solid back wall at a height of 1.0 m above the container door. Different experiments were performed with the nozzle directed upwards and downwards. The storage tank was filled with hydrogen at different pressures, ranging from 0.6 to 2.4 MPa(g), and the

steel container was then filled with hydrogen through the steel tube. The fuel supply was controlled by a ball valve with a pneumatic actuator. Details of the gas handling units are presented in Figure 3.3 and Figure 3.4. The fuel supply system was controlled remotely from the control room.

Figure 3.4 Gas storage tank and fuel supply system.

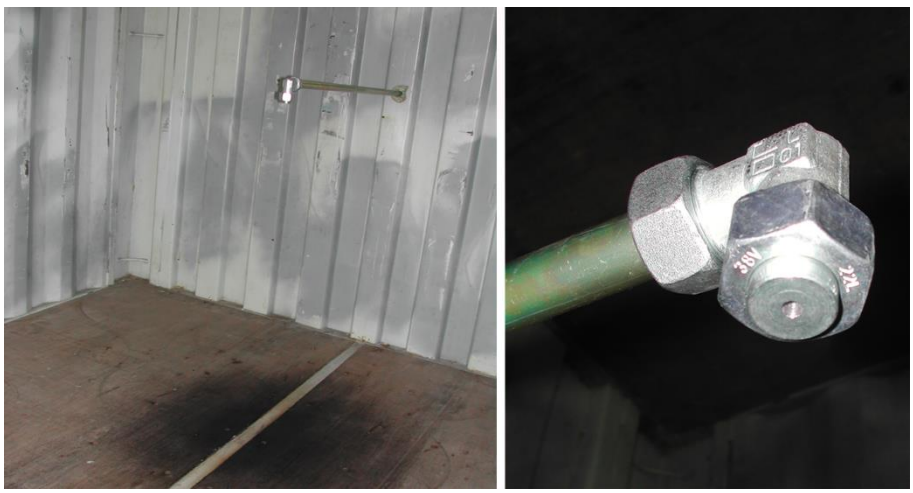

Figure 3.5 Nozzle details, 9 mm.

3.2.3 Ignition system

The ignition source was a continuous spark system, built up by two electrodes and a Siemens ZM 20/10 220 V transformer with an output voltage of approximately 5 kV. The electrodes, shown in Figure 3.6, were mounted in the roof, 100 mm below the roof of

the container. The spark electrodes were located at two different positions during the experiments, at 1 m from the door opening, and 1 m from the closed end wall, respectively. The two ignition locations are shown in Figure 3.2 and Figure 3.3.

Figure 3.6 Spark electrodes used as ignition source mounted in the roof of the container.

Spark duration was not logged; however, the ignition was continuous until confirmed ignition. An extension cord from the container and ignition source to the control room were put up to control the ignition remotely.

3.2.4 Instrumentation

Three Kistler 7001 piezo-electric pressure transducers (P1, P2, P3) measured the explosion overpressure inside the container. These pressure transducers are hermetically sealed and have a stainless-steel body. A quartz crystal measuring element transforms the measured pressure [bar] into an electrostatic charge [pC]. The transducers were mounted in brass brackets sealed with silicone and were located as shown in Figure 3.2 and Figure 3.3. Grease were applied on P1-P3 flush with the brass brackets. The pressure transducers were connected to Kistler charge amplifiers, type 5011B, from which the electrical charge was converted into a proportional voltage signal. The pressure transducers were triggered by the first input voltage signal, corresponding to the first pressure peak in the explosion. The digital logger had a built-in pre-trigger of 100 ms, allowing for a complete pressure-time development to be recorded and stored. The pressure transducer amplifiers were calibrated by measuring

two C-4 high explosives detonations, with 10 and 100 g of C-4 respectively (amplifier details are provided in Appendix 3).

Two LC-33 pressure transducers (P4 and P5 respectively), were positioned outside the container, at several positions during the course of the experiments. P4 and P5 were mounted on rods, which were positioned perpendicular to the blast wave, to measure side-on pressure. The pressure signals from P4 and P5 were recorded on a transient digital data logger, using the same trigger system as mentioned above. Pressure measurement details are shown in Figure 3.7.

Figure 3.7 Instrumentation for pressure measurements. Top left: Kistler 7001, top right: Kistler 7001 mounted in brass plate in container wall, top middle: LC-33 pencil shaped transducer mounted on a pole located outside of the container. Bottom: Kistler charge amplifiers.

For experiment 38 and experiment 39, the far-field monitors P4 and P5 were positioned as indicated in Figure 3.8. Figure 3.9 shows a photo of the P4 and P5 pressure

transducers mounted on rods located outside the container. Analysis and plotting of pressure data was done using MATLAB.

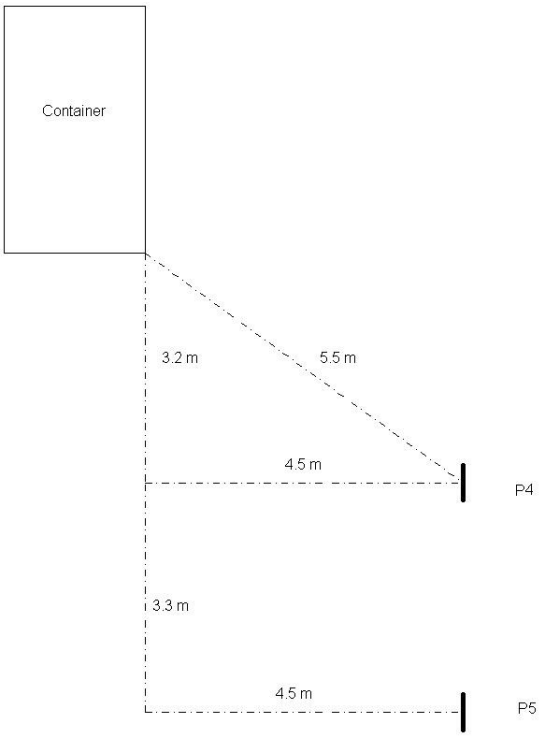

Figure 3.8 Positions of transducers P4 and P5 during experiment 38 and 39

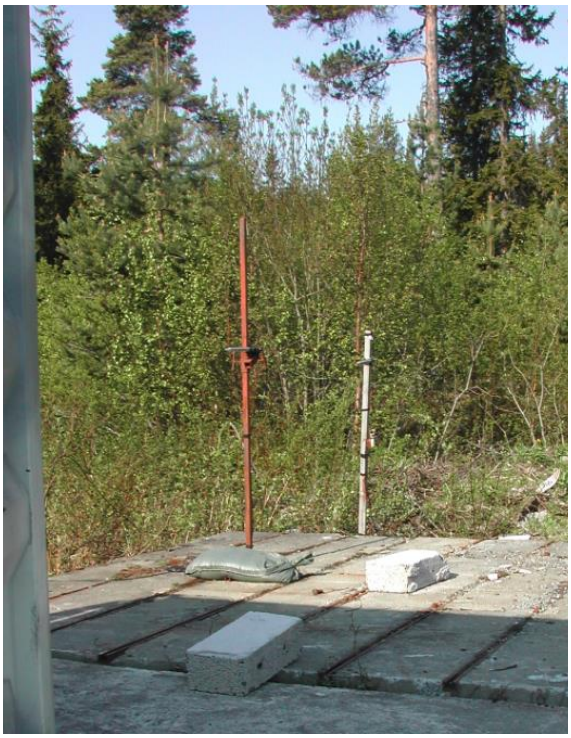

Figure 3.9 Photo of P4 and P5 located outside the container

The hydrogen storage tank pressure was monitored with a Kistler 428xAE50 pressure transducer mounted at the end wall of the tank, and the pressure recorded on a LeCroy 9314M oscilloscope. The pressure drop in the storage tank was therefore logged during each experiment. The tank pressure recordings are compared with leak rate calculations to verify these calculations, presented in 3.4.5.

Each experiment was also recorded with two high-speed video cameras. A Photron Ultima APX-RS high-speed monochrome camera with a Nikkor 50mm f/1.2 lens, was recording the explosion events at a rate of 3000 fps. A Photron FASTCAM-APX 120KC colour high-speed camera recorded the events at 500-1000 fps. The cameras were

triggered manually, at the exact time as the explosion occurred, using a pre-trigger function embedded in the camera software.

Video recordings of each test were made, using a Sony digital camera placed outside of the container.

Figure 3.10 Photron APX-RS high-speed camera used in the ISO container experiments.

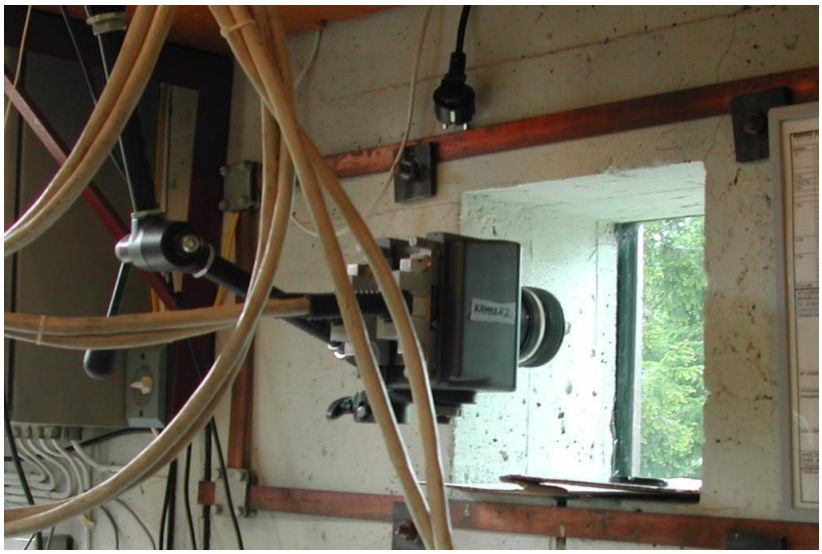

Figure 3.11 Photron FASTCAM-APX 120KC colour high-speed camera used in the ISO container experiments.

3.3 Experimental matrix

From the full experiment series of 39 tests, a set of 13 experiments with the 9 mm nozzle are presented here, shown in Table 3.1. The 22 experiments not reported included basic tests to check instrumentation- and fuel supply system, and a series of tests with low tank pressures and low amounts of hydrogen which did not ignite at all.

The first column in Table 3.1 represent the original experiment number, the second column denotes the storage tank overpressure [MPa] prior to the release, with the corresponding calculated flow rate in column 3 (calculations presented in Appendix 1). The fourth column describes the nozzle direction and position from the solid end wall, the fifth column shows the time of ignition [s] after the release were initiated, and the last column show calculated initial mass of hydrogen in the tank. This matrix has a set of results where the storage tank pressure varies between 0.6 and 2.4 MPa. All but 3 of the 9 mm experiments were ignited after 15 s of hydrogen release.

Table 3.1 Experimental matrix, 9 mm nozzle.

Experiment	Initial tank pressure [MPa] (g)	Initial flow rate[1)] [kg/s]	Nozzle direction and position	Ignition [s]	Mass H_2 [1)] [kg]
23	2.0	0.08	downwards, 1 m	After 15 s	0.46
24	2.0	0.08	downwards, 1 m	After 15 s	0.46
25	2.0	0.08	downwards, 1 m	After 10 s	0.46
26	2.4	0.1	downwards, 1 m	After 15 s	0.55
27	1.2	0.05	downwards, 1 m	After 15 s	0.27
28	0.6	0.03	downwards, 1 m	After 15 s	0.13
29	0.6	0.03	downwards, 1 m	After 16 s	0.13
30	2.0	0.08	downwards, 1 m	After 15 s	0.46
35	2.0	0.08	downwards, 1 m	After 7.5 s	0.46
36	2.4	0.1	downwards, 1 m	After 7.5 s	0.55
37	2.4	0.1	downwards, 1 m	After 15 s	0.55
38[2)]	2.4	0.1	downwards, 1 m	After 15 s	0.55
39[3)]	2.4	0.1	downwards, 1 m	After 15 s	0.55

[1)] calculated values. [2)]obstacles (2 pallets, ref. Figure 3.19). [3)]obstacles (8 pallets ref. Figure 3.20).

Table 3.2 presents the experimental matrix for the 4 successful experiments performed with the 5 mm nozzle. The layout is the same as for Table 3.1.

Table 3.2. Experimental matrix, 5 mm nozzle.

Experiment	Initial tank pressure [MPa] (g)	Initial flow rate[1)] [kg/s]	Nozzle direction and position	Ignition [s]	Mass H_2 [1)] [kg]
31	2.0	0.08	upwards, 1 m	After 30 s	0.46
32	2.0	0.08	upwards, 1 m	After 15 s	0.46
33	2.0	0.08	upwards, 1 m	After 7.5 s	0.46
34	2.0	0.1	downwards, 1 m	After 15 s	0.55

[1)] Calculated values

3.4 Results and discussion

In general, most of the experiments reported here were performed with a nozzle diameter of 9 mm. The time of ignition were varied from 7.5 s to 30 s, although the major part of the experiments was ignited at 15 s. The direction of the nozzle was primarily downwards, but the experiment series contained both upwards and downwards directed discharges. 13 experiments performed with the 9 mm nozzle and 4 experiments with the 5 mm nozzle are documented here. Not all reported experiments yielded high quality pressure recordings from all the 5 pressure transducers (P1-P5). As expected, the explosion overpressures increased as the initial storage tank pressure were increased. A complete test matrix with comments are found in Appendix 3.

The results are presented in four topics; nozzle size and direction, initial tank pressure, time of ignition and effect of obstructions. Apart from the section related to nozzle size, the results presented here are related to the 9 mm nozzle size only.

3.4.1 Nozzle configuration

Four experiments with the 5 mm nozzle were successfully performed. The time of ignition varied from 7.5 s to 30 s. All the experiments with the 5 mm nozzle were performed in an empty container. The maximum explosion pressures were quite low, in the order of 2-4 kPa. Figure 3.12 shows a comparison of the 4 experiments. The figure presents the pressure records from P1, the pressure transducer placed closest to the solid end wall. The time in experiments 31, 32 and 33 have been adjusted according to experiment 34, to enable direct comparison of the data. The experiments were manually triggered; hence the experiments do not share the same zero. The results are filtered

with a moving average of 10 (i.e. window size = 10, MATLAB filter function), to reduce the level of noise.

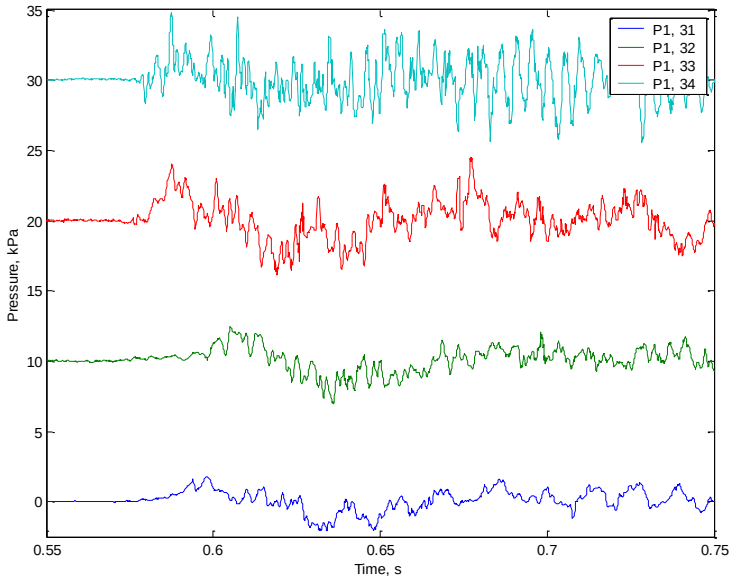

Tank pressure	Nozzle dir.	Time of ignition
2.0 MPa	Down	15 s
2.0 MPa	Up	7.5 s
2.0 MPa	Up	15 s
2.0 MPa	Up	30 s

Figure 3.12 Pressure records from the P1 transducer, experiments 31, 32, 33 and 34 (5 mm nozzle). The different experiments are separated with an offset of 10 kPa. The table on the right summarizes experimental details.

The 5 mm nozzle experimental results are quite similar with respect to explosion characteristics. After a short build-up, the transducer records a first maximum peak. The pressure then decreases, starting a series of oscillations. The oscillating periods are in the order of 1.5 to 2.7 ms, and is quite consistent during the explosions. The other pressure transducers did not record higher maximum explosion pressures. In three of the experiments treated here, the pneumatic valve was closed as soon as the gas ignited. The remaining storage tank pressure were approximately 1000 kPa, meaning a lower level of hydrogen contributed to the explosion. This were the case for experiments 32, 33 and 34.

The results from the experiments with the 5 mm nozzle show that the explosion pressure is relatively low in this geometry. The pressure records are quite similar, even though the release times are different. In a closed container, and with ideal conditions, the mass of released hydrogen would be different due to the difference in the release times. Flow rate calculations imply cumulative mass of hydrogen to be 0.1 kg in the 7.5 s experiment (33), 0.19 kg for the two 15 s experiments (32 and 34) and 0.3 kg for the 30 s experiment (31). Assuming 100 % of the released hydrogen would contribute to the explosions, the explosion pressures would also be different. In the current experimental setup, this indicate that the gas cloud formed in the container have been vented out of the container during the release. As the two doors were open, the ventilation of the container was relatively good. Any release of hydrogen on the outside of the container prior to the ignition has not been detected in the high-speed films for these experiments.

Experiment 30 were the only 9 mm experiment performed with the discharge directed in the upwards direction. The forces acting on the steel pipe providing the gas were so strong that the pipe moved, therefore affecting the dispersion and mixing process. After the experiment were complete, the pipe was directed upwards at an angle, and the nozzle was almost close to the container roof. Due to lack of comparable data from experiments with the 9 mm nozzle, this topic will not be discussed further.

Experiments 1-5 with low tank pressure (> 1.2 MPa) combined with the smallest nozzle diameter (5 mm) did not ignite at all, nor did they give visible ignition in the high-speed films. In these experiments, the ignition source was located 1.0 m from the container door opening. See Appendix 3 for further details.

The experimental campaign did not include 5 mm experiments with obstructions, and results from the 5 mm experiments will thus not be discussed further.

3.4.2 Initial tank pressure

The effect of initial tank pressure was investigated in experiments 26, 27, 28 and 29, where the 9 mm nozzle were directed downwards and all with comparable times of

ignition (15 s). The initial tank pressures were 0.6 MPa in experiments 28 and 29, 1.2 MPa in experiment 27 and 2.4 MPa in experiment 26.

In test 27 a vibrating sound was heard as the explosion propagated. The test recorded a maximum pressure of 2 kPa, and the pressure slowly decreased in a time span of 1.8 s. The high-speed film from this test show flames coming out of the container. The container roof oscillated to some extent.

In test 28 the gas did not ignite, probably due to too low hydrogen gas concentration close to the ignition source. In test 29, the gas ignited after approximately 16 s, after 1 s of continuous ignition. The pressure records from the experiments with an initial tank pressure of 0.6 MPa show no clear pressure peaks, but a continuous pressure oscillation of ±0.5 kPa. High-speed films from experiment 29 show a small blurred gas cloud and a small movement in the container floor. During the experiments, it became clear that the 0.6 MPa tank pressure were the limiting case for successful ignition in this geometry.

Test 26 show a pressure rise from 0 to 2 kPa in a period of 70 ms. The first pressure peak has a maximum of 6.5 kPa, and the global maximum pressure is 14 kPa. The high-speed film from this test show flames coming out of the container, and a significant lift of the container roof. In this experiment, three Leca® Blocks (i.e. Weber expanded clay lightweight aggregates) were placed outside of the container in the longitudinal centreline, 2, 4 and 6 m from the container opening, respectively. The explosion pressure from this experiment was sufficient to topple all the blocks.

Figure 3.13 shows a comparison of pressure recordings from monitor P1 between the cases where the initial tank pressure was varied from 0.6 MPa, 1.2 MPa, to 2.4 MPa (test 29, 27 and 26 respectively). It is clear that the experiment with the highest tank pressure also provide the highest explosion pressure. This can be due to the mass of hydrogen involved in the different experiments, as well as different levels of mixing. The far-field pressure sensors detected a pressure pulse in experiment 26 only.

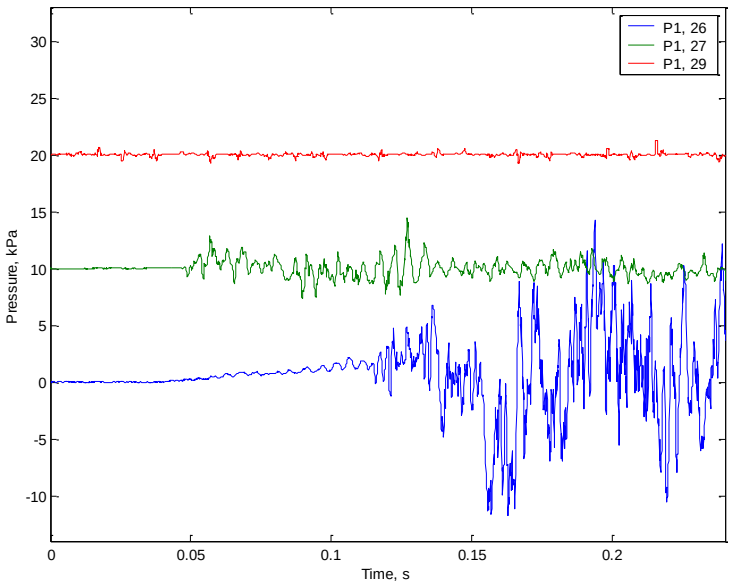

Tank pressure	Nozzle dir.	Time of ignition
0.6 MPa	Down	Ca. 16 s
1.2 MPa	Down	15 s
2.4 MPa	Down	15 s

Figure 3.13 Pressure records of monitor P1, experiment 26, 27 and 29. The time of ignition was 15 s. The different experiments are separated with an offset of 10 kPa.

Experiment 35 and 36 were ignited after 7.5 s, with an initial tank pressure of 2.0 MPa and 2.4 MPa, respectively. The high-speed films show that these explosions were fairly strong. The explosions were visible outside the container due to movement of dust on the ground. Figure 3.14 shows a comparison of the pressure recordings from monitor P1 from experiment 35 and 36, with an offset of 10 kPa. The pressure records show a close correlation, where the pressure build-up and overall trend in the beginning of the explosions are quite similar. In monitor P1, the maximum pressures are 8.0 kPa in both test 35 and 36. In monitors P2 and P3 the results show a similar trend. The far field pressure monitors (P4 and P5) did not record any pressure readings higher than 0.5 kPa in these two experiments.

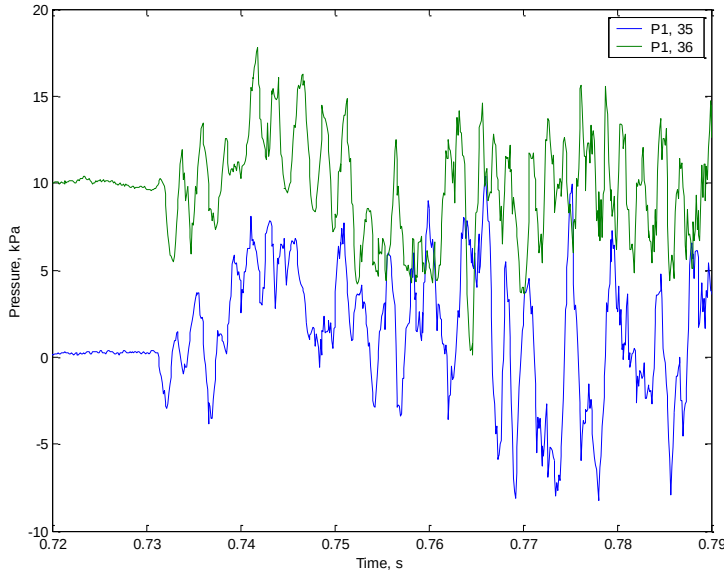

Tank pressure	Nozzle dir.	Time of ignition
2.4 MPa	Down	7.5 s
2.0 MPa	Down	7.5 s

Figure 3.14 Pressure records of monitor P1, experiments 35 and 36. The results are separated with an offset of 10 kPa.

The results show that the explosion overpressures are relatively low, despite the relatively large scale of the experiments. One probable reason for the low explosion pressures could be the fact that the container was without any obstacles for the majority of the experiments. Prior to ignition, some of the hydrogen in the gas cloud could therefore be vented outside unhindered, in addition to a lower degree of turbulence and resulting pressure build-up in the explosion phase. Rai et al. (2014) presented experimental work on hydrogen gas releases in a similar shape as the ISO container, where the same effect was seen.

3.4.3 Time of ignition

The time of ignition was varied throughout the experimental matrix. This section presents results and discussions related to this.

Experiments 24, 25 and 35 were all done with an initial tank pressure of 2.0 MPa. The difference in the time of ignition were as follows; 7.5 s for experiment 35, 15 s for

experiment 24 and 10 s for experiment 35. The maximum overpressure in experiments 24 and 25 were measured between 4 and 6 kPa, as for experiment 35 a maximum overpressure of 20 kPa was recorded. The pressure recordings in these experiments are quite similar, and show the same level of oscillations. Figure 3.15 shows the pressure records in monitor P1 from experiments 24, 25 and 35 (separated with an offset of 20 kPa). As expected, the results show that the later the gas cloud is ignited, the higher is the maximum explosion pressure. However, the relatively similar explosion pressures in experiments 25 and 35 may be explained by the small difference in time of ignition; after 10 s and 7.5 s, respectively. As the initial tank pressure is fairly high, there is a possibility that an amount of hydrogen gas had escaped the container prior to ignition, due to high impulse and a high degree of turbulence.

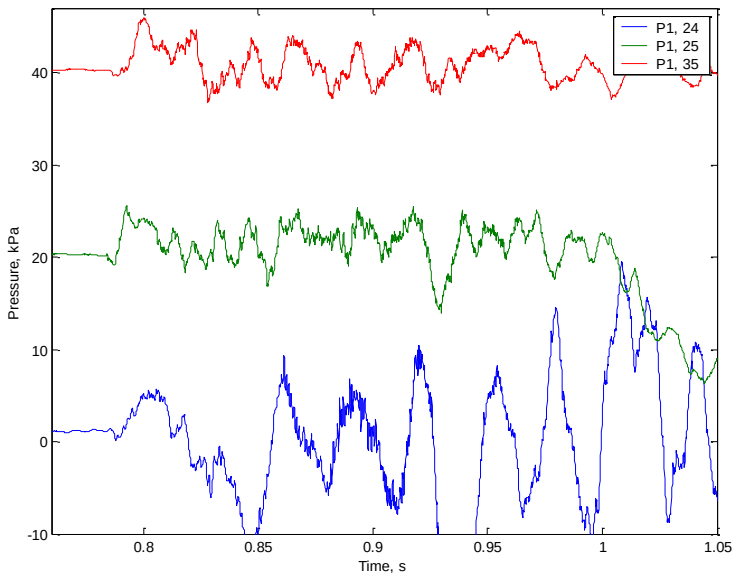

Tank pressure	Nozzle dir.	Time of ignition
2.0 MPa	Down	7.5 s
2.0 MPa	Up	7.5 s
2.0 MPa	Up	15 s

Figure 3.15. Pressure records of monitor P1, experiments 24, 25 and 35. The results are separated with an offset of 20 kPa.

A similar comparison has been done for two experiments with an initial tank pressure of 2.4 kPa. From comparing experiments 36 and 37 the results show that the time of ignition do affect the explosion pressure. The recorded measured pressures are higher

in test 37, as the time of ignition; and also probably the amount of flammable gas, is higher than in test 36. The comparison is visualized in Figure 3.16, which shows the pressure records from pressure transducer P1. The first pressure peaks in experiments 36 and 37 have maximum at 4 kPa and 8 kPa, respectively.

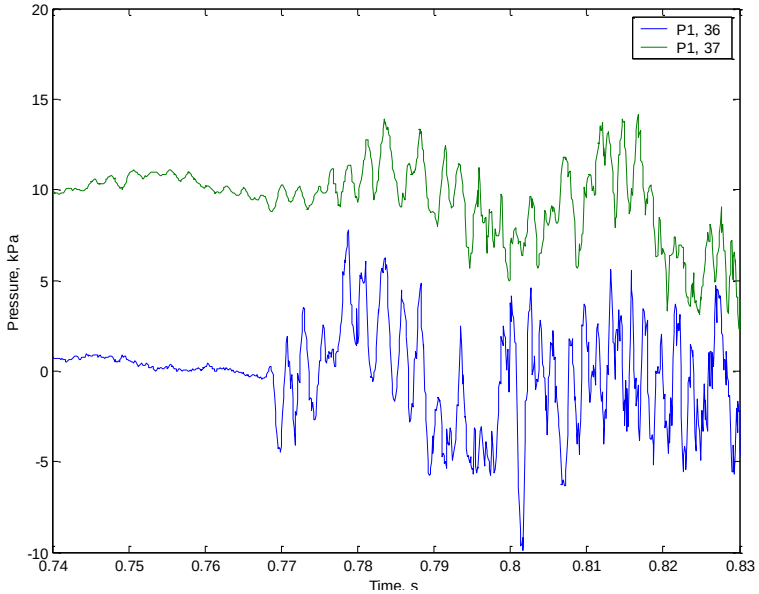

Figure 3.16 First pressure peaks in monitor P1, experiments 36 and 37 (offset 10 kPa).

3.4.4 Effect of obstructions

Obstacles can have a strong influence on a gas explosion. In this section, this phenomenon is briefly explained theoretically, before presenting the experimental results.

In a gas explosion, the laminar flame will normally accelerate and transit into a turbulent deflagration if there are obstructions present. The flow field ahead of the flame becomes turbulent, due to the interaction of the flow field with the obstructions (equipment, piping or other structures). The expansion of the combustion products causes the unburnt gas to be pushed ahead of the flame and a turbulent flow field can be generated in the wake of the obstacles. When the flame propagates into a turbulent flow field the burning rate increases. The mechanisms causing the increased burning rate are the wrinkling of the flame front by large eddies and the turbulent transport of

heat and mass at the reaction front, as discussed in Bjerketvedt et al. (1997). Flame acceleration due to obstacles entails a strong positive feed-back loop.

In an accident situation, it is important to avoid strong flame acceleration of deflagrations that may cause a transition from deflagration to detonation (DDT). The topic of deflagrations and DDT in obstructed channels has been investigated extensively. A detailed study, based on experiments performed at Raufoss in the early 1980s can be found in Lee and Moen (1980).

The effect of obstructions in the explosions have been studied by comparing the explosion pressures from experiments 26, 38 and 39. These three experiments had the same initial storage tank pressure of 2.4 MPa, but with different levels of obstructions. Test 26 had no obstructions, 38 had 2 Euro pallets and 39 had 8 Euro pallets.

Experiment 26
In experiment 26 the first pressure peak was in the order of 5 kPa inside the container, and rose to 12 kPa in the second peak. The far-field side-on pressure was 2 kPa. The high-speed film from experiment 26 shows that the container roof and walls responded to the pressure build-up, and started to oscillate. The container itself moved slightly, both upwards in the open end as well as in the longitudinal direction opposite of the door. The pressure records from this experiment are discussed further at the end of this section, where 3 experiments are compared.

Experiment 38
In experiment 38, two standard wooden Euro Pallets, with dimensions 0.8 m by 1.2 m and a height of 0.12 m, were suspended 0.4 m from the container roof to generate turbulence during the explosion. This turbulence is mainly caused by the interaction of the flow with the obstacles. The increase in turbulence contributes to an increase in the overall burning rate, therefore creating a more violent explosion compared to an empty container. The distribution of the obstacles is shown in Figure 3.19.

The explosion was significantly stronger than the previous experiments. Pressure records from this test are shown in Figure 3.17 where the five pressure transducers are

plotted with an offset of 20 kPa. The maximum pressures were 20 kPa in P1, 11 kPa in P2, and 29 kPa in P3, all measured in the first peaks. The far-field sensors P4 and P5 recorded 2.5 kPa pressure maximums. It is interesting to note that the highest pressure was recorded in P3, which were placed in the middle of the container lengthwise, and close to the roof. The innermost transducer, P1, recorded a much lower pressure. This can be explained by the location of P3 closer to the obstructions compared with P1, leading to a pressure build-up at P3. As the figure shows, the pressure decreases after the first peak, in a series of oscillations. The pressure then increases, after 240 ms.

The second pressure peak, not pictured here, were in the order of 10 kPa in P3, followed by two smaller pressure peaks successively. The high-speed film from experiment 38 show the roof lifting approximately 0.34 m as the pressure built up, based on pixel measurements. A flame ball came out of the container during this period. After this first shock, a flame tongue exited through the container opening, and reached more than 6 m shown in Figure 3.18. The container was lifted to some extent. The two longest walls were bent outwards by the forces involved in the explosion, and left permanent deformations along the full length of the steel wall plates.

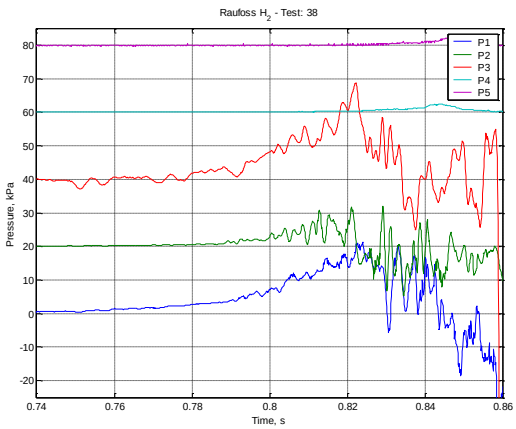

Figure 3.17 Pressure records from test 38, with 5 pressure transducers. The offset is 20 kPa.

Figure 3.18 Flames in experiment 38, image from high-speed film.

Experiment 39

In experiment 39, eight Euro pallets were placed inside the container to generate turbulence in the explosion. Four pallets were suspended 0.4 m from the ceiling, spaced apart with ca. 1 m between. The last four pallets were distributed on the floor, in a staggered pattern. The distribution is shown in Figure 3.20 (Appendix 4 contains drawing with detailed measurements). The nozzle was directed vertically downwards 0.2 m above one of the obstacles, ensuring that the hydrogen would disperse violently.

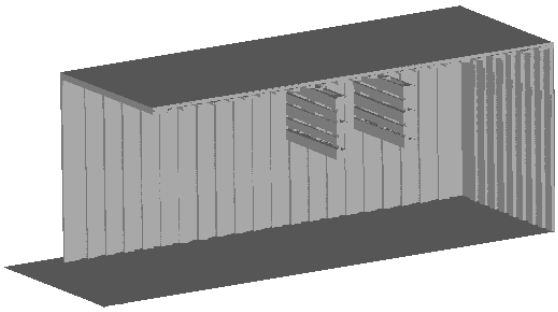

Figure 3.19 Distribution of obstacles in experiment 38.

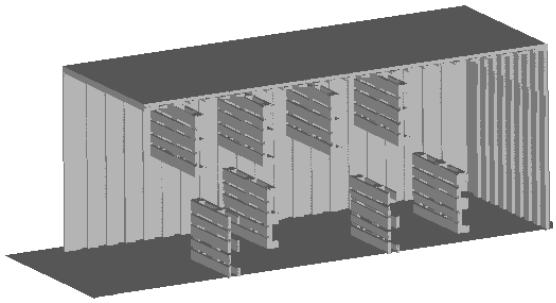

Figure 3.20 Distribution of obstacles in experiment 39.

During this experiment, the container lifted approximately 0.5 m off the ground, as shown in Figure 3.21.

Figure 3.21 Image series of Experiment 39, captured by the Photron FASTCAM-APX 120KC colour high-speed camera. The images were captured with a frame rate of 500 fps; the time between the middle frame and the right frame is 36 ms.

The lifting caused the pressure sensors located inside of the container to fail. The overpressure at the origin of the explosion is unknown. The first peak from monitor P1 was recorded though, and shows a maximum pressure of 49 kPa. The two pressure transducers located outside of the container, P4 and P5, gave pressure records as shown in Figure 3.22. These two transducers located 6.5 and 8.7 meters from the container door. In the case of P4, the maximum pressure in the first peak were 16 kPa, with a rise time of 0.1 ms. The pressure then decreased to 10 kPa over a period of 1.1 ms, before the explosion generated a second pressure peak with a maximum of 24 kPa. Pressure transducer P5 recorded two peaks, similar to P4. Here the peak pressures were approximately 14 kPa at both peaks. The time of arrival of the shock wave between the first peaks in P4 and P5 were approximately 3 ms.

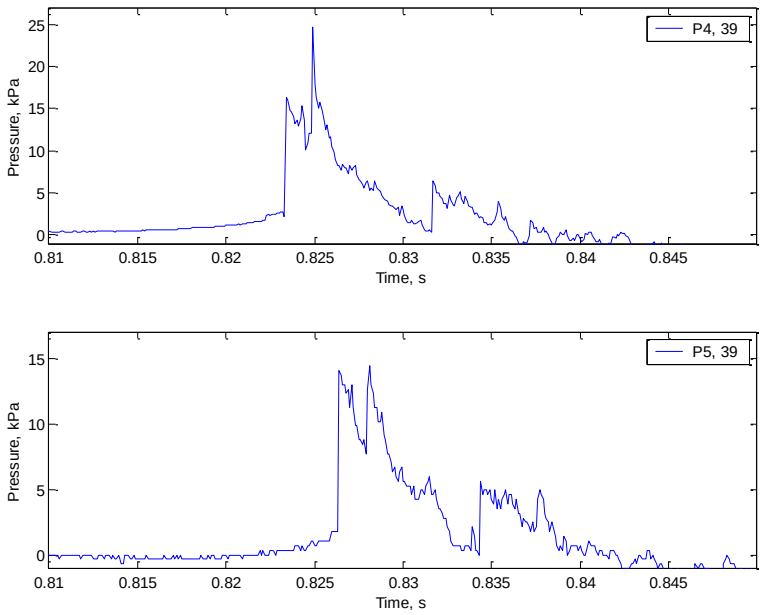

Figure 3.22 Pressure records from experiment 39. Pressure sensor P4 and P5 were mounted outside the container, 6.5 and 8.7 meters from the container doors.

The high-speed film from experiment 39 show a violent explosion. The container walls and roof were deformed, and the stronger support beams running along the corners of the container were bent during the explosion. The curvature on the back end wall were at a maximum when the flame and explosion products become visible on the outside of

the container. The welded seams along the roof and end wall were ruptured, allowing burnt gas to escape. Some of the wooden floor panels were lifted upwards and broken due to the explosion. Figure 3.23 shows the explosion in four different time steps. The trigger system involved in the pressure measurements and the trigger of the high-speed camera did not have a common zero. The first frame in the high-speed films are therefore undefined, with respect to the time of ignition and pressure build-up. The figure shows the frames 460, 500, 570 and 760, corresponding to a time of 153 ms, 166 ms, 190 ms and 253 ms, respectively (counted from the first frame). Figure 3.23 visualize the deformation of the container, as well as the movement of the pallets used as obstructions in the explosion. Typical values of the fragments' velocities were 20-70 m/s, or 72-250 km/h. The shock wave in experiment 39 is further investigated in Chapter 4, where the shock wave is treated by evaluating the high-speed films.

Figure 3.23 High-speed images from experiment 39, at time steps 153, 166, 190 and 253 ms, counted from camera trigger time.

Figure 3.24 shows the pressure records from monitor P1 for experiments 26, 38 and 39. The time vectors have been adjusted to match the first peaks in each experiment. The P1 pressure transducer in experiment 39 failed later, and the results from this experiment are therefore uncertain. The figure shows comparable initial trends in the three experiments. The P1 first peak maximum pressures were 6.5 kPa in experiment 26, 31 kPa in experiment 38 and 49 kPa in experiment 39. Details of the P1 pressure records of experiment 39, where the first local maximum of 49 kPa is shown in Figure 3.25.

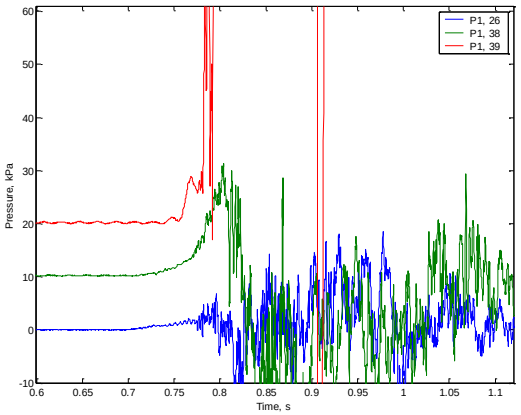

Figure 3.24 Comparison of pressure records from P1 in experiments 26, 38 and 39.

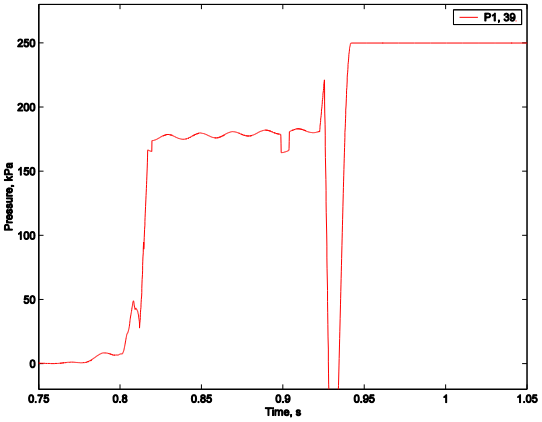

Figure 3.25 Details of P1 pressure records in experiment 39.

The far-field pressures are presented in Figure 3.26 comparing results from the P5 monitor from experiments 26, 38 and 39. The pressure records show a clear pressure peak in test 39, whereas the pressure in both test 26 and 38 are comparatively low. The results from P5 show a decrease in the measured pressure in experiment 26 after the first pressure peak; this may be noise or other kinds of error. There are therefore uncertainties related to the data from P1 in this experiment.

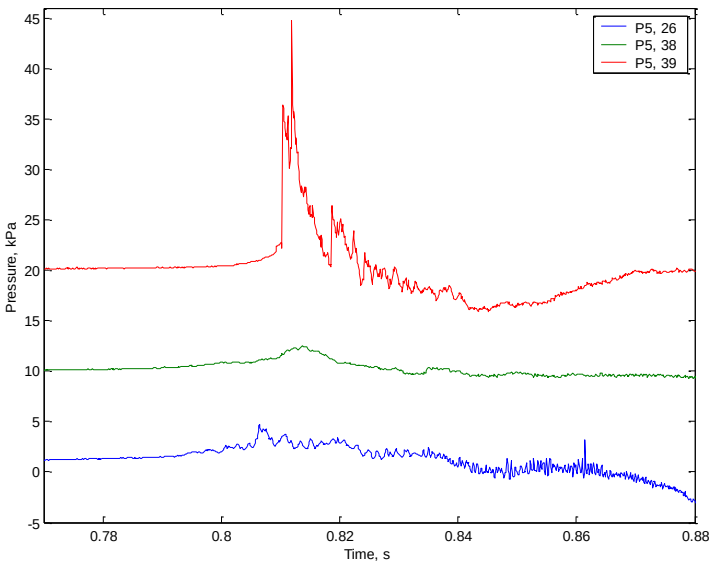

Figure 3.26 Comparison of pressure records from P5 in experiments 26, 38 and 39.

3.4.5 Storage tank pressure data

The storage tank pressure was monitored during each experiment. Figure 3.27 shows the tank pressure (kPa) recorded in experiment 39. Isentropic, ideal gas calculations on the pressure drop in the tank is inserted for comparison. The theory and method of these calculations are presented in Appendix 1. The flow rate calculations show that the calculated transient tank pressure correspond well with the experimental recordings. Calculations presented here were performed with a discharge coefficient, CD = 0.7.

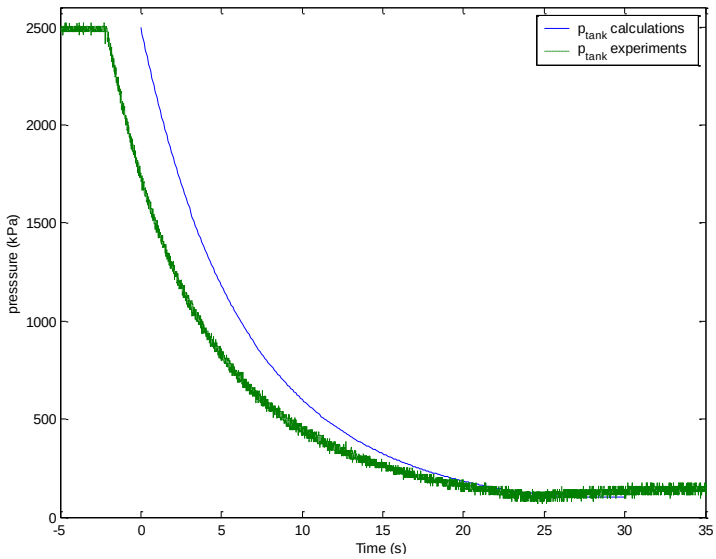

Figure 3.27 Tank pressure comparison of recordings from experiment 39 and calculations. The graphs are offset by 2 s to ensure visibility

The leak rate calculations were used to estimate the total mass of hydrogen released in the experiments. Figure 3.28 shows the calculated cumulative mass flow from experiment 39. As the time of ignition was 15 s in this experiment, the total mass released in the ISO container prior to ignition was approximately 0.5 kg.

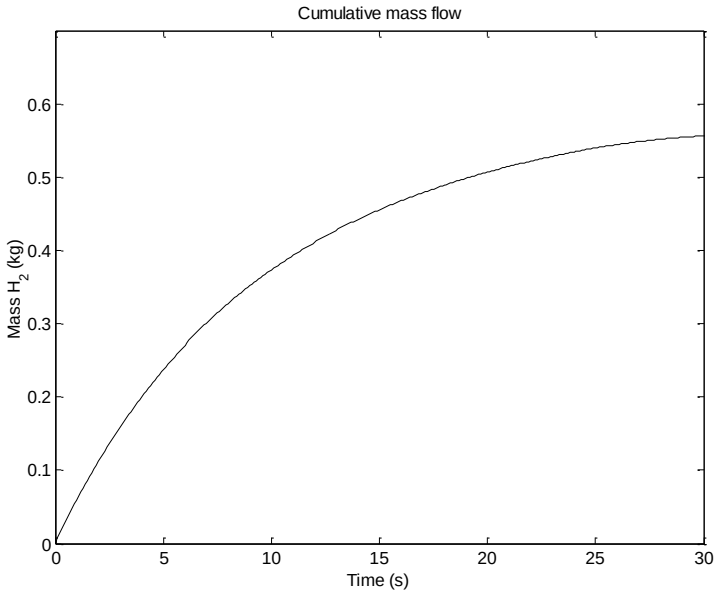

Figure 3.28 Calculated cumulative mass flow, experiment 39. Calculations are described in Appendix 1.

3.5 Conclusions

Field-scale experiments were performed on pressurized releases of hydrogen inside a 6 m long ISO container, having a 2.4 m width and 2.4 m high cross section. The main objectives of these experiments were to obtain pressure and high-speed data from explosions of inhomogeneous hydrogen-air clouds. Test parameter variations included nozzle configuration, jet direction, reservoir back pressure, time of ignition after release and degree of obstacles. The results show that the experiments without obstacles had explosion pressures in the range of 0.4 to 7 kPa, whereas in the experiments with obstacles the gas exploded more violently producing pressures in order of 100 kPa.

In hindsight it becomes clear, when evaluating the relatively careful start of the test series, that there were uncertainties related to the magnitude of the explosion overpressures that could be expected.

The experiments sought to produce scenarios that could give further insight to factors that could explain overpressures experienced in the N1 accident. Evidently, hydrogen gas explosions in the same geometry may be very different in terms of explosion overpressures and combustion phenomena. As proven in these experiments, a relatively small amount of hydrogen can either generate an explosion with significant overpressures, or low-pressure combustion of gas. As the hydrogen gas easily vents out to open air, none of the parameters initial tank pressures or time of ignition gave new insight to which factors might have contributed to the chain of events in the N1 accident. The experiments show two key parameters that determine the strength of the hydrogen gas explosion; the nature of the dispersion and the degree of obstructions. The effect of obstructions in the explosion is significant when comparing overpressures in experiment 26 and experiment 38. These two experiments differed only by two pallets in the geometry.

Experiment 39 was even more violent, and differs from experiments 26 and 38 in the number of obstructions, but also in the way the dispersion was influenced, as the jet was impinged directly on a pallet. The contribution of each of these two main factors

cannot be quantified, but the effect of the pallet directly downstream of the nozzle is believed to play a significant role. This finding is supported by the CFD simulations presented in Chapter 5.

4 Shock wave investigations

4.1 Introduction

This chapter describes the application of a flow visualization technique of density gradients called background-oriented schlieren (BOS). The technique is often used to obtain quantitative measurements of shock waves from explosions by processing high-speed digital video recordings. After a short introduction, the image processing technique is presented. The last part of the subsection describes the results and discussion on the topic.

The last hydrogen experiment in the ISO container, experiment no. 39, described in Chapter 3, has been the subject of a more extensive investigation, in order to learn more on the topic of field-scale explosions. The results from this work were presented at the international colloquium on Dynamics of Explosions and Reactive Systems (ICDERS) in 2007, and have been published as an article in the journal Shock Waves (Sommersel et al. 2008). One of the reasons for the in-depth analysis of this test was the violent nature of the explosion, compared to the rest of the experiments. In order to determine more thoroughly the maximum overpressure generated in this explosion, the high-speed films were analysed. The explosion in the experiments generated a shock wave that was visible on the high-speed films. Based on the theory of the background oriented schlieren technique, it was possible to extract pictures of this shock wave propagating from the container opening.

The technique is illustrated by an analysis of two explosions, a high explosive test and the gas explosion experiment, test no. 39. The C-4 high explosives test were originally performed as a calibration method for the pressure sensors (as the blast overpressure to a known mass of high explosives is also a known quantity). The C-4 test was performed with 100 g of C-4 mounted and detonated on a wood pole (set up in front of the container, see Figure 4.2). The C-4 test is used as a control sample of the BOS technique. The last part of the section presents the hydrogen case, where the same method is used to estimate the shock wave overpressures.

4.2 Image processing

Background Oriented Schlieren is described by Klinge et al. (2003) as an optical measurement technique, for visualizing density gradients. The principle is the deviation of light rays that pass through a density gradient, which is well known from the Schlieren and shadowgraph techniques. The deviation is caused by the variation of the refractive index of the transparent media (i.e. air) (Venkatakrishnan and Meier, 2004). The common steps of the method are imaging of a background through a flow of interest, and then performing software analysis that manipulates the data to find the density gradients. In its simplest form, BOS makes use of simple background patterns of the form of a randomly generated dot-pattern. The size of the pattern should ideally be optimized according to the magnification of the set-up. In the ISO container experiment no. 39, the background was a forest (i.e. a row of spruce trees). The technique could probably be improved by using a random dot pattern, but would be impractical due to scale of the experiment. The visualized shock surface is not always visible along its entire contour, and present gaps as shown in the right-hand image of Figure 4.1. These gaps are caused by the absence of background, as the shock front propagates higher than the trees, especially in the right-hand side of the images.

Figure 4.1 Principle of the image processing: Subtraction of an undistorted image (middle image) from a distorted image (left image) yields the result shown in the right image

As illustrated in Figure 4.1, the image processing technique entails subtracting an undistorted image from a distorted image. The resulting image was then manipulated

by a logarithmic intensity transformation. The positions of the shock front were read from the resulting image manually. If the shock surface was thicker than one pixel, the position was defined at the outermost pixel. The shock front gaps mentioned above did not affect the analysis, because of the manual procedure. The time vector used in the calculations were the logarithm of the product of sound speed in air and the time extracted from the high-speed movie, made by the basis of frames pr. sec in the high-speed movie, as there was one shock wave reading for each frame (time step). The distance vector was also logarithmic. The time and distance data set were curve-fitted using both a 3- and a 4-degree polynomial (the polyfit.m function in MATLAB). Calculations with polynomials of higher degrees had large oscillations, and could not present the data correctly. The data were used to calculate the shock front velocity, hence the shock Mach number. The predicted shock front pressures were calculated from the Mach number using the relation defined in Wilcox (2003)

$$\frac{\Delta p}{p_0} = \left(\frac{2\gamma}{\gamma + 1}\right)(M^2 - 1) \qquad 5.1$$

where Δp denotes the pressure difference between the pressure in the undisturbed fluid p_0 and the pressure lying behind the shock, the Mach number is M and the specific heat ratio (C_p/C_v) is denoted γ. In these calculations γ is assumed to be 1.4. In Appendix 1 normal shock waves are treated in more detail.

The numerical algorithms were developed in MATLAB for the image processing and pressure calculations. The code also generated videos from the manipulated images.

4.3 Results and discussion

Figure 4.2 Manipulated image from the C-4 test.

A manipulated image of the C-4 test is shown in Figure 4.2. Figure 4.3 shows the predicted shock front pressures from the C-4 test compared with a pressure-distance curve based on the Kingery and Bulmash free air burst TNT curve, found in Lees (1996). This curve is based on TNT data, so to compare with the C-4 experiment, the curve needed to be corrected to a C-4 equivalent. According to UFC (1997), the factor for a C-4 to TNT equivalence conversion is 1.2 at this pressure, hence 100 g C-4 equals 120 g TNT, shown as the solid line in Figure 4.3.

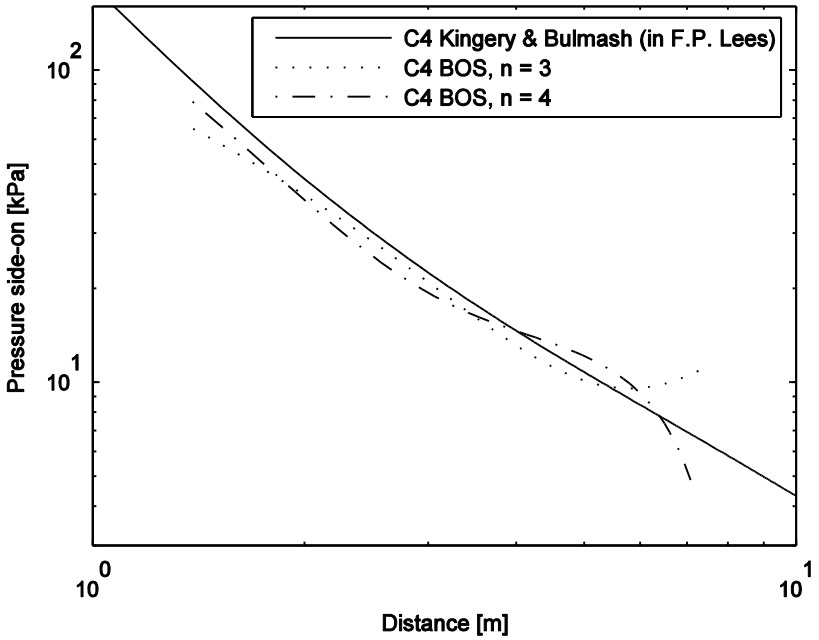

Figure 4.3 Predicted shock front pressures from the C-4 test. Third and fourth degree polynomial from experiments compared with the Kingery & Bulmash theoretical TNT curve, Lees (1996).

The length scale is based on the number of pixels in the BOS movie, corrected by the known length of the container, yielding a factor of 24.43 pixels/m. This factor is an important parameter, as to get the length scales defined correctly. Figure 4.3 shows good agreement between the corrected C-4 curve and the experimental data. The end points of the experimental curves are deviating from the theoretical curve. This is caused by the polynomial curve fitting. Calculations with polynomials of higher degrees had large oscillations, and could not present the data correctly. Even though the predicted shock front pressures deviate in the end points of the data set, the average value is following the Kingery and Bulmash curve quite well. The result shows that it is possible to estimate shock front pressures from a high explosive detonation by using a high-speed digital video recording of the event.

The highspeed movie from experiment no. 39 was treated in the same manner as with the C-4 experiment. Figure 4.4 shows one of the manipulated images from the hydrogen gas explosion test. From the manipulated images two sets of shock trajectories have been extracted along the vertical and horizontal axes. The upper left corner of the

container was defined as a known reference point. The highspeed movie treated with the BOS technique clearly show that the shock wave propagates from the origin of the axes in Figure 4.4. In this experiment, a flame propagates from inside of the container and a vortex is generated at the upper part of the door opening. This is probably excess hydrogen that is burnt on the outside of the container. The vortex rotates and is shown as a white, almost spherical flame ball in Figure 4.4. The centre of this cloud also defines the centre from where the shock wave propagates. The transient development of the shock front in experiment 39 was initially read manually using a projector and a whiteboard, as shown in Figure 4.5. Detailed pixel reading was later performed using the Photron Fastcam Viewer software, PFV (2015).

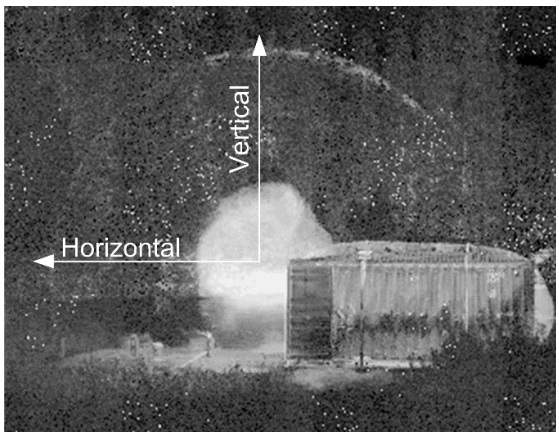

Figure 4.4 Manipulated image from the hydrogen gas explosion test with defined axes.

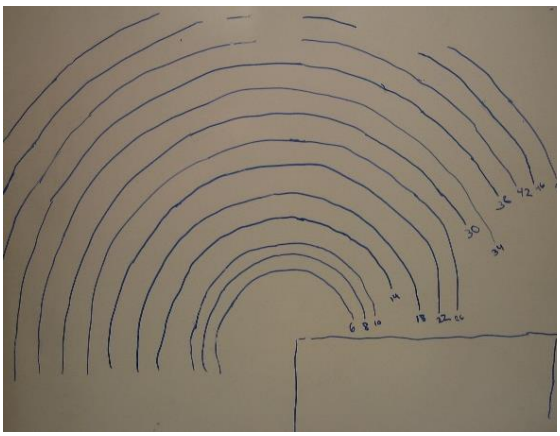

Figure 4.5 Image from manual reading of shock front development in experiment 39 using a projector and a whiteboard. Numbers indicate the timestep in the high- speed video.

Figure 4.6 shows the trajectories in a time-distance diagram for the shock front propagation along the vertical and horizontal axes. The figure also shows the time-distance results for the second shock wave, read along the vertical direction. The data from the hydrogen gas explosion test were treated in the same manner as the C-4 experiment, with the same pressure-Mach number relation (Equation 5.1).

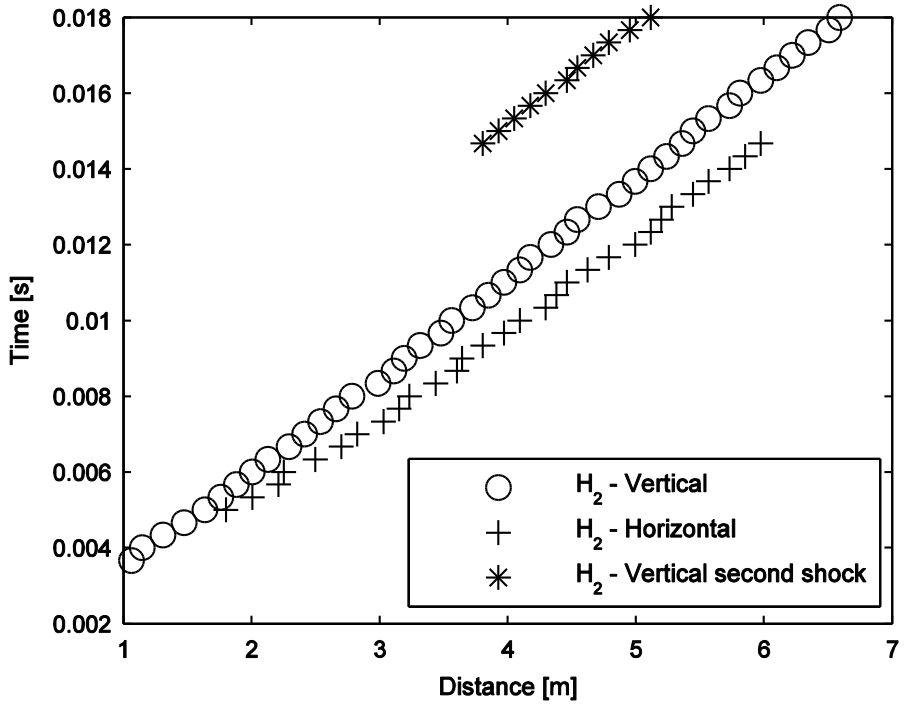

Figure 4.6 Shock propagation in the hydrogen gas explosion test along the axes defined in Figure 4.4.

The estimated shock front pressure versus time can be found in Figure 4.7. The shock in the horizontal direction propagates at a higher velocity than in the vertical direction. CFD simulations with the FLACS code (FLACS 2008) indicated that the flow velocity ahead of the shock cannot explain the differences in horizontal and vertical shock velocities. The details on the numerical work are discussed in Chapter 5.3.4. The asymmetrical shock is expected to be a result of the reflection off ground and the momentum in horizontal direction of the jet from the explosion inside the container and possibly also the external explosion. The asymmetrical shock phenomena have been investigated among others by Forcier and Zalosh (2000), Chiu et al. (1977) and Harrison and Eyre (1987).

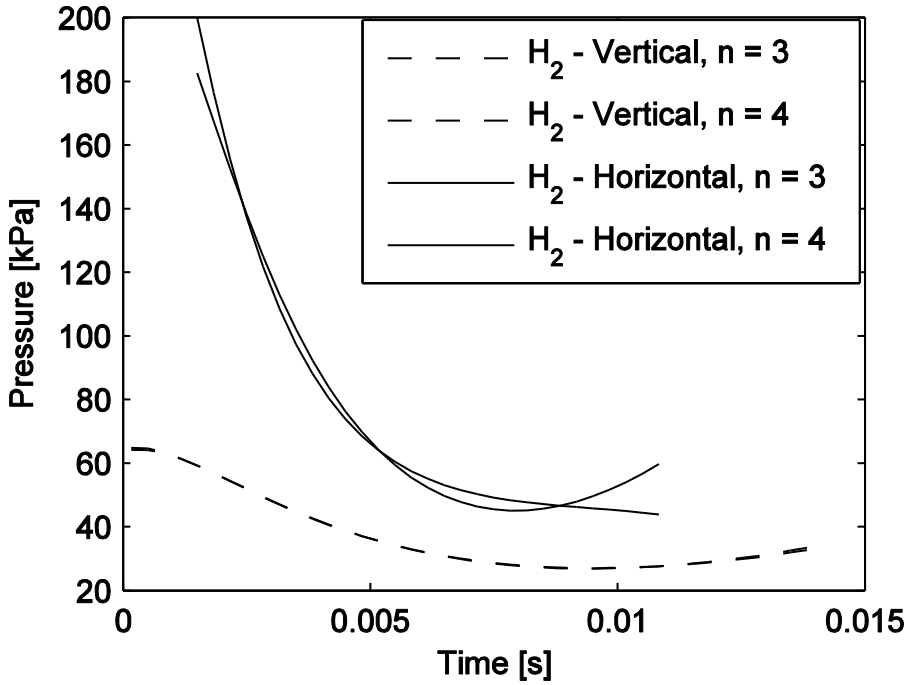

Figure 4.7 Estimated shock front pressure vs. time for experiment 39.

It is interesting to note that on the manipulated video several shock waves follow the first shock wave. Figure 4.8 shows an image of the manipulated video where the first shock wave is followed by a second shock. The second shock wave is harder to recognize, and appears only in the late half of the movie.

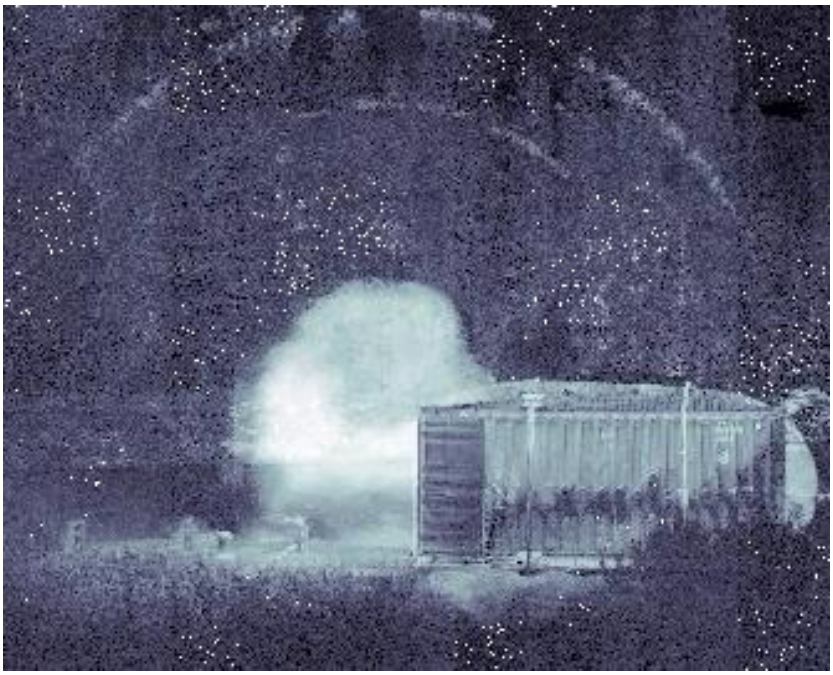

Figure 4.8 A second shock wave following the first shock. Manipulated image from the high-speed movie of experiment 39.

Figure 4.9 shows the estimated shock front pressure versus distance. FLACS simulations (see Chapter 5.3.4) and experimental pressure records from P4 and P5 are also shown in the figure. In the FLACS simulations a homogeneous 20% hydrogen-air gas cloud were assumed to fill the upper half of the container volume.

The estimated shock front pressures in the horizontal direction is relatively linear in the log-log diagram, up a distance of around 5 m from the defined origin. Inaccuracy or difficulty in the manual reading of the shock front can explain the divergence at longer distances. The shock is not visible in the high-speed film close to the origin, leaving an opening in the data set.

The estimated shock front pressures seem reasonable compared with the FLACS simulations (presented in 5.3.4) and the experimental pressure measurements. Relevant uncertainties of the method are related to the manual readings of the shock front, the calibration of a known distance and the defined origin of the explosion.

However, the results from this technique indicate that the maximum overpressure in experiment 39 was at least 200 kPa.

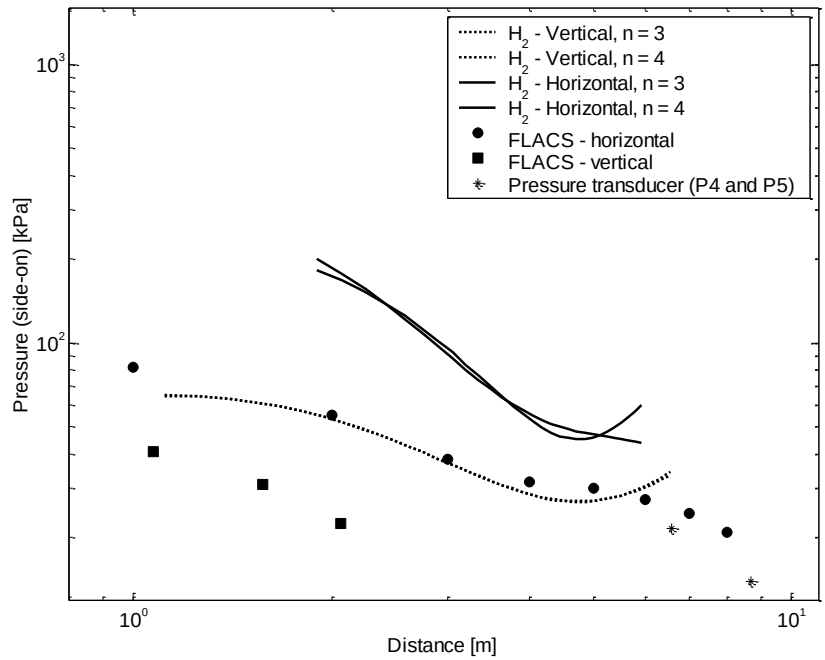

Figure 4.9 Estimated shock front pressure vs. distance for experiment 39.

4.4 Conclusions

The use of the BOS technique is proven to be useful for estimating explosion overpressures from high explosives and gas explosions. One example of use is the work by Mizukaki et al. (2015).

For high explosives, the method agreed quite well with a standard curve for side-on shock pressures. For the gas explosion, it was found that the shock wave propagated faster in the horizontal direction than in the vertical direction. Clear observations were made of the fact that the first shock wave was followed by several other shock waves.

The results obtained by this technique gives reason to believe that the maximum explosion overpressure in experiment 39 was at least 200 kPa.

5 Numerical simulations, ISO container

This chapter describes the numerical simulations with FLACS of the experiments performed in the ISO container, discussed in Chapter 3. The experiments involved hydrogen gas dispersion and ignition at the NDEA test facility at Raufoss, Norway. The results consisted of pressure records and highspeed films. The same experiments have been simulated in FLACS. One goal was to compare the results from simulations and the experiments in terms of explosion pressures. The simulations have been used to investigate the propagation of the hydrogen gas prior to ignition, along with the ignition of the inhomogeneous gas cloud. This work contains three different parts:

1. A set of dispersion/ignition cases based on the nine most interesting experimental tests.
2. A set of explosion simulations with a homogeneous premixed gas cloud, with comparison to the most violent experiment; experiment 39.
3. Simulations on premixed clouds compared with shock wave propagation from experiment 39, discussed in Chapter 4.

One of the main goals of this thesis has been to study the N1 accident with FLACS. This chapter will make use of the field scale to compare the FLACS simulation results with experimental data obtained in the ISO container. This comparison will be used to study the quality of the FLACS simulations of the N1 accident, presented in Chapter 6.

5.1 General setup for all simulations

The geometry was modelled in a Cartesian grid as similar to the real container as possible. The inner dimensions were x = 6.0 m, y = 2.4 m and z = 2.4 m. The experimental container had walls and roof made of corrugated steel plates with angular trusses, and these were modelled in FLACS to 90-degree angles. The total simulation volume was x = 15.2 m, y = 12.6 m and z = 5.0 m, where the container was placed in the centre. The container doors at one end were open. Figure 5.1 shows the geometry details of the

container, with the roof removed for better visualization. A program within the FLACS package was used to calculate the flow rate and discharge area of the jet. A hydrogen jet was positioned inside the container 1.0 m from the back wall, at a height of 1.0 m above the container floor. The ignition source position was 1.0 m from the solid back wall, and 50 mm below the roof. Pressure monitors P1-P5 were placed at the same positions as in the experiments, presented in Figure 3.2 on page 26.

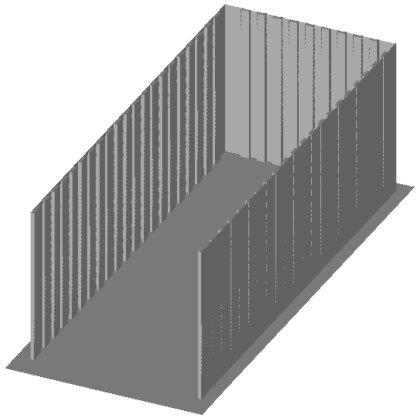

Figure 5.1 ISO container model used in the FLACS simulations.

In the dispersion calculations, the grid was refined to 0.04 m near the jet, along the x- and y-axis, and 0.1 m in the z-direction. The overall grid size inside the container was 0.2 m, and stretched with a stretch factor of 20 % on the outside, yielding a total number of grid cells up to around 350 000 in the dispersion simulations. The explosion simulations were simulated with a uniform grid with 0.2 m grid cells, giving a total of 340 000 grid cells. Here the grid in the z-direction were maintained from the dispersion calculations. After each dispersion simulation, the results were loaded into a new set of files, adjusted to new grid and ignited. The jet continued after ignition, to maintain turbulence levels. Experiments 38 and 39 were performed with ordinary wooden Euro pallets, with dimensions 0.8 m by 1.2 m and a height of 0.12 m. The pallet geometry drawn in FLACS is shown in Figure 5.2.

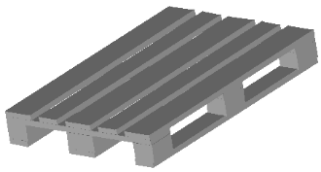

Figure 5.2 Standard Euro pallet used as obstacles in FLACS simulations of experiments 38 and 39.

5.1.1 Geometry details for experiment 38

In experiment 38, two euro pallets were introduced to the geometry to generate turbulence. The pallets were positioned in the middle of the length-wise axis (x), 0.38 meter from the container roof, and 1.8 and 2.8 meter from the closed back end wall, respectively. The distribution of obstacles in experiment 38 is shown in Figure 5.3. The jet was directed downwards, originating from a tank pressure of 2.4 MPa.

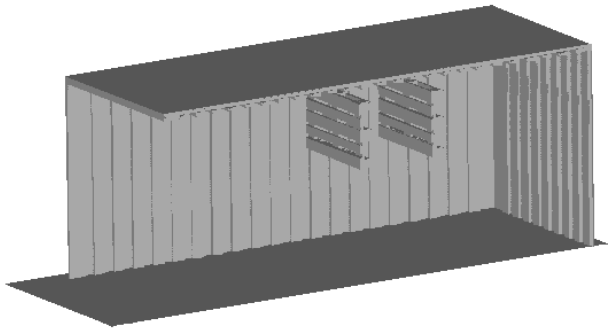

Figure 5.3 Distribution of obstacles in experiment 38.

5.1.2 Geometry details for experiment 39

The eight pallets used as obstructions in experiment 39 were distributed as shown in Figure 5.4. Four pallets were placed on the floor; the first one directly under the nozzle (1.1 m from the back-end wall) and with three pallets positioned on the floor in a staggered pattern. The four remaining pallets were suspended 0.4 m from the ceiling, centred in the container. A detailed sketch of the obstacle distribution is found in Appendix 4.

The jet was directed downwards, originating from a tank pressure of 2.4 MPa. The grid cells in the explosion simulation from this experiment were cubic, with dimensions 0.1 m to ensure the minimum number of control volumes to be 10 along the full length of the gas cloud. Here the thickness of the gas cloud was in the order of 0.5 m prior to ignition.

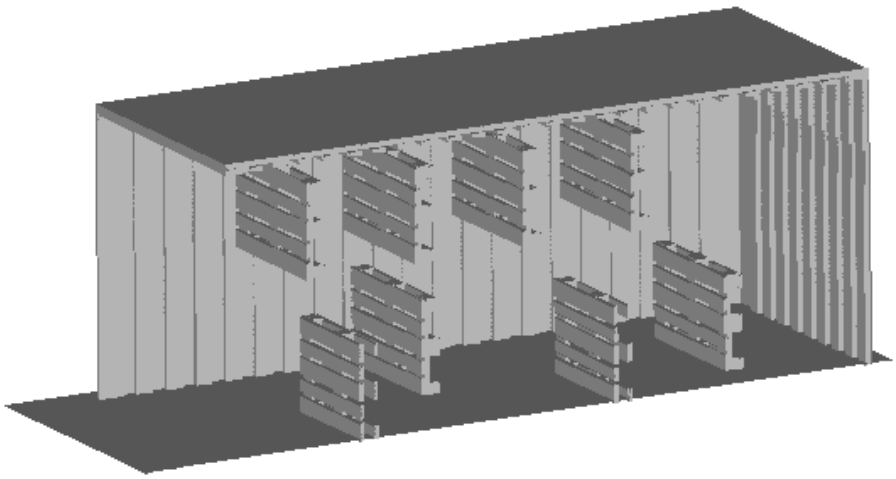

Figure 5.4 Distribution of obstacles in experiment 39.

5.2 Simulation matrix

Table 5.1 summarises the simulated scenarios. Each case was first simulated as a dispersion, and then ignited. Each case has therefore 2 simulations. Base case is experiment no. 30, i.e. 2.0 MPa overpressure inside the tank, with a 9 mm nozzle directed upwards. Furthermore, simulations were performed on experiments 24, 28, 26 and 27. These simulations represent a set of results where the tank pressure varies between 6 and 2.4 MPa, and with different direction of the jet. Experiments 33 and 34 used a 5 mm nozzle.

Table 5.1 FLACS simulation matrix, ISO container experiments.

Case	Exp.	P_{tank}(MPa)	D_{Nozzle} (mm)/ direction	Ignition	Release case	Ignition case
1	38	2.4	9 mm/1m downwards	after 15 s	010309	010310
2	39	2.4	9 mm/1m downwards	after 15 s	010305	010306
3	30	2.0	9 mm/1m upwards	after 15 s	010313	010314
4	24	2.0	9 mm/1m downwards	after 15 s	010315	010316
5	28	0.6	9 mm/1m downwards	after 15 s	010317	010318
6	26	2.4	9 mm/1m downwards	after 15 s	010311	010312
7	27	1.2	9 mm/1m downwards	after 15 s	010319	010320
8	34	2.0	5 mm/1m downwards	after 15 s	010321	010322
9	33	2.0	5 mm/1m upwards	after 7.5 s	010323	010324

5.3 Results and discussion

The results from the numerical simulations on the ISO container are presented here. Simulations on experiment 38, experiment 39 and experiment 26 are presented in different sections throughout the chapter. Simulations on homogeneous gas clouds based on experiment 39 are presented in Chapter 5.3.4. Additional results from FLACS; calculated pressure records for remaining cases (i.e. experiments 30, 24, 28, 27, 34 and 33) are presented in Appendix 2.

Table 5.2 shows the mass of hydrogen that have been released prior to ignition in the dispersion simulations. The values vary between 0.106 and 0.433 kg, represented by experiment 33 and 38, respectively.

Table 5.2 Mass of hydrogen prior to ignition.

Case	Exp.	P_{tank}(MPa)	Mass hydrogen (kg)
1	38	2.4	0.43
2	39	2.4	0.31
3	30	2.0	0.39
4	24	2.0	0.38
5	28	0.6	0.12
6	26	2.4	0.43
7	27	1.2	0.23
8	34	2.0	0.19
9	33	2.0	0.11

5.3.1 Experiment 38

Figure 5.5 shows the development of the experiment no. 38 gas cloud in a series of 2D cut planes in the middle of the container (x-axis), at the jet position for timesteps 0.1 s, 5.0 s, 10.0 s and 15.0 s. The concentration level is represented by colours, where the dark blue is 2 vol. %, the lighter blue is the lowest flammable concentration, 4 vol. %, and up to red which is above 30 vol. % (ref. figure legend). As shown in the upper left figure, the gas hits the container floor almost immediately, and is then diverted to the sides. The pictures show that after 15 seconds the whole container volume is filled with a hydrogen cloud, and also that an amount of gas have escaped the container. At the time of ignition, the hydrogen concentration is above 16 vol. % in the inner part of the container, where the ignition unit is located. The simulations indicate that the mass of hydrogen prior to ignition was 0.43 kg.

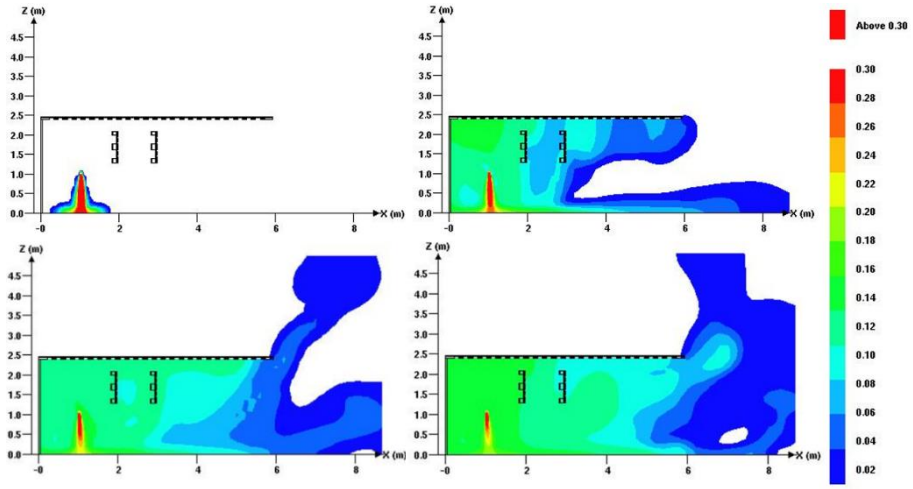

Figure 5.5 Centreline 2D cut plane of FLACS simulation of the hydrogen dispersion in experiment 38. The figure shows the volumetric hydrogen concentration during the release with timesteps 0.1 s, 5.0 s, 10.0 s and 15.0 s.

Figure 5.6 shows a pressure-time diagram from the 5 points, located at the same position as the pressure transducers in the experiments. The figure also contains the experimental pressure records from monitor P1, where the time is adjusted to fit the numerical results. The numerical results show a relative correlation with the

experimental results. However, the maximum pressure of P1 is overpredicted by a factor of 2.

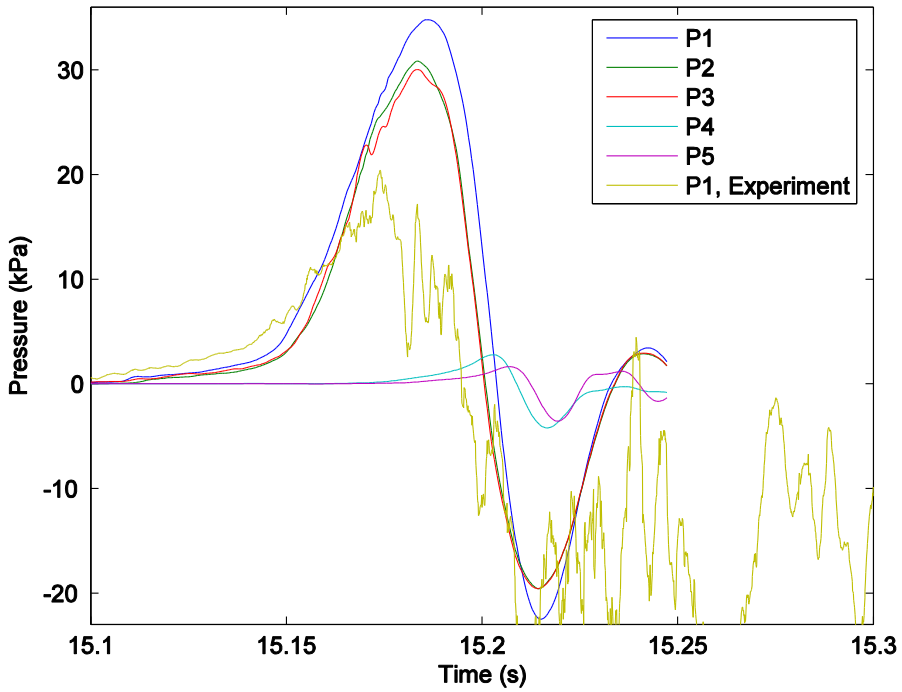

Figure 5.6 Pressure records from FLACS simulation on experiment 38, along with the pressure records from P1 in experiment 38.

5.3.2 Experiment 39

Experiment no. 39 have been studied in several FLACS simulations. The FLACS simulations on homogeneous clouds from this experiment is reported in Chapter 5.3.4. The results from the dispersion simulations on experiment no. 39 is shown as a volume plot in Figure 5.7, where the iso-surface is 8 vol. %, representing the flammable gas cloud. The timesteps used are 0.1 s, 3 s, 6 s, 9 s, 12 s and 15 s, read from top left. The mass of hydrogen prior to ignition was 0.31 kg, leading to the conclusion that an amount of gas had escaped the container as well as the computational domain before ignition.

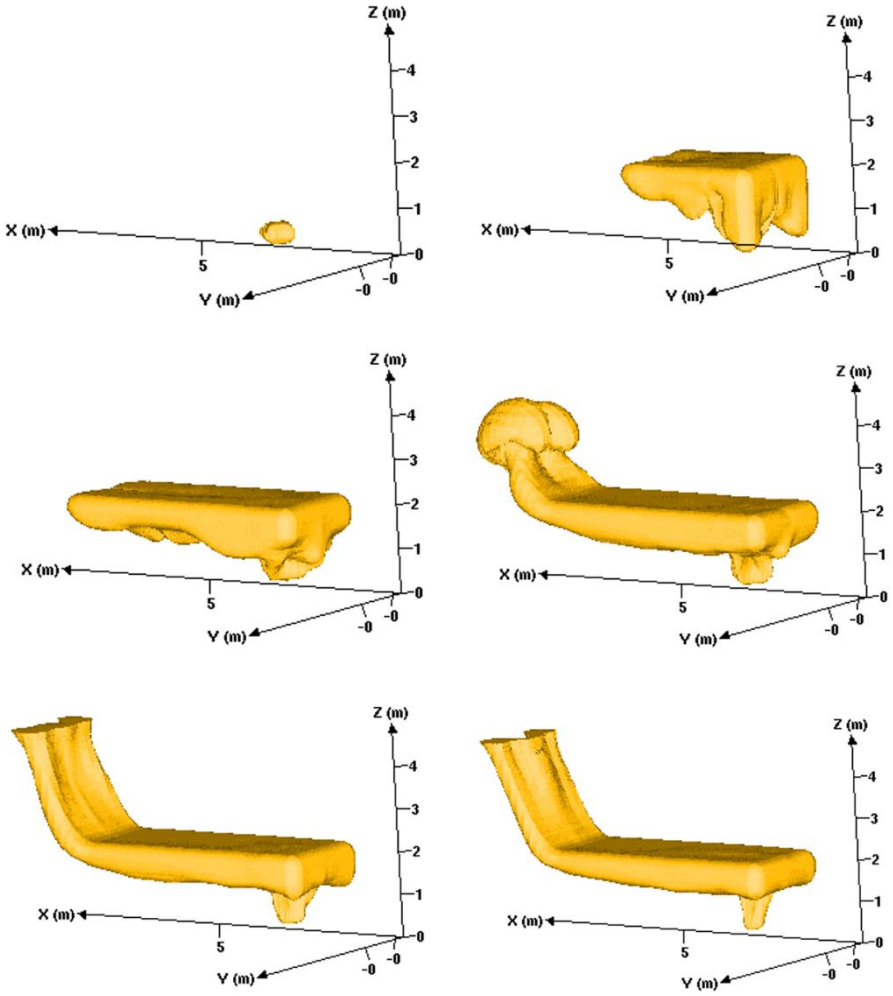

Figure 5.7 3D dispersion results from FLACS for experiment no. 39. The orange colour corresponds to 8 percent hydrogen gas concentration by volume. The timesteps are 0.1 s, 3 s, 6 s, 9 s, 12 s and 15 s, read from the top left image. Geometry removed for visibility.

Figure 5.8 presents the development of the volumetric concentration of hydrogen gas as contours in a 2D cutplane in the container centreline (along the x-axis), with timesteps 0.1 s, 5.0 s, 10.0 s and 15.0 s. The colour scheme used is dark blue representing 2 vol. %, and up to red, representing concentrations above 30 vol. % (ref. figure legend). This experiment was the only one performed with an obstruction in the jet zone, and the effect is clearly visible in the figures. The jet hits the pallet, placed 0.2 m from the nozzle, and the gas is diverted outwards and upwards. After 5 s, a highly concentrated gas is formed directly above the jet. The gas cloud is then forced through the pallets

suspended from the ceiling, and out of the container. The head of the gas form a thicker cloud as it escapes the container, shown in the lower left image, before the gas leaks from the container in a steady manner, shown in the lower right.

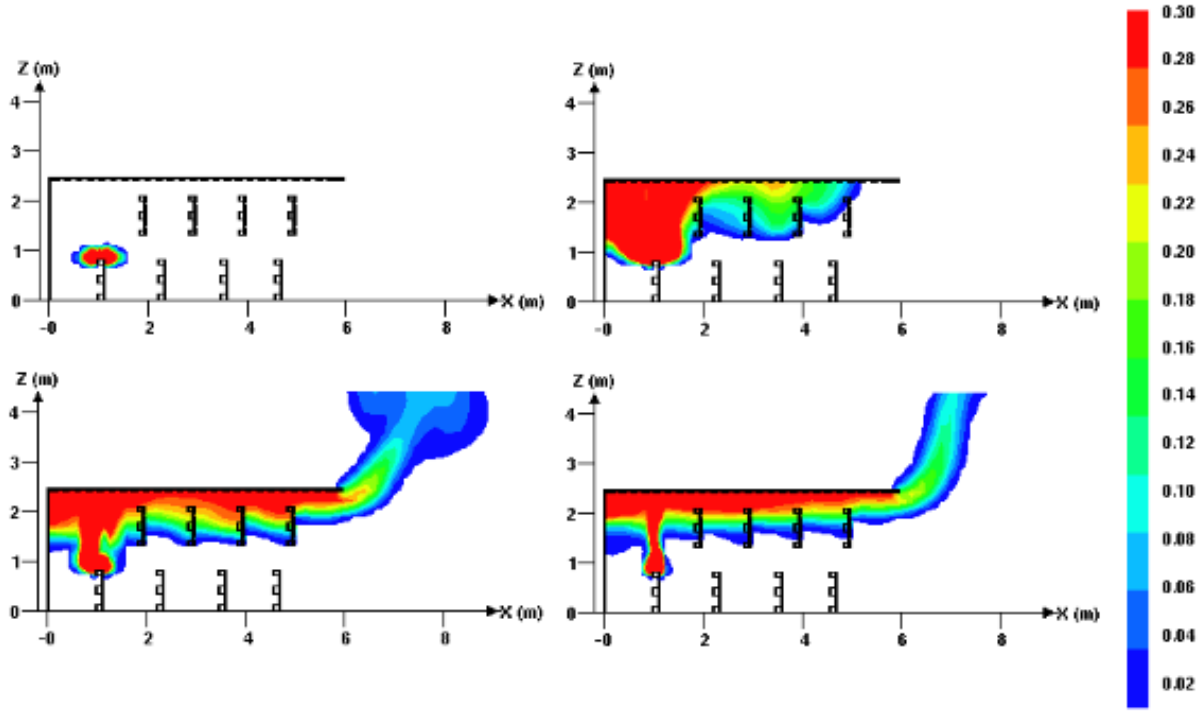

Figure 5.8 centreline 2D cut planes of FLACS simulation of the hydrogen dispersion in experiment 39. The figure shows the volumetric hydrogen concentration during the release with timesteps 0.1 s, 5.0 s, 10.0 s and 15.0 s.

In this simulation, the explosion pressure was above 200 kPa in monitor P2, shown in Figure 5.9. Monitors P1, P2 and P3 cannot be fully compared with the experiment, due to transducer failures.

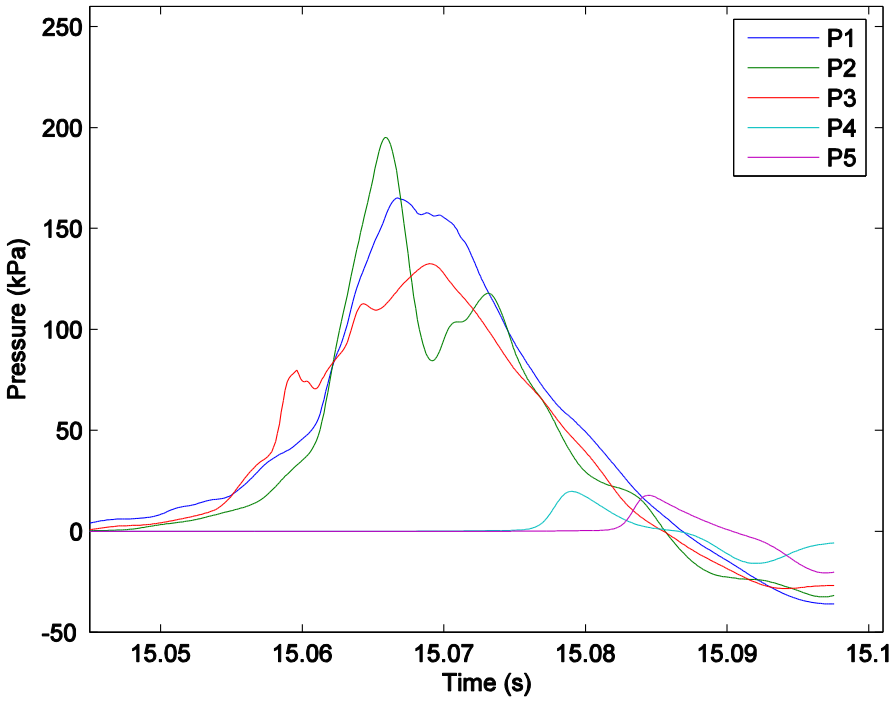

Figure 5.9 Pressure records for points P1-P5 from FLACS simulations of experiment 39.

A comparison of the experimental pressure transducer records from P1 and FLACS is presented in Figure 5.10. Compared to the first local maximum of the experimental data, the FLACS simulation indicates a higher explosion overpressure. One question is whether the local maximum overpressure inside the container was higher than 70 kPa. Given the uncertainty of the data in this experiment, it is difficult to conclude. However, the impulse on the experimental data is lower than in the FLACS simulations, where one explanation can be the lack of instrumentation, thus comparable data.

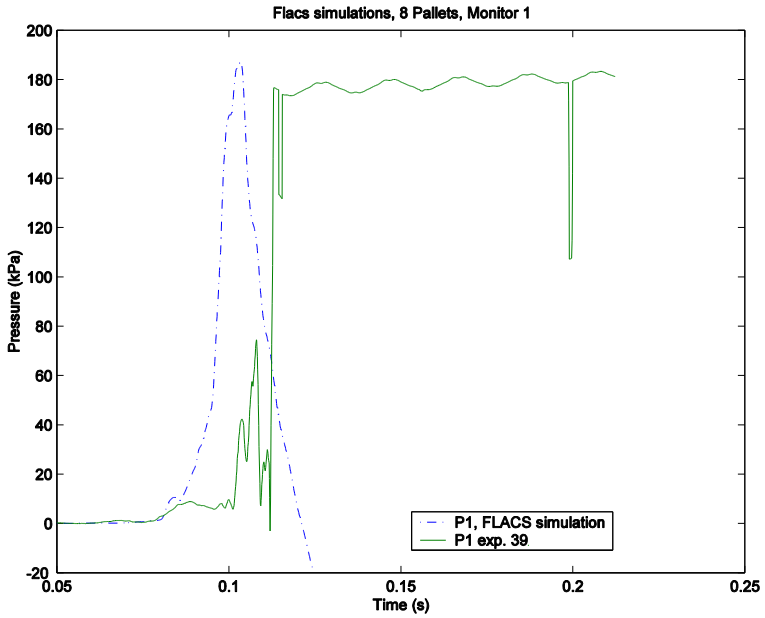

Figure 5.10 Comparison of pressure records of monitor P1 FLACS simulation and available experimental recordings

The pressure recorded in the far-field pressure transducers (P4 and P5) are compared with the experimental results in Figure 5.11 showing P4 in the upper part and P5 in the lower part of the figure. The overall trend in the results from the simulations corresponds quite well with the experiments, although the simulation over-predicts the explosion pressures to some degree. In terms of rise time, the results from FLACS deviate from the experimental results. As shown in Figure 5.11, the calculated first pressure peaks are not located consistently in both transducers. As the time in the experiment is adjusted to fit the FLACS results, it becomes clear that the time for the pressure peak to arrive to P5 is 2.5 ms longer in the simulations than in the experiments, measured from peak to peak. The far-field impulse of the experimental data and the FLACS simulations are quite comparable. Thus, it can be concluded that the estimated energy in the FLACS simulations is fairly accurate.

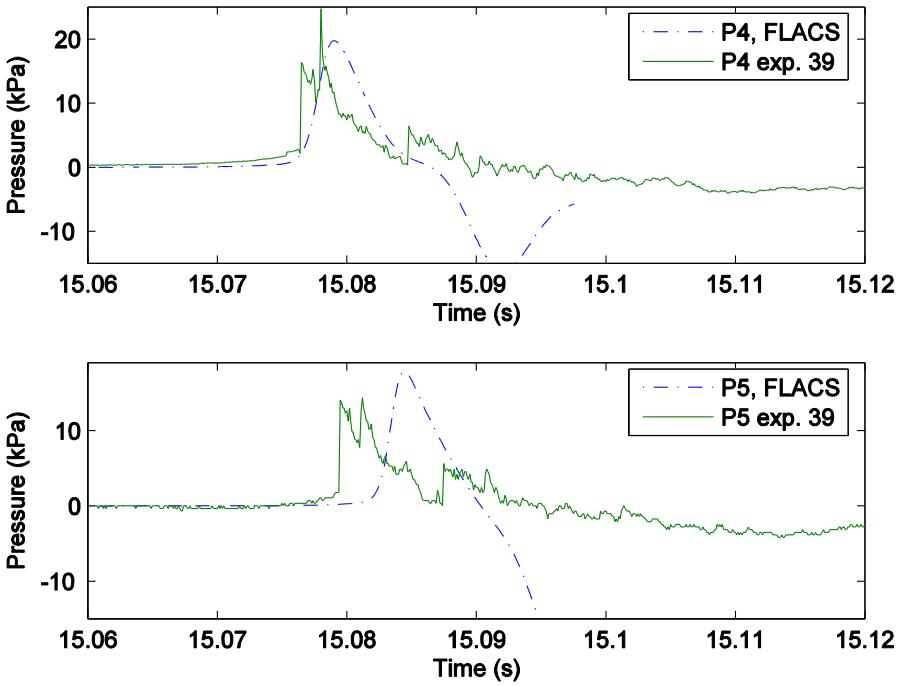

Figure 5.11 Pressure records from experiment 39, compared with FLACS simulations. The time in the experimental results are adjusted to fit the simulations, but are the same in both P4 and P5.

5.3.3 Experiment 26

Figure 5.12 shows the development of the flammable cloud in experiment 26, simulated. The lower hydrogen concentration shown in orange corresponds to 8 vol. %. The geometry is removed to visualize the gas cloud only, and the time-steps in the figure are from top left 0.1 s, 3 s, 6 s, 9 s, 12 s and 15 s. The figure does not tell anything about the concentration levels inside the gas cloud, but is illustrative for the transient gas dispersion development. When compared to the dispersion scenario of experiment 39, Figure 5.7, it is clear that the dispersion is quite different in the two experiments. In experiment 26, the gas cloud fills up the total volume of the container, whereas in experiment 39, only the upper half is filled with hydrogen. However, the gas concentration is higher in experiment 39. This, in combination with the presence of obstacles can explain the generation of a significantly stronger explosion in experiment 39. In both experiments the ignition source was located in the roof of the container.

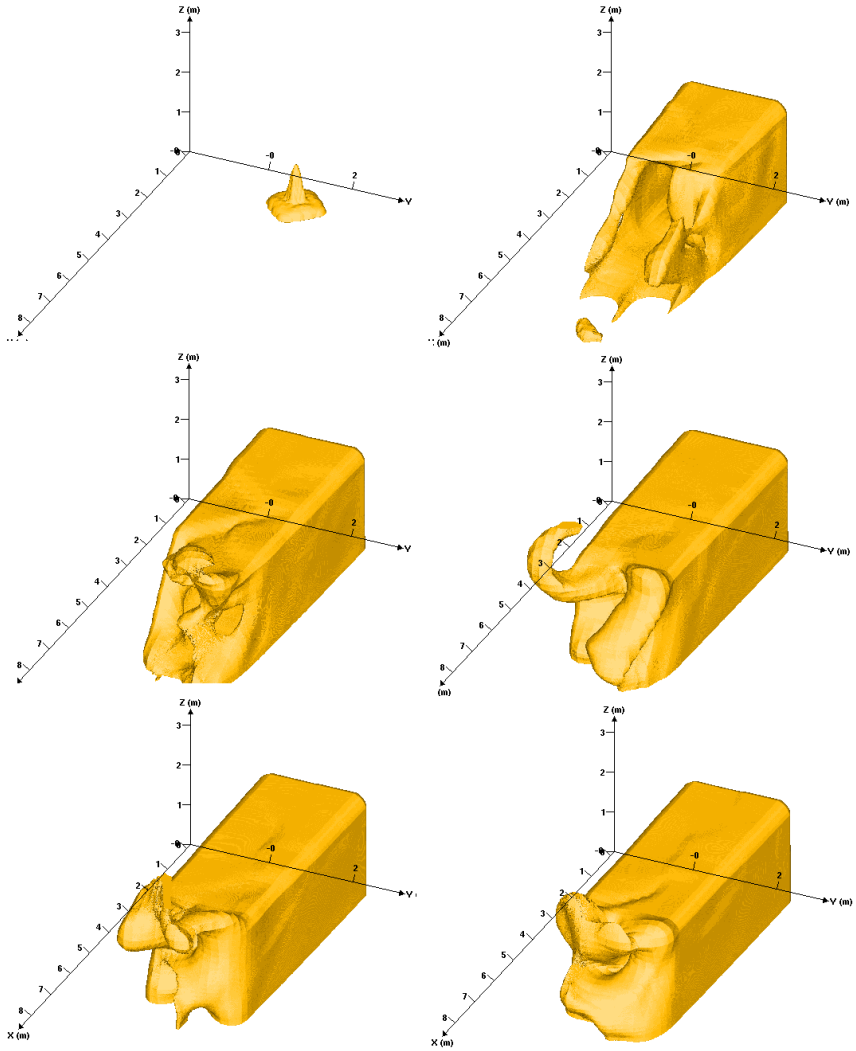

Figure 5.12 Dispersion results from FLACS, experiment 26. The orange colour corresponds to 8 vol. % hydrogen gas concentration. a) = 0.1 s, b) = 3 s, c) = 6 s, d) = 9 s, e) = 12 s and f) = 15 s. Geometry removed for visibility.

The development of the concentration as contours in a 2D cutplane in the centreline of the container is displayed in Figure 5.13. The figure shows results from timesteps 0.1 s, 5.0 s, 10.0 s and 15.0 s. The colour scheme used is blue representing 2 vol. % concentration, and up to red, representing concentrations above 30 vol. %. The FLACS simulations show that within 10 s the downwards directed jet has filled the container

with hydrogen. In the inner part of the container the concentration is in the order of 15 vol. %.

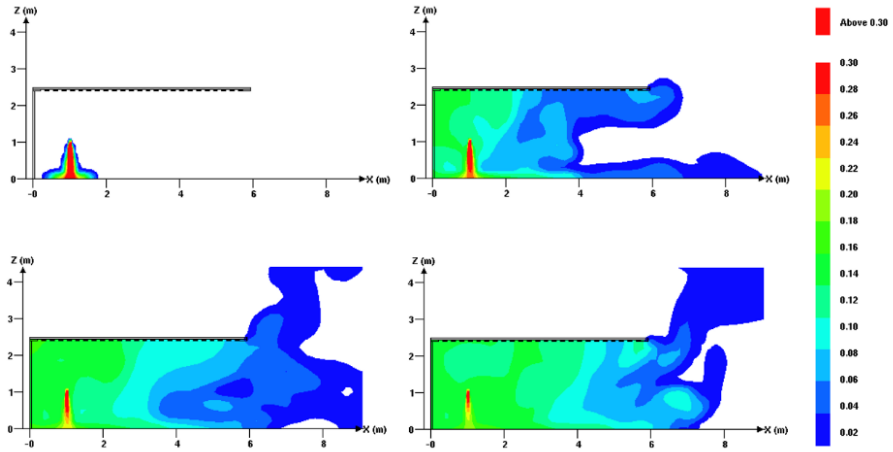

Figure 5.13 Concentration contours from simulations on experiment 26. Timesteps from top left are 0.1 s, 5 s, 10 s and 15 s.

The FLACS simulations of experiment 26 show explosion overpressures of 25-29 kPa in transducers P1-P3. These are substantially higher than the experimental records of P3, which was 3 kPa at first local maximum. The FLACS manual states that the simulation tool may underpredict overpressures resulting from explosions in “empty” enclosures (with vents) due to missing models for flame instabilities. This can explain the discrepancy between the experimental and numerical results in experiment 26. However, an improvement to this issue is expected in a future release, according to the most recent FLACS manual (FLACS (2015)).

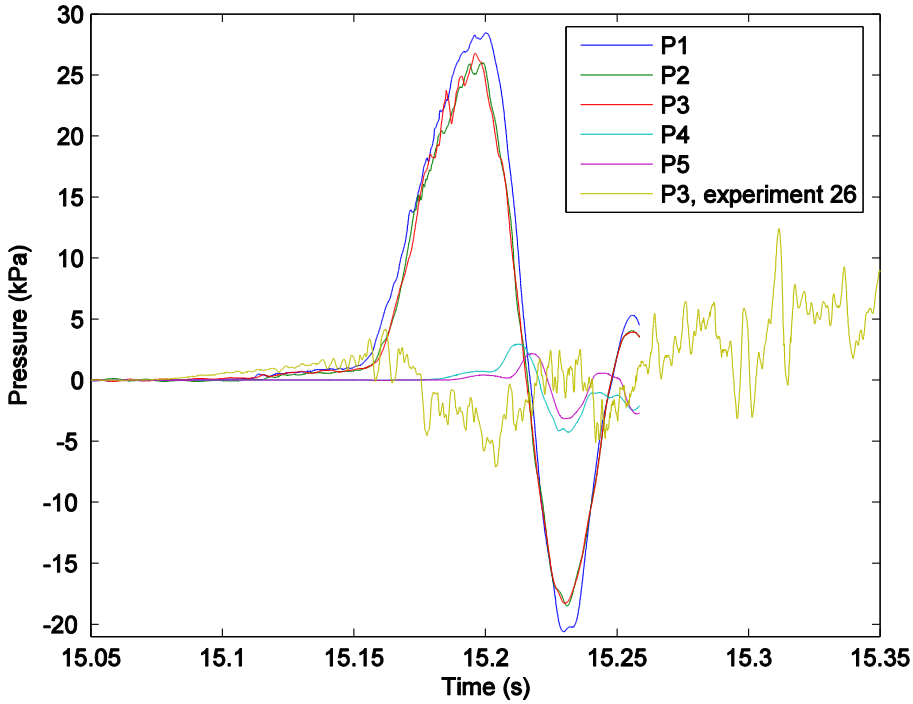

Figure 5.14 Pressure records from simulation on experiment 26, compared with the pressure records from P1 in the same experiment.

Additional FLACS simulations on the ISO container are presented in Appendix 2.

5.3.4 Homogeneous gas clouds, experiment 39

In addition to the combined dispersion and explosion, i.e. simulation with inhomogeneous gas clouds based on experiment 39, a set of simulations with homogeneous hydrogen-air mixtures have been performed. These simulations were run to further study experiment 39. One key feature of these simulations is the low computational time, compared to the more elaborate dispersion-ignition simulations. A first assumption in this work, based on the findings presented in Chapter 2, was that the upper half of the container would fill with a homogeneous hydrogen-air mixture, and that the lower half would contain pure air. Simulations with concentrations ranging from 10 to 30 vol. % in the upper half were performed. In addition, the same gas concentrations were simulated with the gas cloud filling the whole container, to further investigate the dispersion regime. The grid cells were cubic, with size of 0.2 m in all the simulations. The locations of the pressure transducers, P1-P5, were the same as in the experiment, as described in Chapter 3.

In terms of explosion overpressures, the results show that the 10 vol. % and 30 vol. % concentration cases were either too low or too high compared to the experiment. Simulations with 15 vol. % and 20 vol. % concentration were comparable with experiment 39.

The maximum pressures from these four remaining simulations (i.e. 15 vol. % and 20 vol. % in both upper half and total volume, respectively) are plotted in Figure 5.15.

The results are presented for transducers P1-P5, in addition to the maximum pressures available from experiment 39. The results show that the scenarios, where the total container volume were gas-filled, produce high maximum explosion pressures, especially for the case with 20 vol. % hydrogen-air mixture. Results from the scenarios where the upper half of the container is filled with homogeneous hydrogen-air mixture, indicate a volume fraction of hydrogen gas between 0.15 and 0.20 as a reasonable estimate, compared with the sparse pressure records from experiment 39.

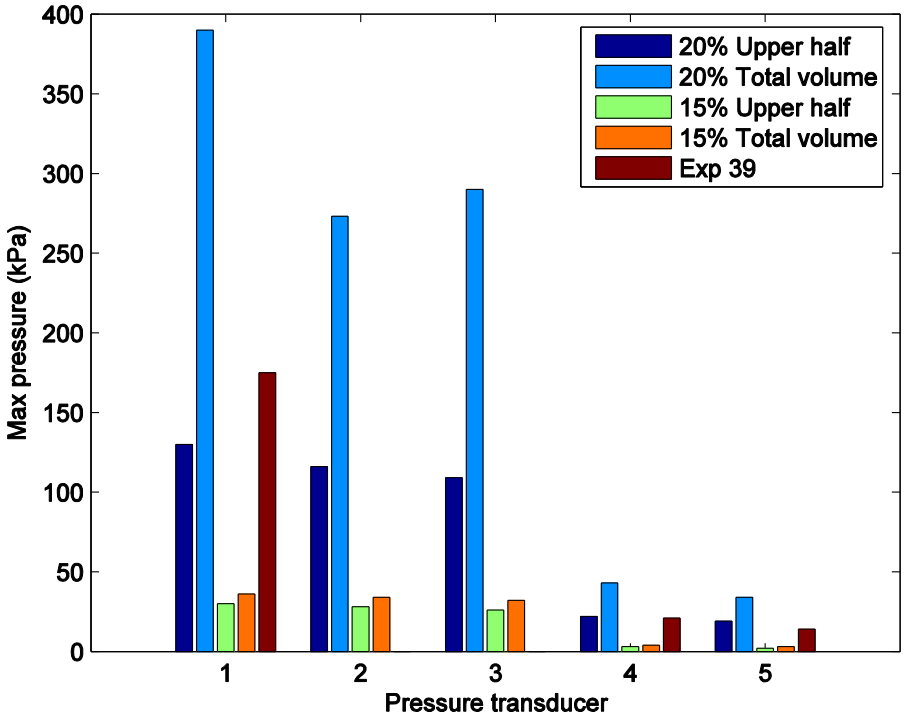

Figure 5.15 Maximum pressures in transducers P1-P5 from FLACS simulations on homogeneous hydrogen-air clouds. Available experimental pressure recordings from experiment 39 are included.

Results from the simulation of the 20% upper half case is plotted in Figure 5.16. The figure shows the simulated shock front pressures as function of distance, and are compared with the experimental results from pressure transducers P4 and P5. The origin is defined as the roof edge above the open end of the container. Compared with the experimental pressure transducers, the FLACS results show comparable maximum overpressures, however with a slight overprediction.

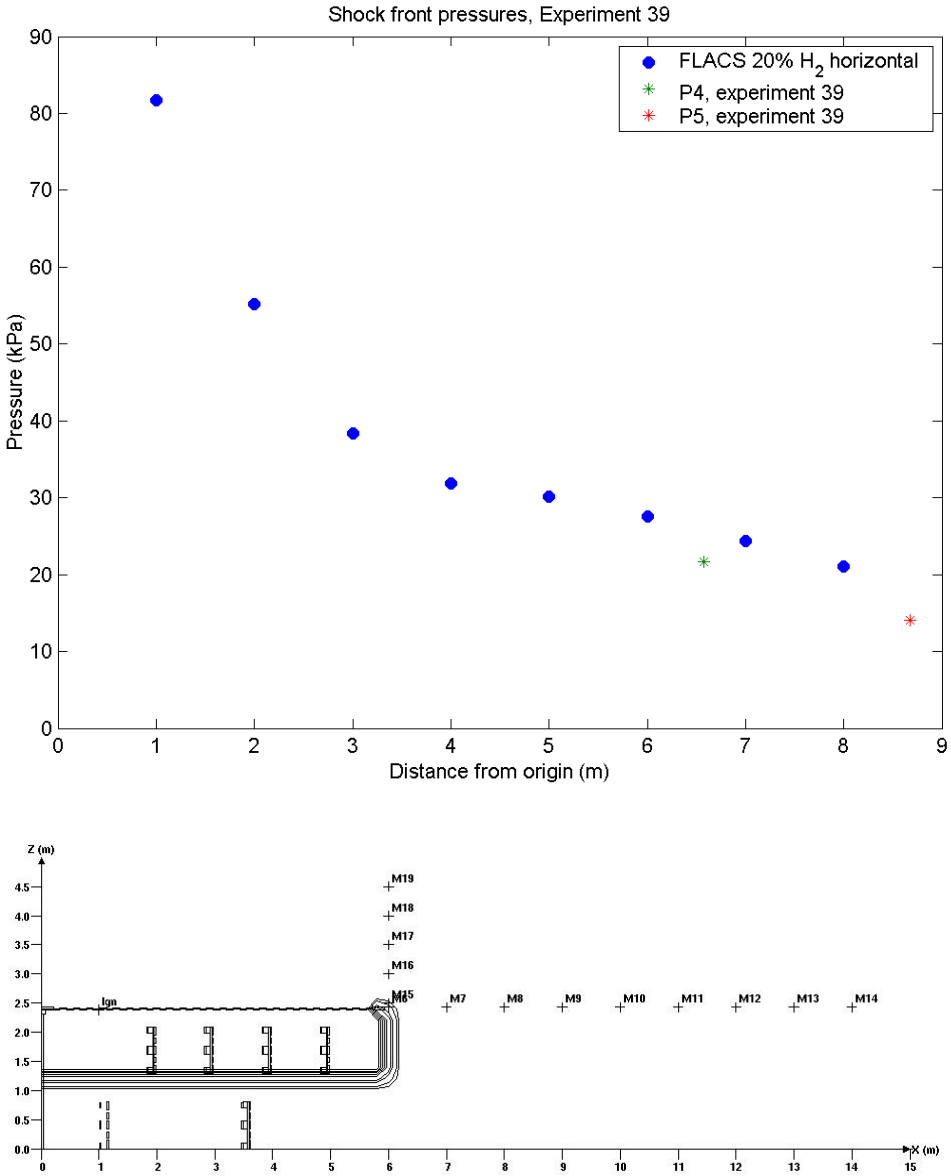

Figure 5.16 Calculated shock front pressure from case with upper half of container filled with 20 vol% hydrogen-air mixture (blue dots). Experimental records from experiment 39 is shown in green (P4) and red (P5)

5.4 Conclusions

FLACS simulations of dispersion and explosion of hydrogen gas in the ISO container indicate that the explosion overpressure in experiment 39 was approximately 200 kPa. This value is comparable with the measured estimated maximum pressure from the shock wave investigations, described in Chapter 4. In the homogeneous gas cloud simulations, the case with a hydrogen concentration of 20 vol. % in the upper half of the container shows comparable pressure records to the FLACS dispersion case of experiment 39. This seems reasonable, as the initial mass of the two FLACS simulation cases are comparable; 310 g for the dispersion/ignition case and 280 g for the case where the upper half of the container was filled with 20 vol. % hydrogen-air mixture.

Given the resolution reported here, the results show that the shock waves are not accurately resolved compared to the experiments. The software indicates some weaknesses when used in a geometry with no obstructions. Simulations with empty container underpredict the explosion pressure to some degree, whereas for the obstructed cases, the results correspond better with the experimental pressure records.

Development of the FLACS code is an ongoing venture. The FLACS version used in this thesis (mainly v8.1) has later been improved, also related to hydrogen dispersion and simulations.

A summary of the FLACS simulations on the ISO container are presented in Table 5.3.

Table 5.3 Results summary of FLACS explosion simulations.

Exp.	P_{tank} [MPa]	Results
24	2.0	Overprediction in FLACS
26	2.4	Overprediction in FLACS
27	1.2	No explosion, burning jet
28	0.6	No ignition in FLACS
30	2.0	Overprediction in FLACS
33	2.0	No explosion, burning jet
34	2.0	No explosion, burning jet
38	2.4	Good correlation
39	2.4	Good correlation

6 N1 FLACS simulations

6.1 Introduction

This chapter describes a series of numerical simulations with release and ignition of hydrogen. The objective of this work was to re-investigate the accidental explosion in an ammonia plant which happened in 1985, using a modern CFD tool. The simulations are based on the factory accident at Herøya, Porsgrunn, which led to two fatalities and complete destruction of the factory building where the explosion occurred.

The N1 ammonia plant accident (with an estimated release of hydrogen of 10-20 kg) was long considered one of the worlds' largest accidental hydrogen-air explosions. An article by Yanez et al. (2015) report that the accident at the Fukushima-Daiichi power plant in Japan, which happened after the tsunami in 2011, had an estimated amount of hydrogen of 130 kg.

In section 6.2 the accidental course of events is described briefly. The numerical simulation setup is described in subsection 6.3, with the following results in section 6.4. An attempt of using the Froude scaling on the N1 factory building is presented in 6.5. A discussion of the results is presented in section 6.6.

6.2 Accidental course of events

The severe hydrogen-air explosion led to two fatalities and complete destruction of the factory building where the explosion occurred (Bjerketvedt and Mjaavatten, 1986). The investigation report states that the event started when a gasket in a water pump was blown out. The pump was feeding water to a vessel containing hydrogen gas at a pressure of 3.0 MPa. The overpressure caused a back flow of water through the pump and out through the failed gasket. The hydrogen gas reached the leakage point after about 3 minutes. Hydrogen was discharged into the building between 20 and 30 seconds before the explosion occurred, with a total mass of hydrogen estimated to 10 to 20 kg. The ignition source was most likely a red-hot bearing located inside a motor casing (motor A). The main explosion was very violent, and the investigation report conclude

that it is likely that the gas cloud detonated. A complete case history of the accident was presented at the First International Conference of Hydrogen Safety in Pisa (Bjerketvedt and Mjaavatten, 2005).

6.3 Numerical simulations setup

The numerical setup was based on the investigation report (Bjerketvedt and Mjaavatten, 1986) and over 1000 pictures from the accident investigation team. The geometry of the building was modelled based on pictures from the accident and layout drawings such as Figure 6.1 and Figure 6.4. The interior was simplified to main components only. Smaller pipes, racks and equipment were left out intentionally, due to lack of precise information.

The findings from the investigation have been the basis of input to the simulations, for example the jet details and ignition source location. Each scenario was first simulated as a dispersion, and then ignited. Each case has therefore 2 coupled simulations.

Five scenarios are presented here. Case 1 is the base case, which gave results closest to the accident scenario. Case 2 represent a jet release directed horizontally towards one of the long sidewalls of the building, used in comparison to Case 1. Case 3 is a simulation with vent openings in the longest side walls, with a 1 m opening in the longitudinal direction at the floor and ceiling. Case 4 is a simulation with no side walls, which was the original design of the building. The last case, case 5 is a re-run of Case 1, but without the roof support beams.

6.3.1 Geometry description

The inner dimensions of the factory building were 100 m long (x), 10 m wide (y) and 7 m high (z). The walls and roof were made of reinforced concrete elements. The roof was supported by several concrete support beams, placed at an interval of approximately 8 m throughout the length of the building. The support beams were 1 m wide. The main process equipment consisted of water pumps A and B, two motors (A and B) and a row of turbines. The water entered the pumps through pipes from the long south wall. Other

equipment was not modelled. A large garage door placed in the north wall, were open. Figure 6.1 shows a schematic of the buildings affected by the explosion at the N1 factory.

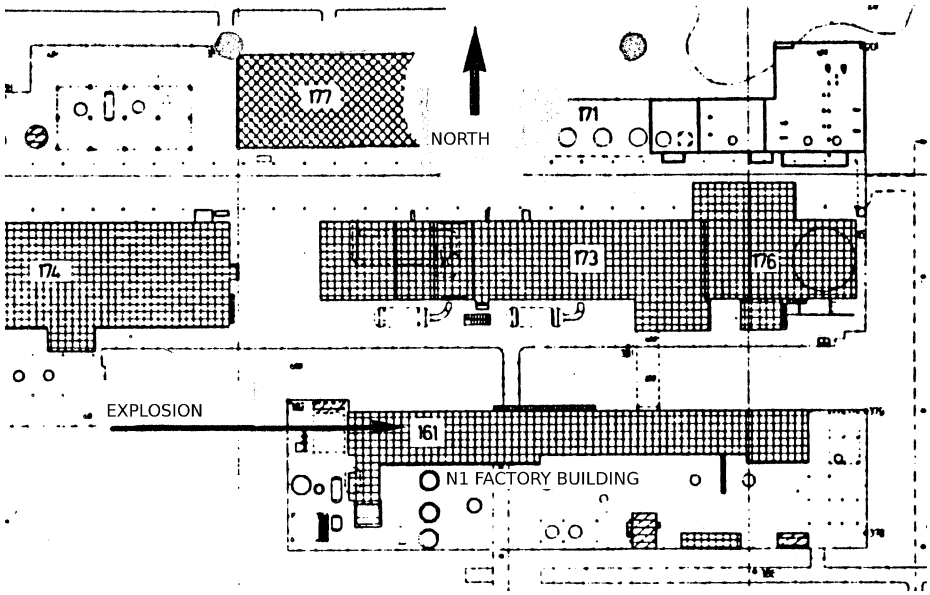

Figure 6.1 Overview of the buildings in the explosion area. Obtained from Bjerketvedt and Mjaavatten (1986).

A photo of the factory building after the accident is shown in Figure 6.2.

Figure 6.2 Photo of the northern wall of the factory building after the accidental explosion (Bjerketvedt and Mjaavatten, 1986). Photo: A. Kjellevold.

The CFD geometry details are shown schematically in Figure 6.3, exported from the FLACS pre-processor CASD. The geometry was simplified. Apart from main equipment, such as the gas supply pipe, pumps and compressors, the factory building was assumed relatively empty. In the simulations, the length of the factory building was 50 m.

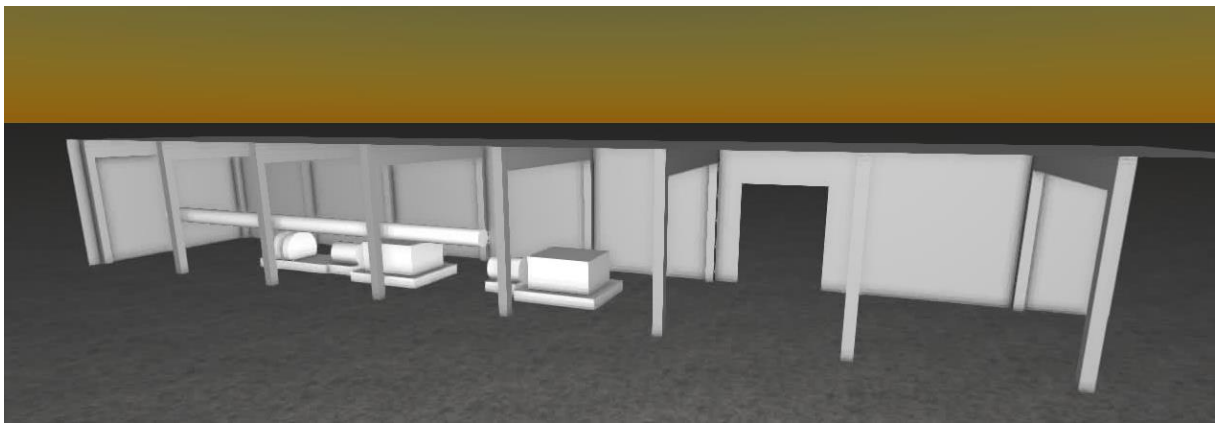

Figure 6.3. FLACS model of the N1 factory building (sidewall removed for visualization purposes).

The ignition point was located at the base of pump A, 1.0 m above the floor. The investigation report concluded that the ignition most likely had happened due to a hot bearing in the driveshaft of this pump. In the simulations, the ignition point was positioned in the direction perpendicular to the jet. Figure 6.4 shows a schematic overview of the location of pump A and pump B.

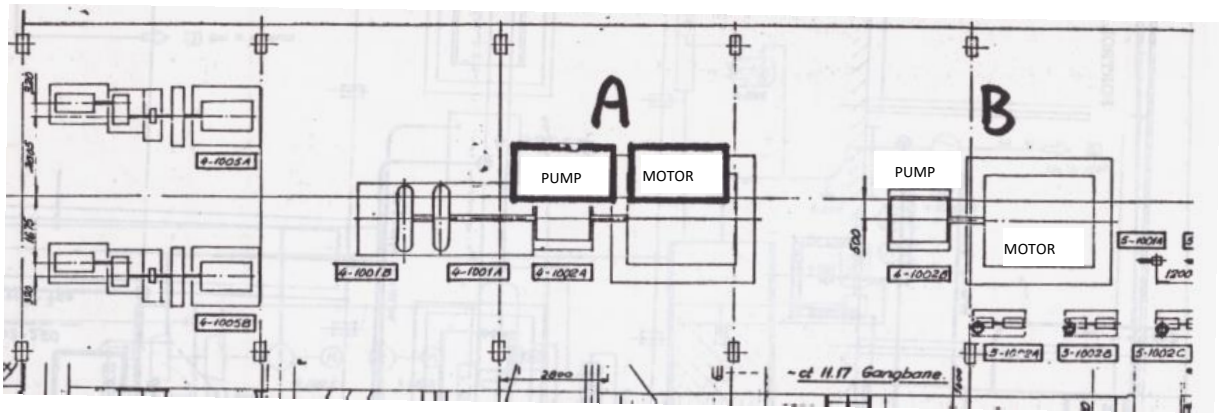

Figure 6.4. Schematic overview of main equipment in the N1 factory building, image from the investigation report by Bjerketvedt and Mjaavatten (1986)

The monitor point distribution is shown in Figure 6.5

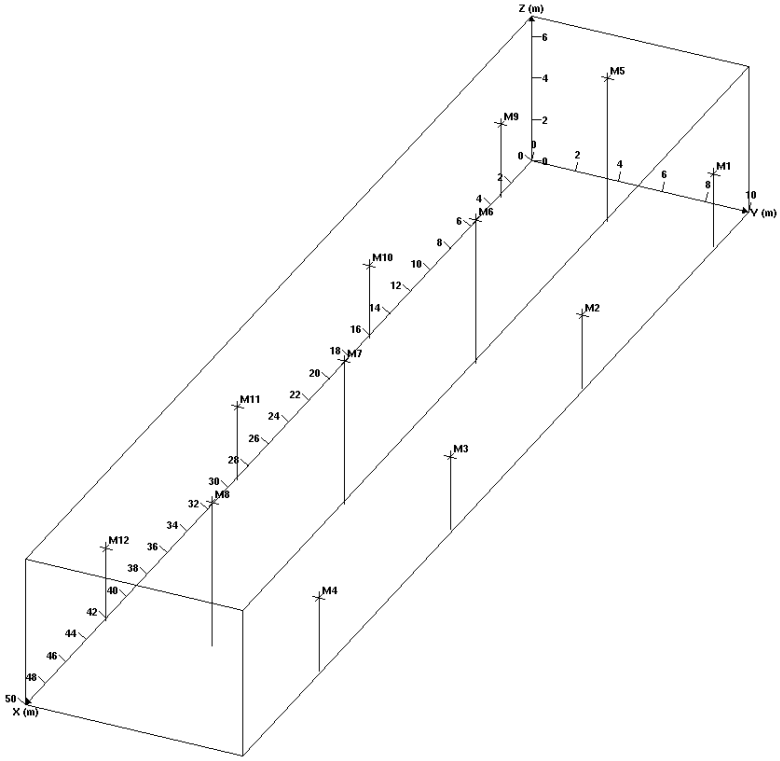

Figure 6.5 Monitor positions for the FLACS simulations performed on the N1 factory building

6.3.2 Simulation description

A series of FLACS simulations have been performed with the abovementioned geometry. The jet direction was varied, to find the most likely dispersion scenario from in the accident. FLACS simulations were also performed to study the effect of natural venting and level of congestion. The height of the longitudinal walls has been varied, leading to different vent openings at floor level, at the ceiling and a combination of the two. This was done on the reported case (case 3) with the results closest to the accident to investigate the effects of congestion with regards to gas cloud formation.

Table 6.1 summarises the simulation matrix. The initial fuel in the rightmost column describes the initial amount of fuel loaded from the corresponding dispersion simulation and into the ignition simulation. These values vary, because of the dilution of hydrogen in the surrounding air in the different scenarios. In case 4, the initial fuel is lower because the walls are removed so that the hydrogen gas exits the computational domain.

Table 6.1 FLACS simulation matrix

Case	Simulation details	Wall details	Initial fuel [kg]	P_{max} [kPa]
1	Release, +x direction Ignition, +x direction	Solid walls Solid walls	14.0	360
2	Release, -y direction Ignition, -y direction	Solid walls Solid walls	14.8	60
3	Release, +x direction Ignition, +x direction	1.0 m opening, top and bottom 1.0 m opening, top and bottom	12.1	10
4	Release, +x direction Ignition, +x direction	No walls No walls	9.94	1
5	Release, +x Ignition, +x	Solid walls, no roof supports Solid walls, no roof supports	14.0	

6.3.3 Jet details

The opening of the accidental release was 6 cm^2. The hole was a blown-out section of a gasket in a water pump, which led to a sector-shaped release. Parts of the jet hit a small vertical steel pipe.

In the simulations, the jet inlet has been calculated in the corresponding jet utility program in the FLACS software package. Table 6.2 shows the input variables chosen for the calculations. Calculations from such an input-file provide a set of data, including Mach number calculations and effective nozzle diameter. The resulting data is presented as a table, where effective nozzle area [m^2], mass rate [kg/s], velocity [m/s] and temperature [K] among others, are listed for successive time-steps. The jet calculation output data set is loaded by the FLACS program during the simulations to provide a time-dependent leak. The reservoir volume was chosen to make sure that the reservoir pressure was treated as a constant, as the value of the reservoir volume was unknown. The investigation report concluded that the pressure was 3.0 MPa prior to the accident.

The simulated release assumed a free jet from a 6 cm^2 circular opening. The discharge coefficient was chosen to 0.62, based on the guidelines in the FLACS software manual. The direction of the jet was changed according to the specification on the different

simulation scenarios. The relative turbulence intensity level was 0.2 in all the calculations. Heat transfer coefficients and wall temperature were 0.

Table 6.2 Jet calculation details

Jet variables	Comments
10000	Reservoir volume [m³]
3.0	Reservoir pressure [MPa, g]
10.0	Reservoir temperature [°C]
0.1	Atmospheric pressure [MPa a]
20.0	Atmospheric temperature [°C]
0.0276	Nozzle diameter [m]
0.62	Discharge coefficient [-]

The calculated mass flow rate was 0.74 kg/s. This is within the estimated mass- and time intervals reported in Bjerketvedt and Mjaavatten (1986).

6.3.4 Grid details

Cases 1 and 2 were run with a simulation domain of 0-50 m in x-direction, 0-10 m in y-direction and 0-7 m in z-direction. This corresponds to the walls of the geometry, and was chosen to minimize computational time. Cases 3 and 4 were run with a simulation volume of 0-55 m in x-direction, -5-15 m in y-direction and 0-10 m in z-direction. The Cartesian grid resolution was standardized to 0.2 m grid cells in all directions, and was stretched 5 % in the outer parts of the simulation volume. A grid sensitivity analysis has been carried out to verify the chosen grid size. Around the jet inlet, the grid was refined to 0.1 m, and smoothened to 0.2 m, 4 control volumes from the inlet. The grid was not refined in the direction of the jet. Examples of simulation grid structures are presented in Figure 6.6 (dispersion) and Figure 6.7 (explosion).

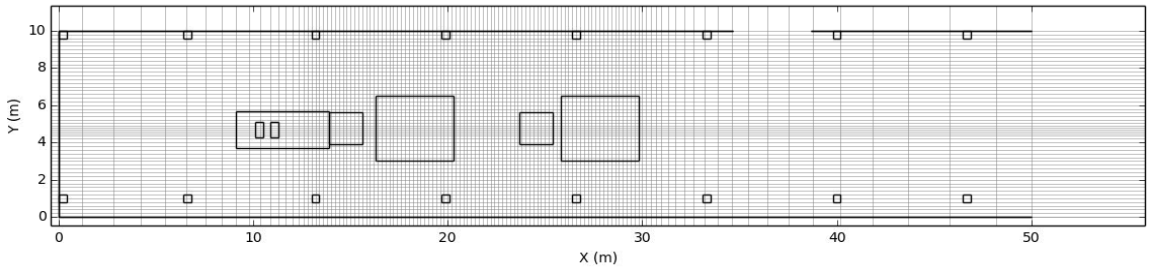

Figure 6.6 Grid details from dispersion simulation, Case 1 (010101). The geometry is viewed from the top, at elevation 0.1 m above floor

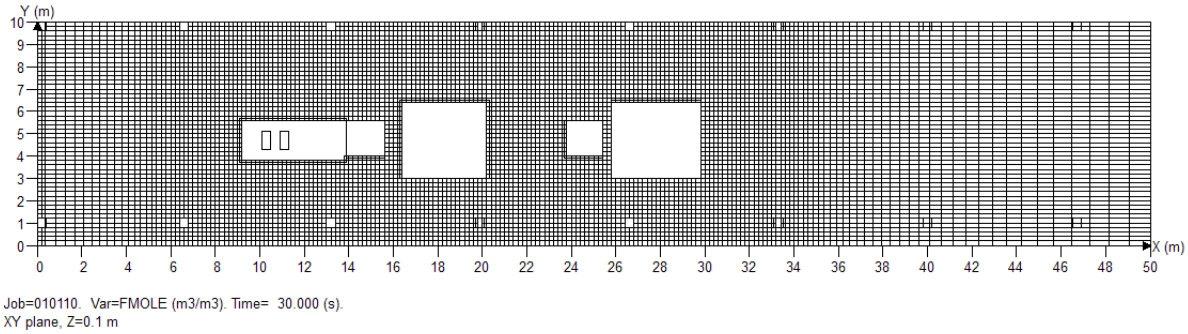

Figure 6.7 Grid details from explosion simulation, case 2 (010110), at elevation 0.1 m above floor

6.4 Numerical results

6.4.1 Case 1

The base case, Case 1, gave reasonable dispersion results compared to the accident. The jet hit the casing of pump A in less than 0.1 seconds, and the gas was diverted in a spherical manner. Some of the gas was directed outwards, hitting the side walls and creating a horizontal circulation zone. Most of the gas was then forced upwards, caused by the concrete foundation of the pump acting as a diversion.

As the gas reached the ceiling, it was directed outwards in all directions. Because of the concrete support beams located under the ceiling, the gas was forced downwards along the side walls of the beams, in addition to the longitudinal walls. This created a large recirculation zone, both in the x- and y-directions. The recirculation zone was fed even

more by the powerful jet in a forced feedback loop. After approximately 6.8 seconds, the flammable hydrogen gas reached the top level of engine A, and after 20 seconds the volume between the ceiling and the floor mounted equipment was above 15 percent. The concentration level at the drive shaft connecting engine A with pump A (1 m above floor) reached 12-15 percent after 20 seconds. The investigation report concluded that a red-hot bearing in the drive shaft of this pump was the likely ignition source. The dispersion results in this FLACS simulation supports this, both the location and the time of ignition after the release started seems reasonable. Figure 6.8 shows the concentration contours in a cut plane in the centre (longitudinal) of the building after a 20 second release.

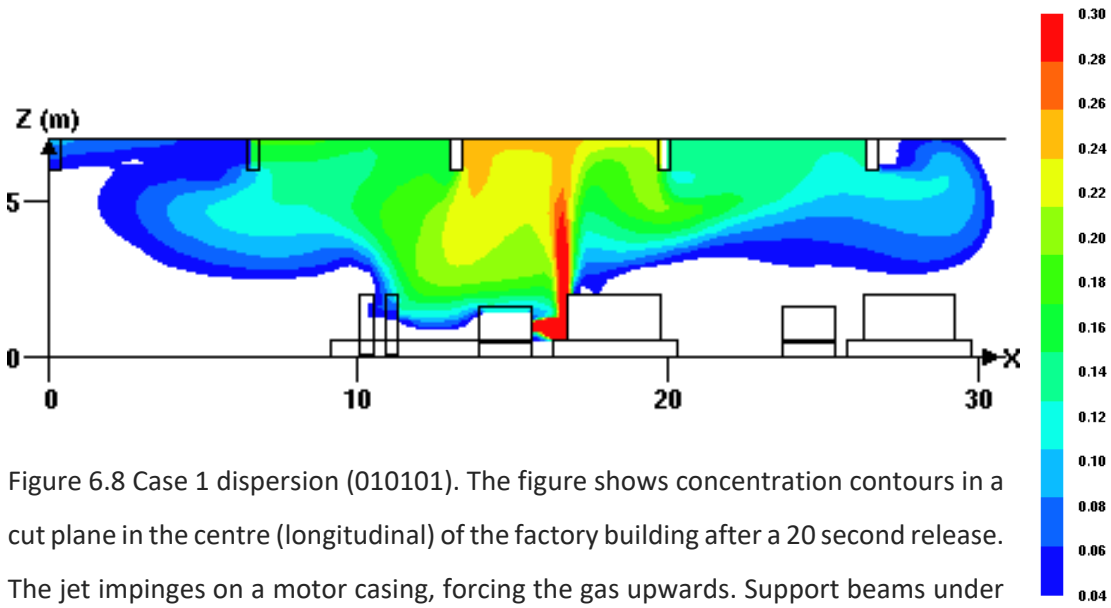

Figure 6.8 Case 1 dispersion (010101). The figure shows concentration contours in a cut plane in the centre (longitudinal) of the factory building after a 20 second release. The jet impinges on a motor casing, forcing the gas upwards. Support beams under the ceiling create a recirculation zone. Colours indicate a range of concentrations from 4 vol. % (dark blue ≥ LFL) to 30 vol. % (red ≥ stoich.). White regions indicate a concentration of less than 4 vol. % (not flammable < LFL).

The ignition of the gas cloud in Case 1 gave high explosion overpressures. The monitor located directly above the jet (M7) recorded a maximum explosion pressure of 210 kPa. One monitor located close to the lower southeast corner of the building gave a maximum of 360 kPa (M1) and recorded the highest maximum overpressure in this

simulation. The pressure records of the monitors M1 and M7 in Case 1 shown in Figure 6.9.

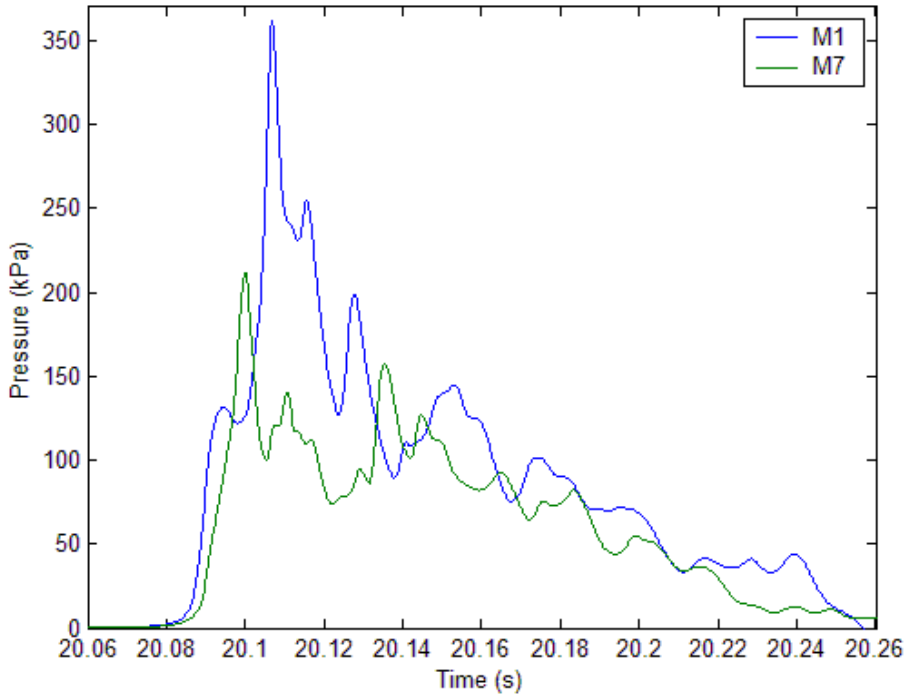

Figure 6.9 Case 1 pressure records from monitors M1 and M7

Simulations with the jet release directed vertically upwards (+z) gave results similar to Case 1, but with even stronger recirculation zones. The explosion overpressures in this simulation were also comparable.

6.4.2 Case 2

Case 2, which had the release directed towards the south side wall, gave a significantly different result than Case 1. The hydrogen gas hit the wall, and was directed to the sides and upwards. The length of the gas cloud was longer than in Case 1, and the development of the cloud was not as controlled by large recirculation zones. The hydrogen concentration in the mixture was lower than in Case 1. Figure 6.10 shows the concentration contours from simulations on Case 2 in a side view cut plane in the centre (longitudinal) of the building after a 20 second release. The figure also represents the concentration contours from top view, in the height of the release (1 m). Compared to Case 1, it is evident that the flammable gas cloud concentration is significantly lower.

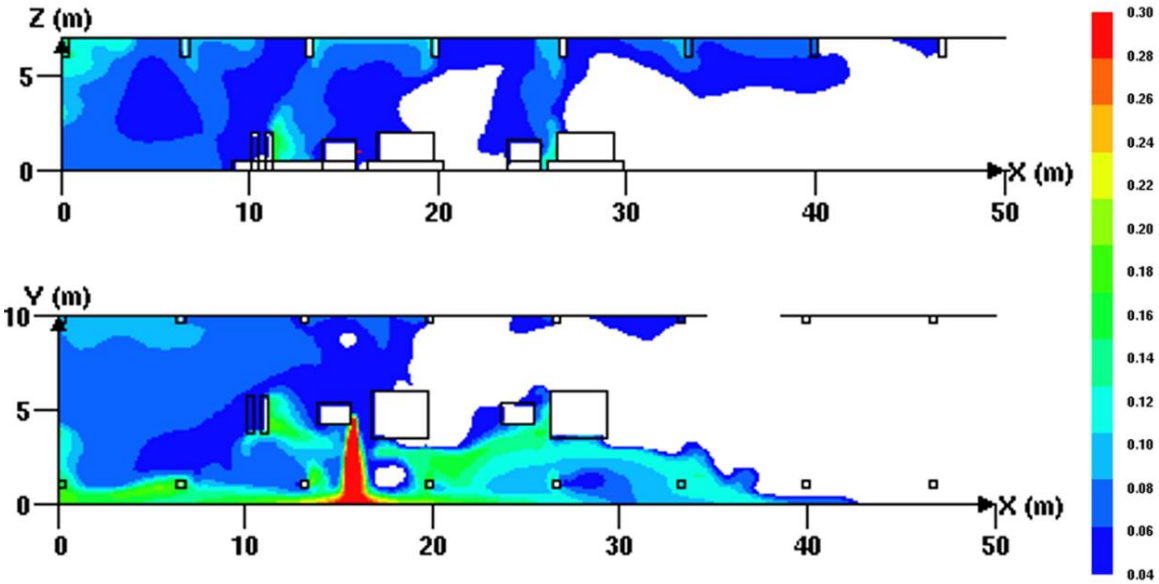

Figure 6.10 Case 2. Concentration contours in cut planes along the x-axis after a 20 s release. Upper figure: Side view cut plane in the centre (longitudinal) of the factory building, Lower figure: Top view cut plane at the height of the release (1.0 m) Colours indicate a range of concentrations from 4 vol. % (dark blue ≥ LFL) to 30 vol. % (red ≥ stoich.). White regions indicate a concentration of less than 4 vol. % (not flammable < LFL)

Pressure records from the explosion simulation show a maximum overpressure of about 50 kPa. Monitors M1 and M7 are shown in Figure 6.11, where M1 recorded the highest maximum overpressure in this case.

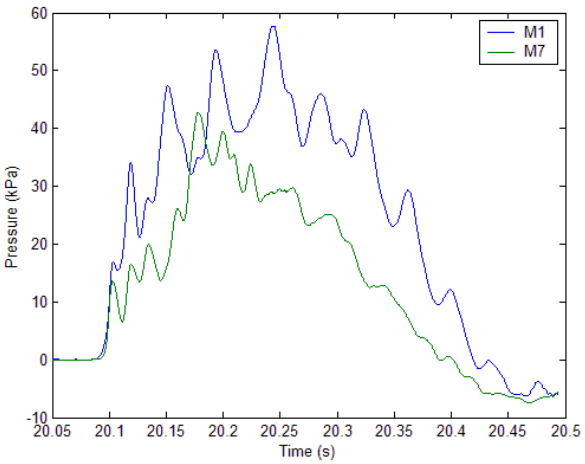

Figure 6.11 Case 2 pressure records from monitors M1 and M7

6.4.3 Case 3

Case 3 was performed to investigate how passive ventilation would work in this geometry. The longitudinal 1 m openings along the floor and ceiling vented some of the gas out of the building. One of the main advantages with this geometry was that the mean hydrogen concentration was lowered from about 20 % in the comparable Case 1 to about 15 % in Case 3. Figure 6.12 and Figure 6.13 show the concentration contours of Case 1 and Case 3 in cut planes located 0.5 m from the jet nozzle, i.e. between the nozzle and pump A.

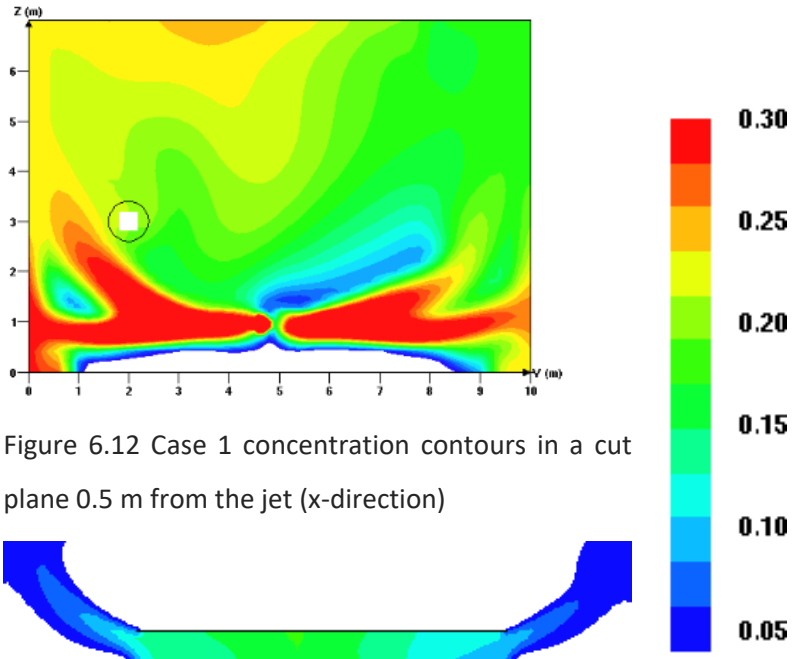

Figure 6.12 Case 1 concentration contours in a cut plane 0.5 m from the jet (x-direction)

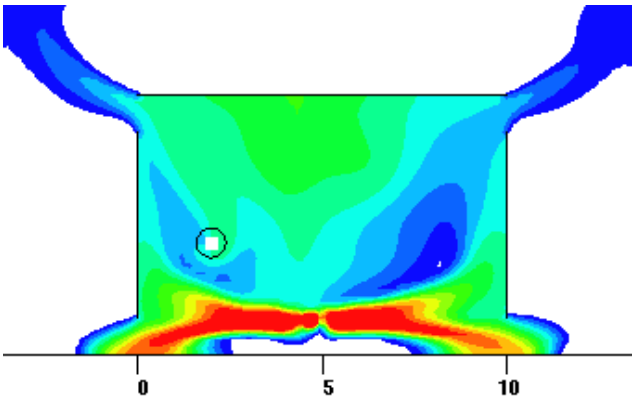

Figure 6.13 Case 3 concentration contours in a cut plane 0.5 m from the jet (x-direction)

A Case 3 side view cut plane concentration contour plot is shown in Figure 6.14. The figure represents the longitudinal centreline of the building after a 20 s release.

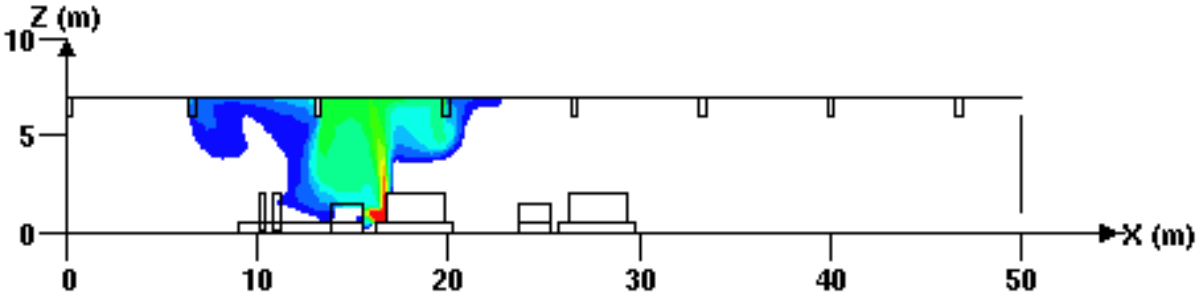

Figure 6.14 Case 3 concentration contours in a cut plane in the centre (longitudinal) of the factory building after a 20 s release. The jet hits a motor casing, forcing the gas upwards. Colours indicate a range of concentrations from 4 vol. % (dark blue ≥ LFL) to 30 vol. % (red ≥ stoich.). White regions indicate a concentration of less than 4 vol. % (not flammable < LFL).

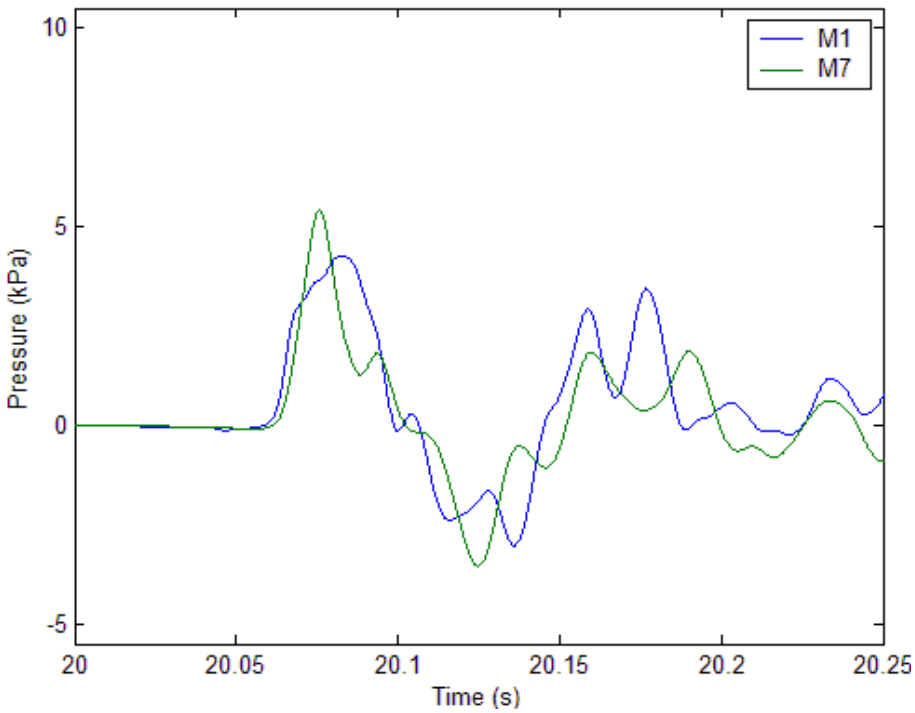

Figure 6.15 Case 3 pressure records from monitors M1 and M7

The results show that in Case 3 a relatively small gas cloud was formed under the factory ceiling. The behaviour of such releases has been reported in Middha and Hansen (2009) and in Sommersel et al. (2008). The explosion simulation of Case 3 gave relatively low

explosion overpressures, compared to the base case. The highest maximum was 10 kPa, recorded in M2 located close to the northern side wall at level with the jet location.

6.4.4 Case 4

FLACS simulations on the factory building without walls were performed to study the development of a hydrogen-air mixture in a more open environment. Originally, the factory was designed without walls. Due to the cold Norwegian winter climate, the walls were added at a later stage to prevent the water inside the building to freeze. The results from simulations on Case 4 show that the hydrogen is effectively vented out of the building, and the potential for an explosion have been dramatically reduced. Figure 6.16 shows the concentration contours in the centre of the building.

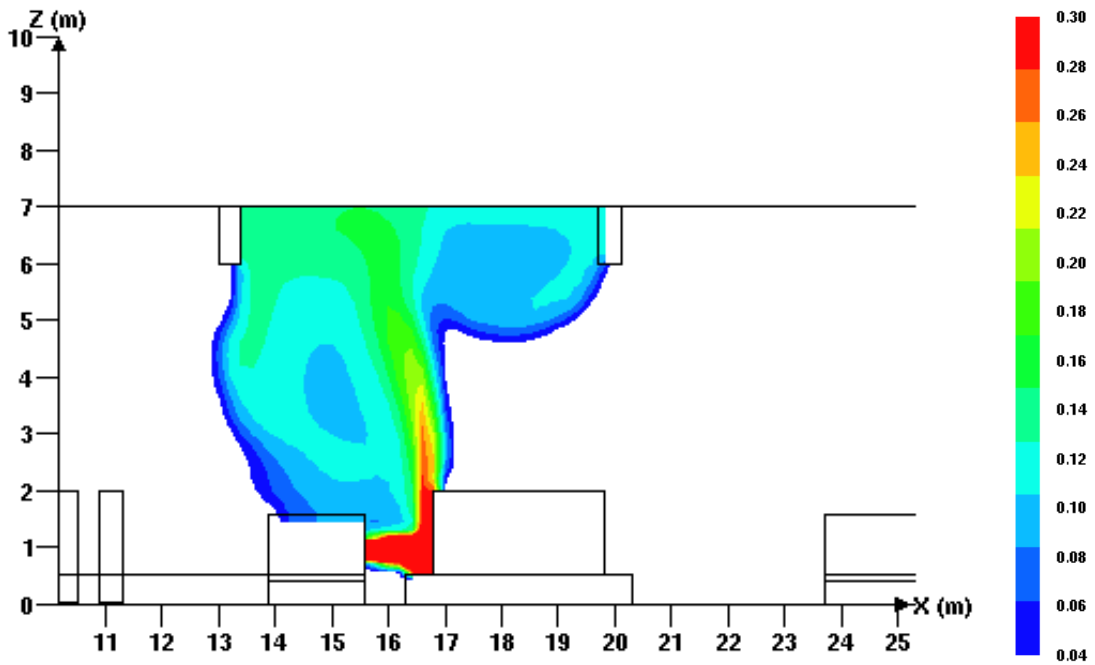

Figure 6.16 Case 4 concentration contours in a cut plane in the centre (longitudinal) of the factory building after a 20 s release. The jet impinges on a motor casing, forcing the gas upwards. The gas then gets forced to the sides and out of the building. Colours indicate a range of concentrations from 4 vol. % (dark blue ≥ LFL) to 30 vol. % (red ≥ stoich.). White regions indicate a concentration of less than 4 vol. % (not flammable)

The consequence of removing the walls is shown in Figure 6.17, where concentration contours in a volume plot shows the effective venting of the hydrogen-air mixture in the more open factory building. This case was impossible to ignite at the same location as the other three cases reported here, indicating that the explosion would probably not occur in this geometry layout. This case was ignited with the ignition located above the release close to the ceiling, in the centre of the factory. The maximum overpressures were in the order of 1 kPa.

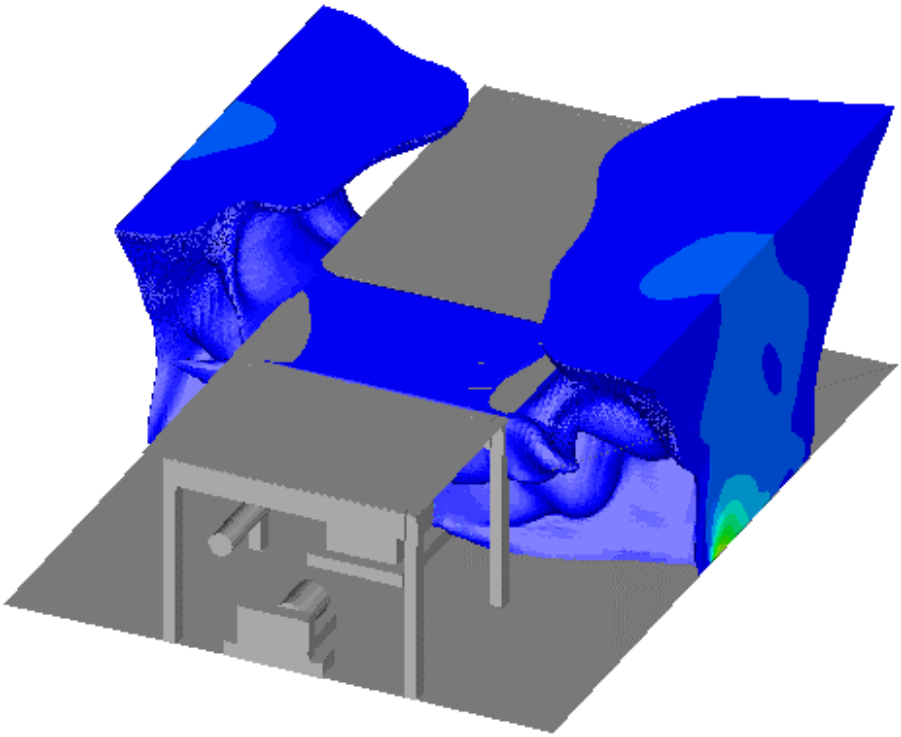

Figure 6.17 Case 4 concentration contours in a volume plot shows the effective venting of the hydrogen-air mixture in the factory building without walls. Colours indicate a range of concentrations from 4 vol. % (dark blue ≥ LFL) to 30 vol. % (red ≥ stoich.). White regions indicate a concentration of less than 0.04 (not flammable)

6.4.5 Case 5

Case 5 is a re-run of the base case (Case 1), but where the roof support beams was removed. The purpose was to investigate the differences in the dispersion and gas cloud build-up between Case 1 and Case 5. In Figure 6.18 and Figure 6.19 the hydrogen dispersion is compared. The figures show concentration contours in cut planes in the centre (longitudinal) of the factory building after a 25 s release. Colours indicate a range of concentrations from 0.04 (dark blue ≥ LFL) to 0.3 (red ≥ stoich.). White regions indicate a concentration of less than 0.04 (not flammable < LFL).

In both Case 1 and Case 5, the jet hits the motor casing, forcing the gas upwards. The simulation results from Case 5 show a reduction in the concentration levels directly above the jet, compared to Case 1.

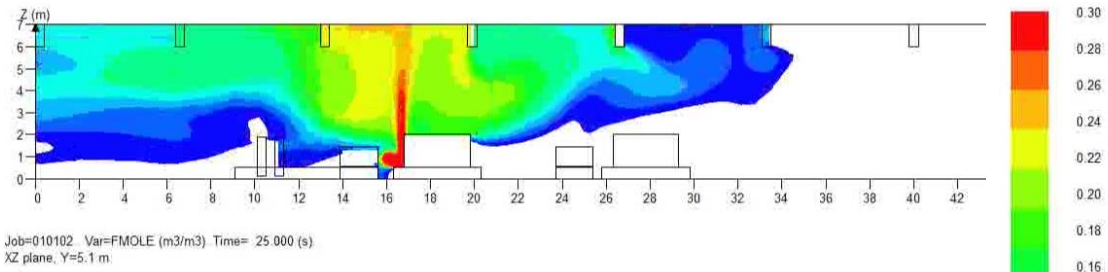

Figure 6.18 Case 1 hydrogen concentration contours in a 2D cut-plane at t = 25 s

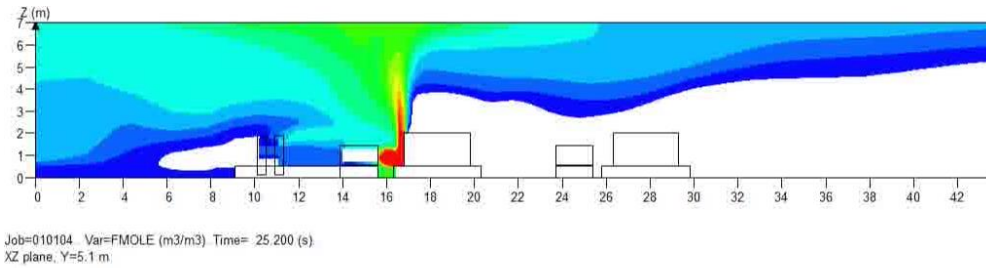

Figure 6.19 Case 5 hydrogen concentration contours in a 2D cut-plane at t = 25 s

6.5 Froude scaling

The propagation of the hydrogen gas cloud in the N1 factory building can be described by the Froude number, using the correlation shown in section 2.3.3. The average frontal velocity can be described as:

$$u_F = \sqrt[3]{\frac{Fr^2 g Q}{w}} \qquad 7.1$$

where the width of the building, w, is 10.0 m. With the Froude number, determined experimentally in Chapter 2.3, to be 0.68, and the dimensionless height Φ = 0.5 (i.e. the average gas cloud filling the upper half of the volume), the average frontal velocity is calculated as function of hydrogen mass flow, shown in Figure 6.20.

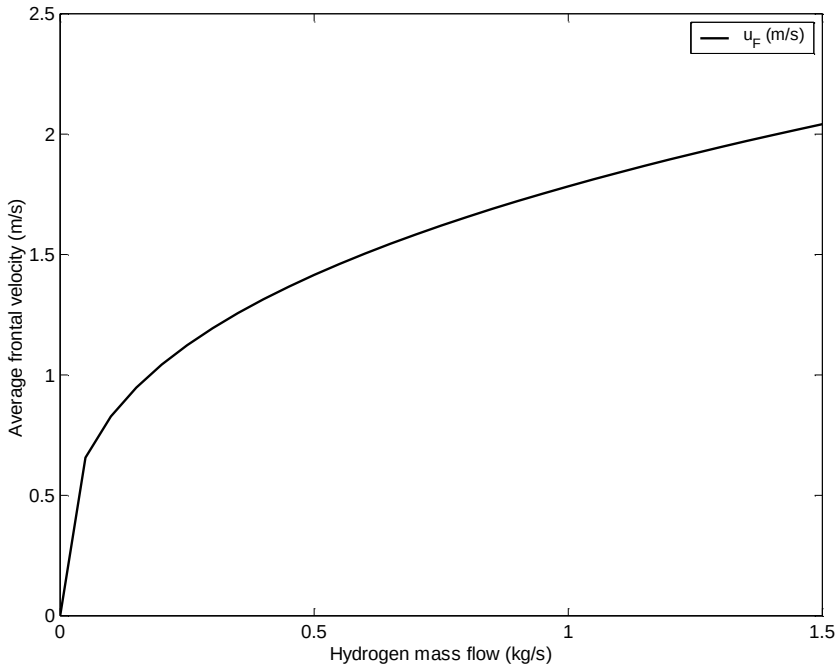

Figure 6.20 Calculated average frontal velocity of hydrogen gas cloud in the N1 accident. Froude number Fr = 0.68, Φ = 0.5

The average concentration of the hydrogen gas cloud is calculated as function of hydrogen mass flow (for Fr = 0.68 and Φ = 0.5), as shown in Figure 6.21. Given a mass flow rate of 0.74 kg/s (dotted lines), the calculated average hydrogen mole fraction is

0.15, which is comparable to the FLACS results of Case 1 and Case 5. This shows that the Froude scaling can be useful in early, fast estimates of hydrogen gas concentration in relevant incidents involving hydrogen dispersion.

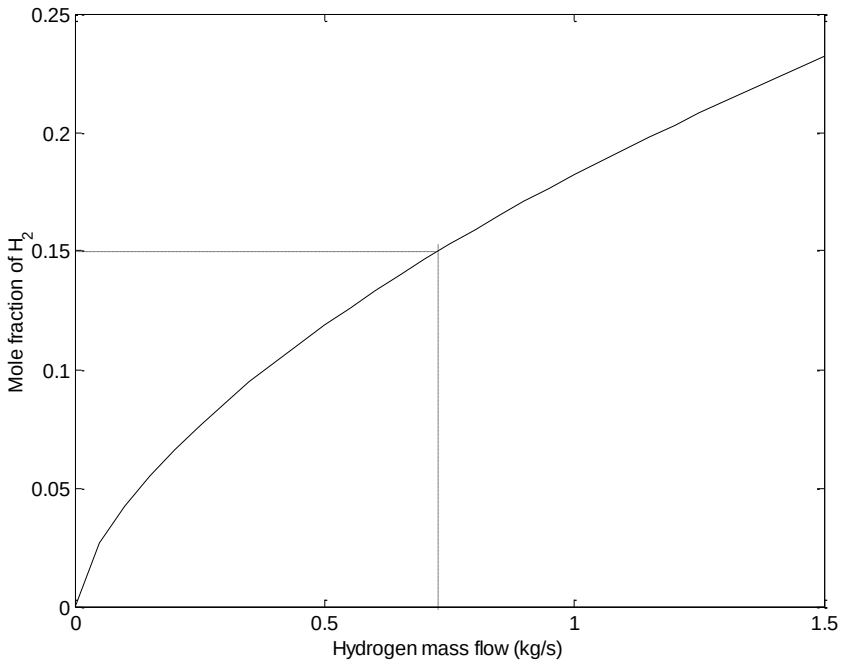

Figure 6.21 Average hydrogen concentration in the cloud, calculated with Φ = 0.5 and Fr = 0.68

6.6 Discussion

Discharge:
The CFD simulations show that the dispersion process is very sensitive with respect to varying the jet direction. Also, obstructions in the jet changes the gas cloud formation dramatically, compared to a free jet. This corresponds well with the results from both the experimental tests and CFD simulations performed in the ISO container (Chapter 3 and Chapter 5, respectively), where one of the tests was carried out with a hydrogen jet hitting an obstacle located only 0.2 m from the nozzle. The same effect is seen in the CFD simulations on the N1 factory.

The investigation report does not contain a clear direction of the release. However, the motor casing that was blown away indicate that the jet has been directed towards the motor. Based on observations on the site, the release was probably sector-shaped. One main assumption in the FLACS simulations have been that the jet release was directed along one of the axes only, which perhaps is too conservative. However, the close distance between the jet exit and the base of Pump A resulted in simulations where the gas was forced upwards and outwards in a fan-shape assumed to resemble the sector-shaped release.

Ignition source:
The investigation report of the N1 accident suggests that the ignition source probably was a red-hot bearing, which is considered to be a weak ignition source by Bond (1991). The ignition of flammable materials by a hot surface is well documented, both for hydrogen and for other materials, such as hydrocarbons, with most researchers showing the lowest temperatures for ignition being associated with large volumes and surface areas, as discussed in the paper by Astbury and Hawksworth (2007). The reported trends show that smaller heated surfaces require higher temperatures, downward facing surfaces showing longer induction times, and surfaces at the top of the test apparatus having longer induction times. Consequently, any hydrogen-air mixture within the flammable range is liable to be ignited by a heated surface, but the temperature and the delay before ignition will depend on the size, geometry, and orientation of the enclosure.

In the N1 ammonia plant accident it is therefore probable that the hot surface could ignite the hydrogen-air mixture containing 12-15 vol. % of hydrogen. Also, the time of ignition is a topic for discussion, given that the investigation report based on process data recordings the time of ignition to be an interval between 20 and 30 seconds.

Walls:
Simulations on the factory building without walls show that 'the best building has no walls', as stated by Trevor Kletz (Bjerketvedt et al., (1997)). As seen in Case 4, the hydrogen-air mixture was effectively vented to the outside of the building, reducing the probability for accidents by a large degree. Also in this case, the explosion overpressures were small.

Efficiency:
According to the investigation report, the total mass released in the accident was in the order of 10-20 kg of hydrogen. The investigation estimated the amount of hydrogen contributing to the explosion was in the interval 3.5-7.0 kg, equivalent of 100-200 kg of TNT. The base case dispersion simulation (Case 1) had a total mass of hydrogen of 14.0 kg at the time of ignition; within the interval of the total mass, but above the estimate of contributing gas. This leads to an efficiency in the base case simulation close to 100%. The CFD simulations performed shows no clear evidence that the gas cloud detonated. FLACS guidelines states that detonation can occur when a set of criteria are met; explosion pressure loads above 6-700 kPa, flame speeds higher than 600 m/s and the factor dP/dx exceeds certain threshold values. Although the CFD simulations do not meet all these criteria, several assumptions have been made on the road to these results. For example, the shape and direction of the discharge, the mass flow rate, the time of ignition and assumed geometry, will largely influence the simulation results. Throughout in this thesis, it has been shown that these parameters influence the dispersion and explosion to a significant degree. The accident investigation team concluded that the accident most likely was a detonation, and the present CFD results cannot exclude this.

6.7 Conclusions

CFD simulations indicate that the gas cloud that formed in the N1 factory was relatively long and narrow. The small-scale experiments presented in Sommersel (2009) are considered representative to model the N1 factory building. The Froude number correlation developed in these experiments was here used to estimate a frontal velocity and an average hydrogen gas concentration. This concentration estimate, although rough, is comparable to the FLACS results of Case 1 and Case 5. The method has potential for use in early, fast estimates of hazard potential in relevant incidents involving hydrogen dispersion.

The CFD simulations of the N1 factory building show that the dispersion is sensitive regarding jet direction and geometry, as shown in the comparison between Case 1 and Case 2. The simulation with solid walls and with an obstruction downstream of the jet (Case 1) shows explosion overpressures of a magnitude that could explain the observed damages from the N1 accident. This scenario has a distinct fan-shaped dispersion caused by an obstruction close to the release point and is assumed to resemble the probable sector-shaped release in the accident. The CFD simulations show that obstructions at roof level also causes formation of a large recirculation zone, where the concentration level rises to above 15 vol. % in short time. The FLACS geometry of the N1 building was simplified, and it is reasonable to assume that the level of obstructions influencing the dispersion (and explosion) was significantly larger than in these simulations.

The N1 factory building was originally designed without walls. The results from the CFD simulations imply that if the walls had not been added, the severe explosion in 1985 would never had taken place. It is not obvious that it would have ignited.

Explosion simulations show a relatively rapid increase in explosion overpressures. However, it is difficult to conclude whether the accident was a detonation or a fast deflagration. The results from the explosion simulations have a degree of uncertainty, when compared with the N1 accident as discussed in Section 6.6. In the accident

investigation report it is concluded that the accident most likely was a detonation, and the present CFD results cannot exclude this.

7 Conclusion

The basis for this thesis is the accident in the N1 ammonia plant hydrogen, where one of the main goals was to re-investigate the chain of events. The N1 factory building has been the model for both small-scale and field-scale experimental campaigns. The objective of the thesis is to get a better understanding of the dispersion of hydrogen and inhomogeneous hydrogen explosions in long buildings, channels and tunnels.

The presentations at the latest International Conference on Hydrogen Safety (ICHS 2017), shows that hydrogen explosions in confined spaces or partially confined spaces, such as buildings, tunnels, garages and repair shops still have the high priority in the hydrogen safety research community and needs further work.

A laboratory scale experimental rig was built for studying dispersion and ignition of hydrogen gas clouds in an open channel. The rig was instrumented with pressure transducers, a continuous ignition source, volume flow control and a digital logging system. The ignition of the hydrogen gas cloud was used as a tool to indicate the front of the flammable gas cloud. A high-speed camera was used to capture the time of ignition of the cloud and the following flame propagation. The rig was designed to study the gas cloud frontal velocity and the generated overpressure in the combustion of the hydrogen released. The experimental campaign was studied numerically, by use of the commercial CFD code FLACS.

A field-scale experimental rig (20´ ISO container) was set up in Raufoss to further study dispersion and ignition of hydrogen gas clouds at a larger scale. This rig was equipped with pressure transducers, hydrogen gas supply system, manual ignition source, digital logging system and high-speed cameras. In this rig, the experimental campaign was designed to study the effects on generated explosion overpressures by varying mass flow rate, jet direction, time of ignition and level of obstructions. Subsequently, the experiments were studied numerically in FLACS.

Finally, FLACS was used to re-investigate the N1 accident through five different scenarios. The scenarios were varied with respect to basic geometry and jet direction.

Each scenario were combined dispersion and explosion simulation, i.e. simulations with inhomogeneous hydrogen gas clouds.

The experimental results from the laboratory scale presented in this thesis show that under the given experimental conditions, the hydrogen-air cloud in the channel behaves as a gravity current, where approximately half of the height of the channel was filled with hydrogen ($\Phi = 0.5$). Based on this observation, a Froude number for the dispersion of the hydrogen gas clouds was determined to be 0.68. The frontal velocity of the hydrogen gas cloud appears to be well described by this method. The fast nature of Froude scaling may give adequate first estimates of both the concentration and the frontal velocity of the cloud in incidents involving hydrogen gas dispersion in channels and tunnels. Numerical simulations with the FLACS code correlate well with the experimentally observed frontal velocities. The Froude number correlation developed in these experiments was also used to estimate an average hydrogen gas concentration of the N1 factory accident. This method has potential for use in early, fast estimates of hazard potential in relevant incidents involving hydrogen dispersion.

The results presented in this thesis strongly suggests that the dispersion of hydrogen gas is highly sensitive to the geometry in which the gas is released. The release from a high-pressure source is mixed rapidly with ambient air, and generates a concentration field due to the turbulence of the jet. If the high-momentum jet is obstructed downstream, the development of the flammable gas cloud is highly sensitive to the local geometry, and could generate significantly differing gas cloud characteristics.

In the ISO container experiments, the time of ignition was varied relative to the release initiation, thus not directly comparable to the laboratory scale experiments. More than 30 experiments were conducted with varying initial conditions, that showed overpressures in the range of 0.4 to 7 kPa. When obstructions were introduced, the explosion overpressures reached levels in the range of 20-100 kPa. In experiment 39, the nozzle was directed towards an obstacle 0.2 m downstream, and generated a violent dispersion and subsequent explosion. This experiment differs from experiments 26 and 38 in the number of obstructions, but also in the way the dispersion was influenced, as

the jet was impinged directly on a pallet. The contribution of each of these two main factors cannot be quantified, but the effect of the pallet directly downstream of the nozzle is believed to play a significant role. This finding is supported by the corresponding CFD simulations. Comparing CFD simulations of experiments 26 and 38 show quite similar dispersion characteristics, despite the obstructions in experiment 38. This supports the assumptions that the combustion process is the main contributor to the difference in explosion overpressures in these experiments. Yet, comparing FLACS simulations 38 and 39, it is seen that the obstruction downstream the jet in 39 strongly affect the dispersion characteristics. The gas cloud in 39 is smaller, but a significant part of the cloud is close to stoichiometric. The FLACS simulations of the N1 factory building show the same pattern.

The use of the BOS technique is proven to be useful for estimating explosion overpressures from high explosives and gas explosions. One example of use is the work by Mizukaki et al. (2015).

For high explosives, the method agreed quite well with a standard curve for side-on shock pressures. For the field-scale ISO container experiment investigated with this technique, there were clear observations of several shock waves. The results obtained by this technique gives reason to believe that the maximum explosion overpressure in experiment 39 was at least 200 kPa.

From a safety perspective, one of the main findings is that minor differences in geometries or discharge directions can cause widely different scenarios for equal amounts of hydrogen:

- Under certain circumstances (i.e. obstructions in jet and geometry), the hydrogen dispersion can generate a forced feedback loop that can accumulate a close-to-stoichiometric gas cloud, posing a serious hazard if ignited. This was seen in the N1 accident.
- There is a dramatic reduction in consequences when the geometry and discharge allow for the released hydrogen to vent unobstructed. This effect is shown in the

N1 factory CFD simulation without side walls, representing the original design of the factory.

The N1 accident is one event that became serious due to modifications made many years prior. This is a reminder of how the safety assessments in an original design can be omitted when considering modifications based on operational requirements and needs. This must be kept in mind when designing and operating facilities involving hydrogen as an energy carrier. If you do the right things, hydrogen will be a safe energy carrier for the future.

The novelty of the project can be summarized as follows:

- A Froude number correlation describing hydrogen gas cloud frontal velocity and average concentration is determined experimentally.
- The background oriented schlieren method with a natural background is used to follow the shock wave from an explosion, and to quantify relevant parameters describing the explosion.
- A unique series of field scale experimental data of discharge and ignition of inhomogeneous hydrogen gas clouds is provided.
- The reinvestigation of the N1 accident provides a reasonable scenario explaining the accident, with a quantitative description of the flammable gas cloud developed during a 20 second release.

7.1 Suggestions for further work

This research project has pointed out that the dispersion characteristics of hydrogen is sensitive to impingement or obstructions close to the leak point. Further work is needed to investigate the level of impact of the obstruction downstream the jet compared with the impact of obstruction in the combustion. Field scale experiments should be performed to quantify this effect. Specifically, it would be interesting to perform an experiment with a setup like the ISO experiment 38, but with an additional pallet obstructing the jet.

Numerical simulations on explosions with homogeneous and inhomogeneous gas clouds in the N1 geometry should be investigated, to numerically prove whether the N1 accident was a detonation or a fast deflagration. The mechanisms for DDT is not yet fully understood, and should be investigated in an industrial scale.

References

Alcock et al. (2001) — Alcock, J.L., Shirvill. L.C., Cracknell, R.F., (2001) Compilation of existing safety data on hydrogen and comparative fuels, European Integrated Hydrogen Project II (EIHP2), deliverable report, WP 5, ENK6-CT2000-00442, Retrieved from http://www.eihp.org/.

Astbury and Hawksworth (2007) — Astbury, G.R., Hawksworth, S.J., (2007) Spontaneous ignition of hydrogen leaks: A review of postulated mechanisms, International Journal of Hydrogen Energy, 32(13):2178-2185

Bain et al. (1998) — Bain, A., Barclay, J.A., Bose, T.B., Edeskuty, F.J., Fairlie, M.J., Hansel, J.G., Hay, D.R. and Swain, M.R., (1998) Sourcebook for hydrogen applications, Hydrogen Research Institute and National Renewable Energy Laboratory

Bjerketvedt and Mjaavatten (1986) — Bjerketvedt, D. and Mjaavatten, A., (1986) Eksplosjonsulykke N1 6.7.85, Eksplosjonsforløp. Sluttrapport., Norsk Hydro, Research Centre, Porsgrunn, Norway, Doc.nr. 86B.BM7. (final report, Norwegian).

Bjerketvedt and Mjaavatten (2005) — Bjerketvedt, D. and Mjaavatten, A., (2005) A hydrogen-air explosion in a process plant: A case history. Conference Proceedings, 1st International Conference on Hydrogen Safety (ICHS), Pisa

Bjerketvedt et al. (1997) — Bjerketvedt, D., Bakke, J.R., Van Wingerden, K., (1997) Gas explosion handbook, Journal of Hazardous Materials, 52 (1), pp. 1-150.

Bond (1991) — Bond, J., (1991) Sources of ignition: Flammability Characteristics of Chemicals and products. Butterwoth Heinemann, Oxford

Brooke (1968) — Brooke Benjamin, T., (1968) Gravity currents and related phenomena, Journal of Fluid Mechanics, vol 31 (2), pp. 209-248.

Chiu et al. (1977) — Chiu, KW., Lee, JH., Knystautas, R., (1977) The blast waves from asymmetrical explosions, Journal of Fluid Mechanics, Vol. 82 (2), pp. 193-208.

Chung (2007) — Chung, S.H., (2007) Stabilization, propagation and instability of tribrachial triple flames, Proceedings of the Combustion Institute 31, pp. 877-892.

Fannelöp (1994) — Fannelöp, T. K., (1994) Fluid Mechanics for Industrial Safety and Environmental Protection,

Industrial Safety Series, vol. 3, Elsevier Science B.V.

FLACS (2008) FLACS User's Guide 98, GexCon AS, Norway.

FLACS (2015) FLACS; www.gexcon.com

Forcier and Zalosh (2000) Forcier T., Zalosh R., (2000) External pressures generated by vented gas and dust explosions, Journal of Loss Prevention in the Process Industries, 13, pp. 411-417, Elsevier Science Ltd.

Gaathaug et al (2010) Gaathaug, A.V., Bjerketvedt, D. and Vaagsaether, K., (2010) Experiments with flame propagation in a channel with a single obstacle and premixed stoichiometric H2-air, Combustion Science and Technology, vol. 182 (11-12), pp. 1693-1706.

Giannissi et al. (2015) Giannissi, S.G., Shentsov, V., Melideo, D., Cariteau, B., Baraldi, D., (2015) CFD benchmark on hydrogen release and dispersion in confined, naturally ventilated space with one vent, International Journal of Hydrogen Energy, 40(8), pp. 2415-2429.

Gröbelbauer et al. (1993) Gröbelbauer, H. P., Fanneløp, T. K., Britter, R. E., (1993) The propagation of intrusion fronts of high density ratios, Journal of Fluid Mechanics, vol. 250, pp. 669-687.

Hansen and Middha (2007) Hansen, O.R and Middha, P. (2007) CFD-Based Risk Assessment for Hydrogen Applications, Process Safety Progress, Vol.27, No.1

Harrison and Eyre (1987) Harrison, AJ. and Eyre, JA., (1987), External explosions as a result of explosion venting. Combustion, Science and Technology, 52, pp. 91-106.

Houf and Schefer (2008) Houf, W., Schefer, R., (2008) Analytical and experimental investigation of small-scale unintended releases of hydrogen. International Journal of Hydrogen Energy, vol. 33, pp. 1435–44.

Hysafe (2004/2017) www.hysafe.org and https://www.hysafe.info/

Klinge et al. (2003) Klinge, K., Kirmse, T., Kompenhans, J. (2003) Application of Quantitative Background Oriented Schlieren (BOS): Investigation of a Wing Tip Vortex in a Transonic Wind Tunnel. Proceedings of 4th Pacific Symposium on Flow Visualisation and Image Processing (PSFVIP).

Lee and Moen (1980) Lee, J.H.S. and Moen, I.O., (1980) The Mechanisms of transition From Deflagration to

Detonation in Vapour Cloud Explosions. Progress in Energy and Combustion Science, 6, pp. 359-389

Lees (1996) — Lees, F.P., (1996) Loss Prevention in the Process Industries, Hazard Identification, Assessment and Control, volume 2, 2nd ed. Reed Educational and Professional Publishing Ltd. (ISBN 0-7506-1547-8) pp. 17/129-132.

Matsuura et al. (2008) — Matsuura, K., Kanayama, H., Tsukikawa, H. and Inoue, M., (2008) Numerical simulation of leaking hydrogen dispersion behaviour in a partially open space. International Journal of Hydrogen Energy 33, pp. 240-247.

Middha and Hansen (2009) — Middha, P. and Hansen, O.R., (2009) Using computational fluid dynamics as a tool for hydrogen safety studies, Journal of Loss Prevention in the Process Industries, 22(3), pp. 295-302.

Mizukaki et al. (2014) — Mizukaki, T., Wakabayashi, K., Matsumura, T., and Nakayama, K., (2014) Background-oriented schlieren with natural background for quantitative visualization of open-air explosions, Shock Waves Vol 24(1), pp. 69–78

Papanikolaou et al. (2010) — Papanikolaou, E.A., Venetsanos, A.G., Heitsch, M., Baraldi, D., Huser, A., Pujol, J., Garcia, J., Markatos, N., (2010) HySafe SBEP-V20: Numerical studies of release experiments inside a naturally ventilated residential garage. International Journal of Hydrogen Energy 35(10), pp. 4747-4757.

PFV (2015) — Software: Photron Fastcam Viewer - For High Speed Digital Imaging, Photron 2001-2008. http://www.photron.com

Phillips (1965) — Phillips, H., (1965) Flame propagation in a buoyant methane layer, 10th. Int. Symp. on Combustion, The Combustion Institute, pp. 1277-1283.

Rai et al. (2014) — Rai, K., Bjerketvedt, D. and Gaathaug, A.V., (2014) Gas explosion field tests with release of hydrogen from a high pressure reservoir into a channel, International Journal of Hydrogen Energy, 39(8), pp. 3956-3962.

Sato et al. (2006) — Sato, Y., Merilo, E., Groethe, M., Colton, J., Chiba, S., Iwabuchi, H. Ishimoto, Y., (2006), Hydrogen Release Deflagrations in a Sub-Scale Vehicle

Tunnel, (presented at 16th World Hydrogen Energy Conference (WHEC))

Settles (2001) — Settles, G. S., (2001) Schlieren and Shadowgraph Techniques: Visualizing Phenomena in Transparent Media. Springer-Verlag Berlin and Heidelberg GmbH & Co. K

Shirvill et al. (2012) — Shirvill, L. C., Roberts, T.A. and Royle, M., (2012) Safety studies on high-pressure hydrogen vehicle refuelling stations: Releases into a simulated high-pressure dispensing area. International Journal of Hydrogen Energy 37(8), pp. 6949-6964.

Simpson, (1997) — Simpson, J. E., (1997) Gravity Currents in the Environment and the Laboratory, 2nd Ed., Cambridge University Press.

Sommersel et al. (2008) — Sommersel, O.K., Bjerketvedt, D., Christensen, S., Krest, O. and Vaagsaether, K., (2008) Application of background oriented schlieren for quantitative measurements of shock waves from explosions, Shock Waves, 18(4), pp. 291–297. Presented at the 21st ICDERS 2007.

Sommersel et al. (2009) — Sommersel, O.K., Bjerketvedt, D., Vaagsaether, K., Fannelop, T.K. (2009) Experiments with release and ignition of hydrogen gas in a 3 m long channel, International Journal of Hydrogen Energy, Volume 34 (14), pp 5869-5874. Presented at the 2nd International Conference on Hydrogen Safety (ICHS) 2007.

Sommersel et al. (2017) — Sommersel, O.K., Vaagsaether, K., Bjerketvedt, D. (2017) Hydrogen explosions in 20’ ISO container, International Journal of Hydrogen Energy, Volume 42 (11), pp. 7740-7748. Presented at the 6th International Conference on Hydrogen Safety (ICHS) 2015.

Swain and Swain (1996) — Swain, M.R. and Swain, M.N., (1996) Passive ventilation systems for the safe use of hydrogen, International Journal of Hydrogen Energy 21(10), pp. 823-835.

Takeno et al. (2007) — Takeno, K., Okabayashi, K., Kouchi, A., Nonaka, T., Hashiguchi, K. and Chitose, K., (2007) Dispersion and explosion field tests for 40 MPa pressurized hydrogen, International Journal of Hydrogen Energy 32(13), pp. 2144-2153.

UFC (1997) — Unified Facilities Criteria (UFC), (1997) Design and Analysis of Hardened Structures to Convential

Weapons Effects. Joint Departments of the Army, Air Force, and Navy and the Defense Special Weapons Agency, TechReport UFC 3-340-01 TM 5-855-1/AFPAM, 32-1147(I)/NAVFAC, P-1080/DAHSCWEMAN-97.

van den Berg (1985) van den Berg, A.C., (1985) The multi-energy method: A framework for vapour cloud explosion blast prediction, Journal of Hazardous Materials, Vol. 12, Issue 1, pp. 1-10.

Venetsanos et al. (2003) Venetsanos A.G., Huld, T., Adams, P. and Bartzis, J.G., (2003) Source, dispersion and combustion modelling of an accidental release of hydrogen in an urban environment. Journal of Hazardous Materials, 105, pp. 1-25

Venetsanos et al. (2009) A.G. Venetsanos, E. Papanikolaou, M. Delichatsios, J. Garcia, O.R. Hansen, M. Heitsch, A. Huser, W. Jahn, T. Jordan, J.-M. Lacome, H.S. Ledin, D. Makarov, P. Middha, E. Studer, A.V. Tchouvelev, A. Teodorczyk, F. Verbecke and M.M. Van der Voort, (2009) An inter-comparison exercise on the capabilities of CFD models to predict the short and long term distribution and mixing of hydrogen in a garage, International Journal of Hydrogen Energy 34 (14), pp. 5912-5923

Venkatakrishnan and Meier (2004) Venkatakrishnan L, Meier EA., (2004) Density measurements using the Background Oriented Schlieren technique, Experiments in Fluids, 37, pp. 237-247.

Yanez (2015) Yanez, J.; Kuznetsov, M. and Souto-Iglesias, A., (2015), An analysis of the hydrogen explosion in the Fukushima-Daiichi accident, International Journal of Hydrogen Energy, 40, pp. 8261 – 8280

ICHS (2017) Keller, J. (2017), Outcome of the Research Priorities Workshop, Lecture at the 6th International Conference of Hydrogen Safety

Wilcox (2003) Wilcox, D. C., (2003), Basic Fluid Mechanics, 2nd Edition, DCW Industries, ISBN 1-928729-03-7.

Appendix 1 Hydrogen discharge calculations

In this text the equations used for calculating a hydrogen discharge are derived and explained (see Chapter 3.4.5). The text was typeset in LaTeX and written by the author.

1 Calculation of temperature and mass flow of a hydrogen jet release from a 300 l vessel.

2 Theory

2.1 Introduction

A shock wave in a gas can be defined as a fully developed compression wave of large amplitude, across witch density, pressure, and particle velocity change drastically (GEH). A shock wave propagates at supersonic velocity relative to the gas immediately ahead of the shock. The propagation velocity of the shock wave depends on the pressure ratio across the wave. Increasing pressure gives higher propagating velocity.

2.2 Normal shock waves

Normal shock waves are handled by Wilcox (2003). He considers a one-dimensional wave propagating into an undisturbed fluid, where the pressure, temperature and density in the undisturbed fluid are denoted p_1, T_1 and ρ_1 respectively. Assuming that the wave is at rest, the undisturbed fluid ahead of the shock moves with a speed of u_1. After the fluid moves through the wave, the flow properties are p_2, T_2 and ρ_2. The latter region is referred to as lying behind the shock.

The fluid is assumed to be inviscid, with no heat transfer or body forces, and the flow is steady. The conservation of mass, momentum and energy can be expressed in terms of Mach number, $M = \frac{Flow\ speed}{Sound\ speed} = \frac{U}{a}$ and the specific heat ratio $\gamma = \frac{c_p}{c_v}$. These equations is called the normal shock relations, and are shown in eq. 1-4.

$$M_2^2 = \frac{1 + \frac{\gamma-1}{2} M_1^2}{\gamma M_1^2 - \frac{\gamma-1}{2}} \tag{1}$$

$$\frac{\rho_2}{p_1} = \frac{u_1}{u_2} = \frac{(\gamma+1)\, M_1^2}{2 + (\gamma-1) M_1^2} \tag{2}$$

$$\frac{p_2}{p_1} = 1 + \frac{2\gamma}{\gamma+1}(M_1^2 - 1) \tag{3}$$

$$\frac{T_2}{T_1} = 1 + \frac{2(\gamma-1)}{(\gamma+1)^2}\left(\frac{1+\gamma M_1^2}{M_1^2}\right)(M_1^2 - 1) \tag{4}$$

where subscript 1 and 2 denotes conditions before and after the shock respectively.

2.3 Laval nozzle

The Laval nozzle is a convergent-divergent nozzle, where the flow upstream of the throat is subsonic. The design condition is sonic flow ($M = 1$) at the throat,

giving an acceleration to supersonic flow at the outlet. Mass conservation gives the area ratio between the inlet and the throat as:

$$\frac{A}{A^*} = \frac{\rho^* u^*}{\rho u} \tag{5}$$

where superscript * denotes conditions at the throat, ρ is the density and u is the velocity. The flow is accelerated isentropically. For a perfect gas, the area ratio can be expressed as a pressure ratio as a function of Mach number, shown in Eq. 6.

$$\frac{p}{p_0} = \left(1 + \frac{\gamma - 1}{2} M^2\right)^{\frac{-\gamma}{\gamma - 1}} \tag{6}$$

where p_0 is the upstream pressure. When the flow at the throat of a Laval nozzle is sonic, we have a condition referred to as choked flow. Substituting $\gamma = 1.4$ and $M = 1$ in eq. 6 gives $\frac{p^*}{p_0} = 0.528$.

2.4 Choked flow

For choked releases, McCaffrey et. al. (1986) states that the exit diameter, D_e, has to be replaced by a hypothetical nozzle, i.e. a convergent-divergent nozzle. The diameter is expressed as a function of the effective Mach number, M_{ef}, as shown in Eq. 7.

$$\frac{D_{ef}}{D_e} = \frac{1}{\sqrt{M_{ef}}} \left[\frac{2 + (\gamma - 1) M_{ef}^2}{\gamma + 1}\right]^{\frac{\gamma + 1}{4(\gamma - 1)}} \tag{7}$$

where Mach number is obtained by solving Eq. 6 with respect to M_{ef}.

$$M_{ef} = \sqrt{\frac{2}{\gamma - 1}\left[\left(\frac{p_0}{p}\right)^{\frac{\gamma - 1}{\gamma}} - 1\right]} \tag{8}$$

Knowing the exit diameter and the exit flow Mach number, all parameters of interest is determined.

3 Calculations

The background for these calculations is a series of experiments done with a hydrogen jet release from a 0.3 m^3 steel vessel. The initial pressure in the experiments ranged from 4 to 24 barg. The nozzle diameter were varied from 5 to 9 mm. In the calculations the hydrogen gas is assumed as an ideal gas, and the flow is isentropic.

Subsonic exit flows are achieved when equation 9 is satisfied, where p_0 is the tank pressure, p is ambient pressure and $\gamma = \frac{c_p}{c_v} = 1.4$ for hydrogen.

$$p_0 < p \cdot \left(\frac{2}{(\gamma+1)}\right)^{\frac{-\gamma}{(\gamma-1)}} \tag{9}$$

When the mach number M is lower than unity, the flow is subsonic. Equation 10 is used to calculate M.

$$M(i) = \sqrt{\frac{2}{\gamma-1}\left[\left(\frac{p_0}{p}\right)^{\frac{\gamma-1}{\gamma}} - 1\right]} \tag{10}$$

The mass flow rate is then

$$\dot{m}(i) = AC_D\sqrt{\frac{\gamma}{R}}\frac{p_0}{\sqrt{T_0}}\frac{M}{\left[1+\frac{\gamma-1}{2}M^2\right]^{\frac{\gamma+1}{2(\gamma-1)}}} \tag{11}$$

where A is the nozzle area $[\mathrm{m}^2]$, C_D is the discharge coefficient, R is the hydrogen gas constant $[\mathrm{J/kgK}]$ and T_0 is the initial temperature $[\mathrm{K}]$. The temperature step dT is calculated as shown in eq. 12.

$$dT = \frac{m(i)}{m(i-1)}T(i-1)(\gamma-1) \tag{12}$$

When the flow is choked the results from McCaffrey et. al. is used. An iteration sequence is performed to determine the Mach number ahead of the shock, M_1, by inserting the initial pressure in Eq. 3 and Eq. 6. Knowing M_1, the Mach number after the shock, M_2, is calculated using Eq. 1. In choked flow, the maximum flow per unit area is

$$\dot{m}(i) = AC_D\sqrt{\frac{\gamma}{R}\left(\frac{2}{\gamma+1}\right)^{\frac{\gamma+1}{\gamma-1}}}\frac{p_0}{\sqrt{T_0}} \tag{13}$$

The temperature is calculated using Eq. 12. The results from the calculations are then updated with the timestep dt, shown in table 1.

$T(i)$	$=$	$T(i-1) - dT \cdot dt$	$temperature\ [K]$
$m(i)$	$=$	$m(i-1) - \dot{m}(i) \cdot dt$	$mass\ [kg]$
$rho(i)$	$=$	$\frac{m(i)}{V}$	$density\ [\frac{kg}{m^3}]$
$p(i)$	$=$	$R. \cdot T(i) \cdot rho(i)$	$pressure\ (Pa)$

In figure 1 is results from 4 different calculations compared with a Flacs jet calculation. The initial tank pressure in the 4 calculations was 6, 12, 20 and 24 bar overpressure respectively.

A Matlab script have been developed. The figures below contains calculated data for temperature, density, Mach number, discharge velocity and tank pressure for an example of a discharge from a 0.3 m³ tank with pressurized hydrogen through a nozzle (representation of discharge in the ISO container experiments, ref. Chapter 3).

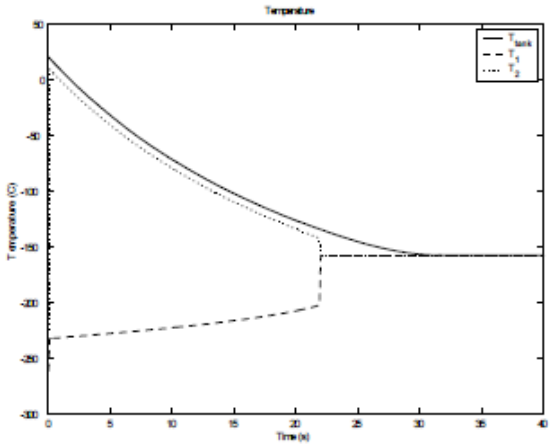

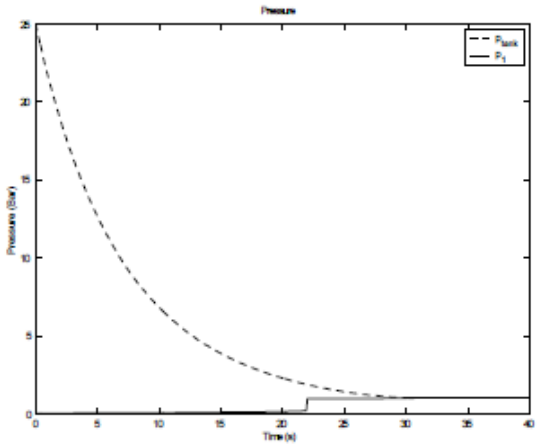

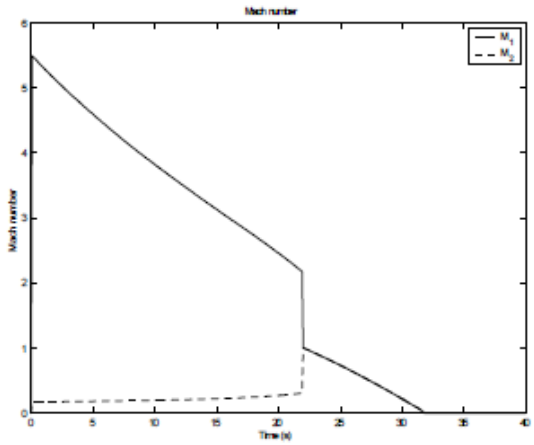

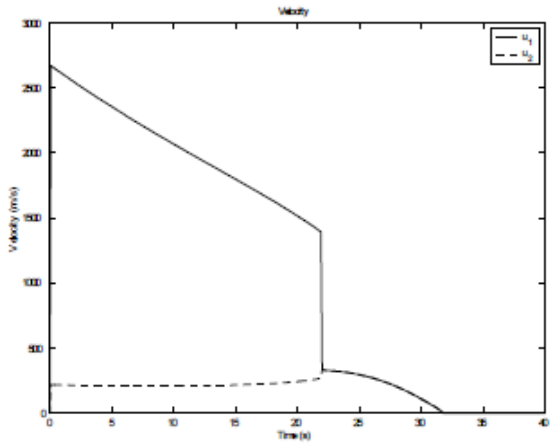

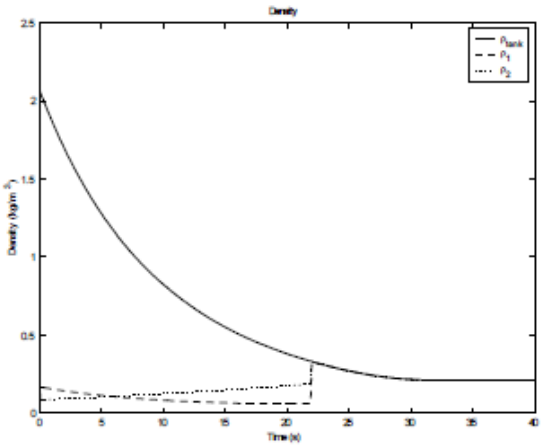

Appendix 2 FLACS simulation results, ISO container

Pressure records calculated in the FLACS CFD code for cases not presented in Chapter 5 (i.e. experiments 30, 24, 28, 27, 34 and 33) are presented in this appendix.

Case 3, Experiment 30:

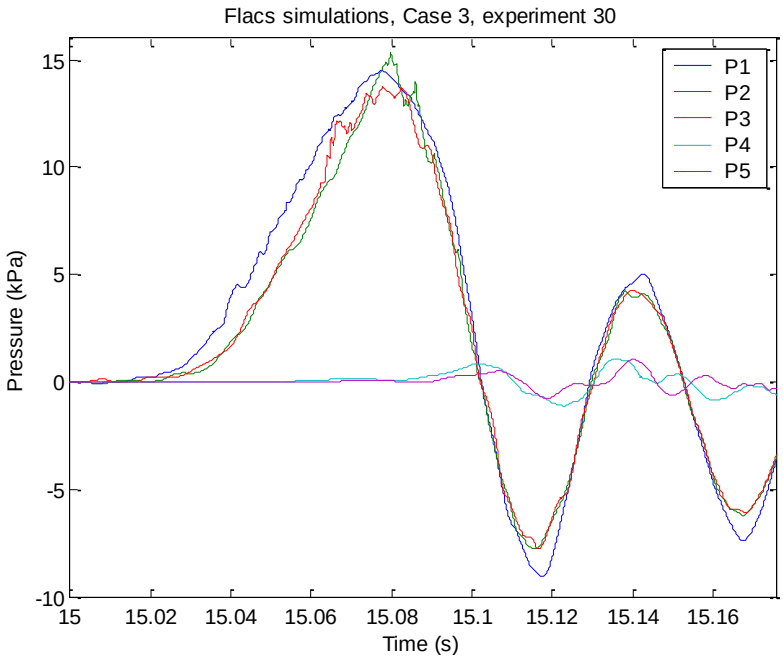

Case 4, Experiment 24:

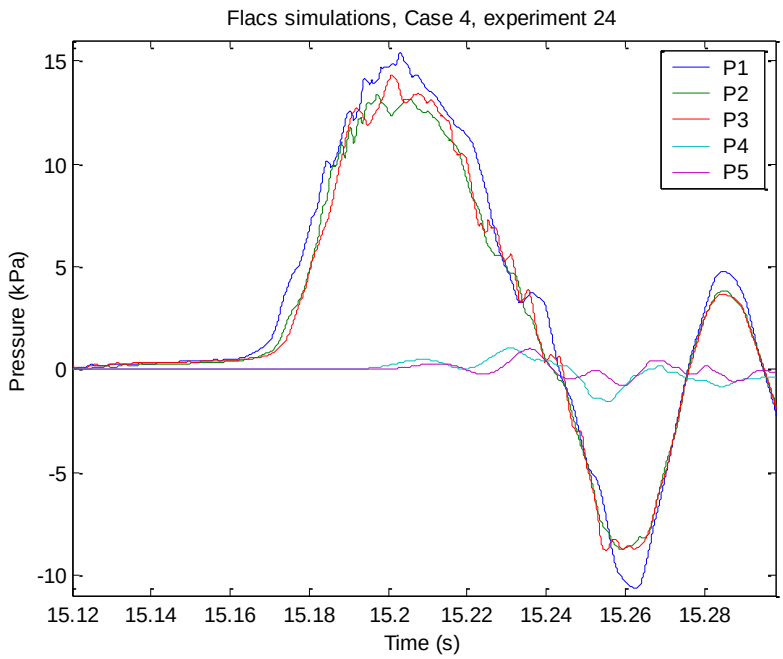

Case 5, Experiment 28

FLACS simulations on Experiment 28 did not report successful ignition. This was as expected, as the gas cloud was too lean. This experiment had an initial tank pressure of 6 kPa, the lowest in the test series. Experimentally, the setup did not generate an explosion.

Case 7, Experiment 27:

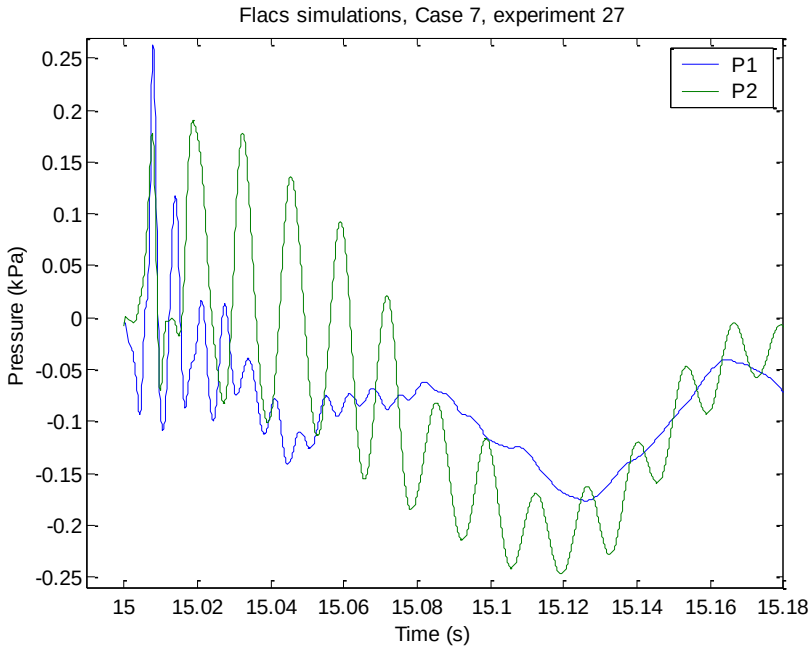

Case 8, Experiment 34:

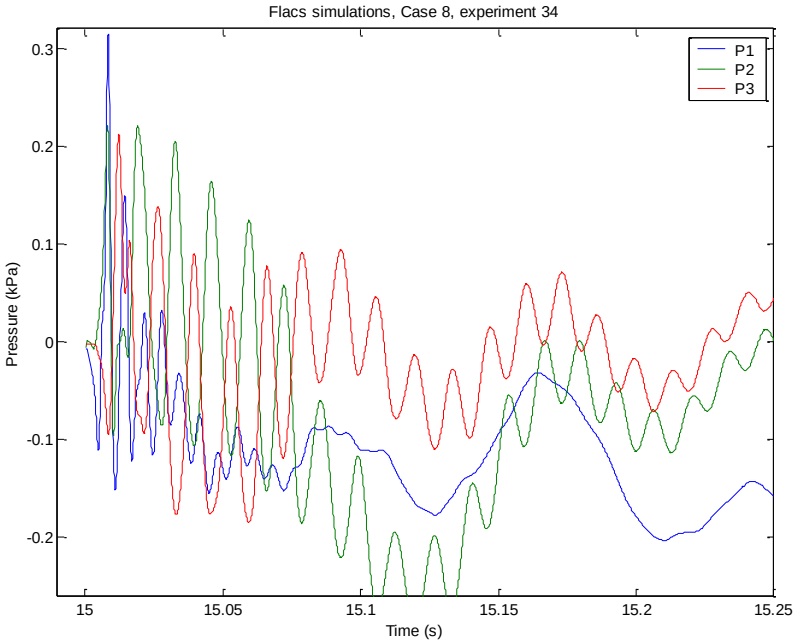

Case 9, Experiment 33

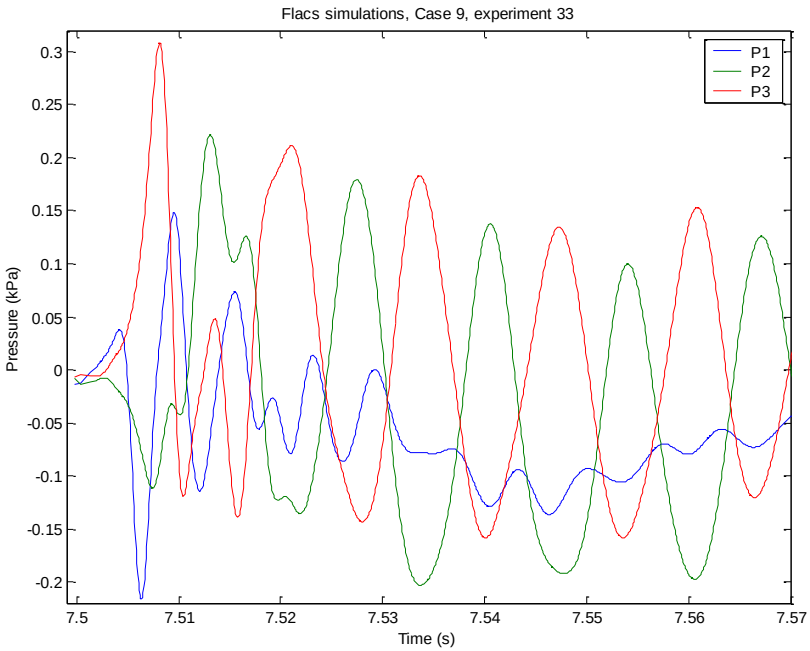

Plot of maximum pressure for all cases; black stars represent results from FLACS simulations, red circles denote experimentally recorded maximum pressures

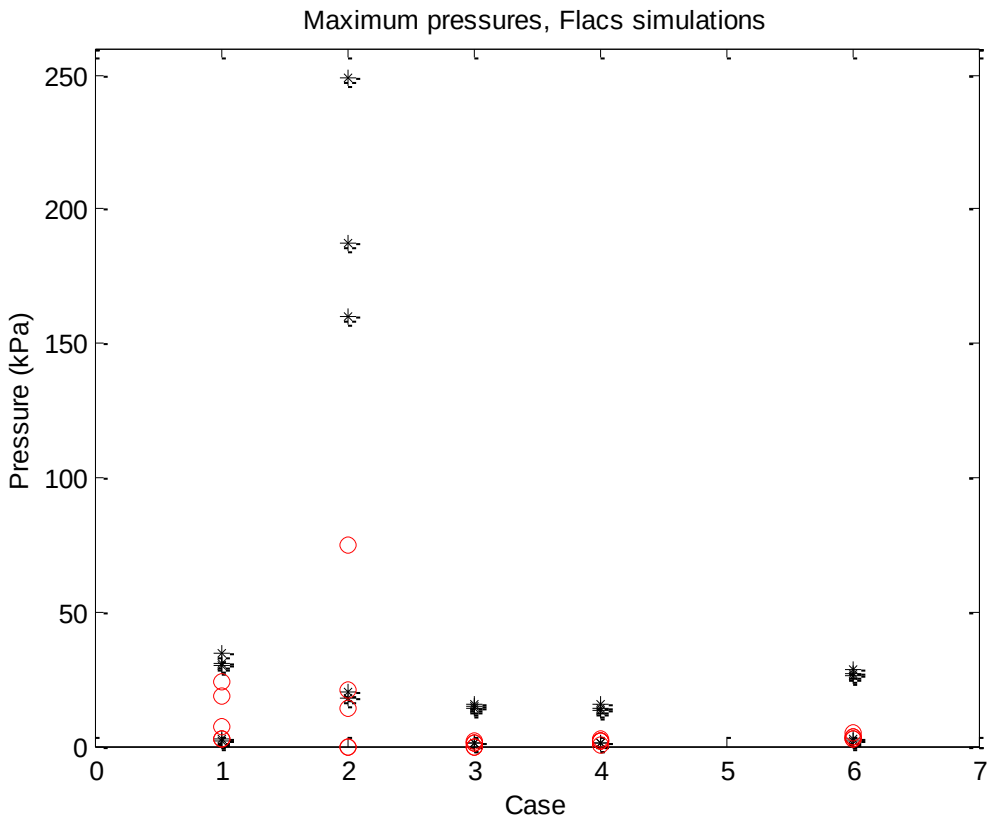

Appendix 3 Test matrix of ISO container experiments

	Experiment #	Tank pressure [bar]	Nozzle (mm) / placement	Ignition comments	P3 pmax	Comments	Amplifier setup [1]	Ignition setup	Highspeed	P tank Scope	Tank pressure Scope intervals (mV)
Not reported in thesis	1		5/1m up	Continuous ignition.		No visible ignition	1	1 m from door		-	
	2		5/1m up	Continuous ignition.		No visible ignition	1	1 m from door		-	
	3	2	5/1m up	Continuous ignition.		No visible ignition	1	1 m from door		skudd03	
	4	3	5/1m up	Continuous ignition.		No visible ignition	1	1 m from door		-	
	5	5	5/1m up	Continuous ignition.		No visible ignition	1	1 m from door		-	354-89
	6	2	9/1m up	Continuous ignition.		No visible ignition	1	1 m from door		-	347-83
	7	5	9/1m up	Continuous ignition.		Fire after 10 s	1	1 m from door		skudd07	347-83
	8	6	9/3m up	Ignition after 20 s.		20 s release.	1	1 m from door		skudd08	347+13
	9	6	9/3m up	Ignition after 20 s.		20 s release.	1	1 m from door		skudd09	347+13
	10	6	9/3m up	Ignition after 10 s.		One door closed, P4 and P5 centered in remaining opening (outside)	1	1 m from door		skudd10	347+19
	11	6	9/3m up	Ignition after 10 s.		No pressure logging	1	1 m from door		skudd11	
	12	6	9/3m up	Ignition after 10 s.		No pressure logging on P4 and P5	1	1 m from door		skudd12	
	13	-		C4 test		C4 test of pressure logging. C4 10 g. NBI Experiments 12 and 13 in same log file.	2	Detonating cord	hs	-	
	14	-		C4 test		C4 test of logging. C4 located inside of container. P1-P3 OK, no pressure logging on P4 and P5	2	Detonating cord		-	
	15	6	9/1m up	Continuous ignition.		Pressure logs show lots of noise	2	1 m from end wall		skudd15	347+21
	16	0	9/1m up	Ignition after 5 s.		Test of trigger and valve (no gas) to check noise in system. Logging OK	2	1 m from end wall		-	
	17	12	9/1m up	Ignition after 15 s.		Bang. Pressure logs on 4 channels (321mV at valve opening).	2	1 m from end wall	hs	skudd17	347+355
	18	-		Hammer stroke test		Test of pressure logging with hammer on container wall	2	-		-	
	19	4,5	9/1m down	Ignition after 5 s.		Succesful ignition after 7-8 s. Valve air hose fell off	2	1 m from end wall		skudd19	347-47
	20	12	9/1m down	Ignition after 15 s.		Pressure logs on 4 channels	2	1 m from end wall	hs	skudd20	347-343
	21	20	9/1m down	Ignition after 15 s.		Bang. No pressure log of tank pressure	2	1 m from end wall		Disk error	159+313
	22	20	9/1m down	Ignition after 15 s.		Pressure transducer location changed. Adapters glued with silicone	2	1 m from end wall	hs	skudd22	
Reported in thesis	23	20	9/1m down	Ignition after 15 s.		Door furthest away closed. Dent in container roof. Grease[2]	3	1 m from end wall	hs	skudd23	147-301
	24	20	9/1m down	Ignition after 15 s.		Successful pressure logging on all transducers	4	1 m from end wall	hs	skudd24	146+293
	25	20	9/1m down	Ignition after 10 s.		Successful pressure logging on all transducers	4	1 m from end wall	hs	skudd25	146+299
	26	24	9/1m down	Ignition after 15 s.	7 kPa	3 Leca blocks located 2,4 and 6m from door opening toppled over	4	1 m from end wall	hs	skudd26	146+371
	27	12	9/1m down	Ignition after 15 s.	0.7 kPa	Strange noise (honk). Leca blocks not toppled. Visible fire out of container	4	1 m from end wall	hs	skudd27	321-36
	28	6	9/1m down	Ignition after 15 s.	-	No explosion. Thermal protection on P4	4	1 m from end wall		skudd28	321-163
	29	6	9/1m down	Ignition after ca. 16 s.	0.4 kPa	Ignition tried at 7 s (unsuccessful). Confirmed ignition after 16 s.	4	1 m from end wall	hs	skudd29	321-163
	30	20	9/1m up	Ignition after 15 s.	0.8 kPa	Gas supply pipe fell. Nozzle ended up close to ceiling (ca. 0.3 m)	4	1 m from end wall	hs	skudd30	321+132
	31	20	5/1m up	Ignition after 30 s.	0.8 kPa		4	1 m from end wall	hs	skudd31	321+120
	32	20	5/1m up	Ignition after 15 s.	1 kPa	Valve closed after ignition. Remaining tank pressure ca. 10 barg (scope 321-86mV)	4	1 m from end wall	hs	skudd32	321+120
	33	20	5/1m up	Ignition after 7.5 s.	1.3 kPa	Valve closed after ignition. Remaining tank pressure ca. 10 barg (scope 321-36mV)	4	1 m from end wall	hs	skudd33	321+122
	34	20	5/1m down	Ignition after 15 s.	0.9 kPa	Valve closed after ignition.	4	1 m from end wall	hs	skudd34	321+130
	35	20	9/1m down	Ignition after 7.5 s.	2.5 kPa	Valve closed after ignition. Remaining tank pressure ca. 5 barg (scope 249+122mV)	4	1 m from end wall	hs	skudd35	321+128
	36	24	9/1m down	Ignition after 7.5 s.	4 kPa	Valve closed after ignition.	4	1 m from end wall	hs	skudd36	249+207
	37	24	9/1m down	Ignition after 15 s.	4 kPa		4	1 m from door	hs	skudd37	314+207
	38	24	9/1m down	Ignition after 15 s.	20 kPa	Obstructions: 2 euro pallets in roof (40 cm from roof)	5	1 m from end wall	hs	skudd38	301+207
	39	24	9/1m down	Ignition after 15 s.		Obstructions: 4 euro pallets in roof (40 cm from roof). 4 pallets on floor (see sketch)	5	1 m from end wall	hs	skudd39	

[1] Amplifier setup (kPa/V)

	Setup 1	Setup 2	Setup 3	Setup 4	Setup 5
P1	5	5	5	2	25
P2	50	5	5	2	10
P3	200	50	50	2	200
P4	71,84	71,84	0,72	0,72	71,84
P5	0,72	71,84	0,72	0,72	7,18

[2] Grease applied flush with brass mount on all Kistler transducers

Appendix 4 Obstructions layout, ISO container experiment 39

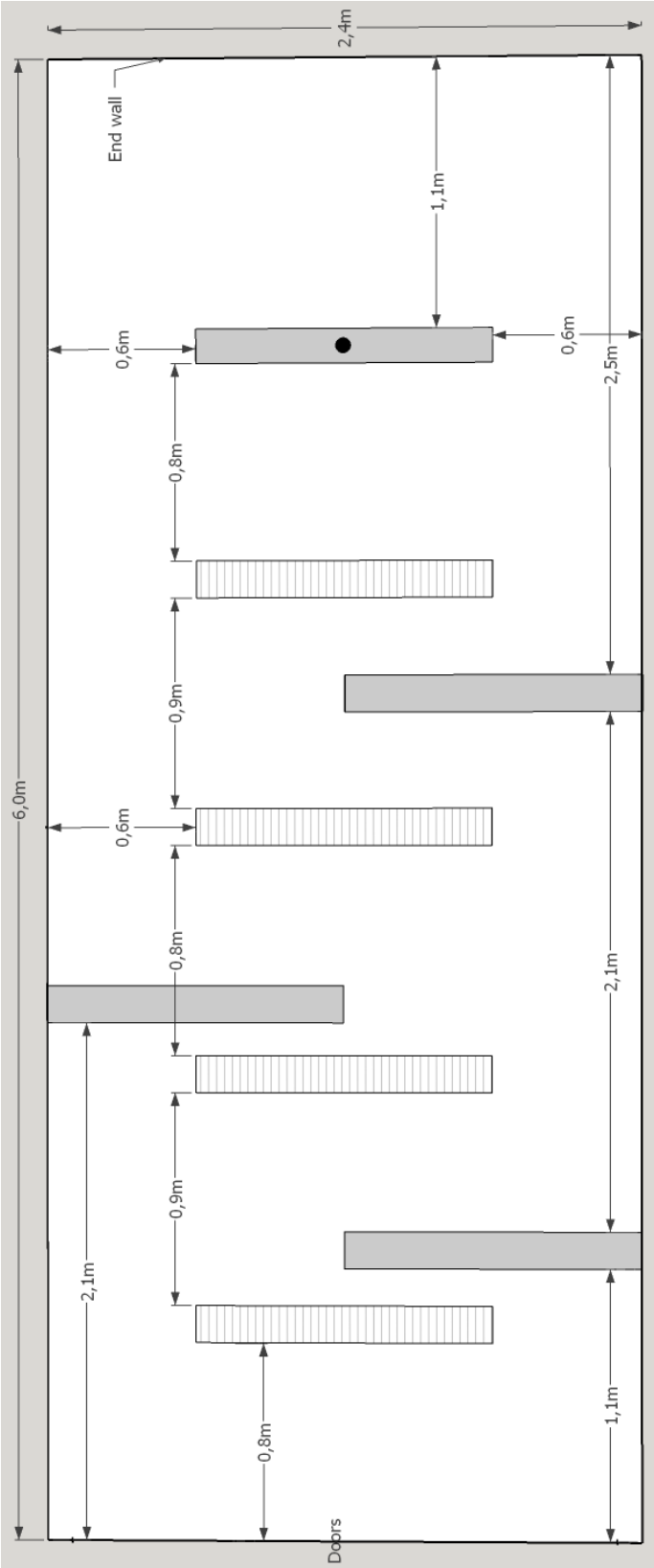

Top view of ISO container with dimensions for the locations of the Euro pallets used as obstructions in experiment 39 (see Chapter 3.4.4) here shown as a top view.

Grey color boxes represents pallets located on the container floor, whereas the shaded white rectangles represent the four pallets mounted 0.4 m from the ceiling. The black circle denotes the nozzle location.